ISSN: 2764-5886
e-ISSN: 2764-622X

Volume 9· N° 5 · May 2026

Journal of Bioengineering, Technologies and Health

An Official Publication of
SENAI CIMATEC

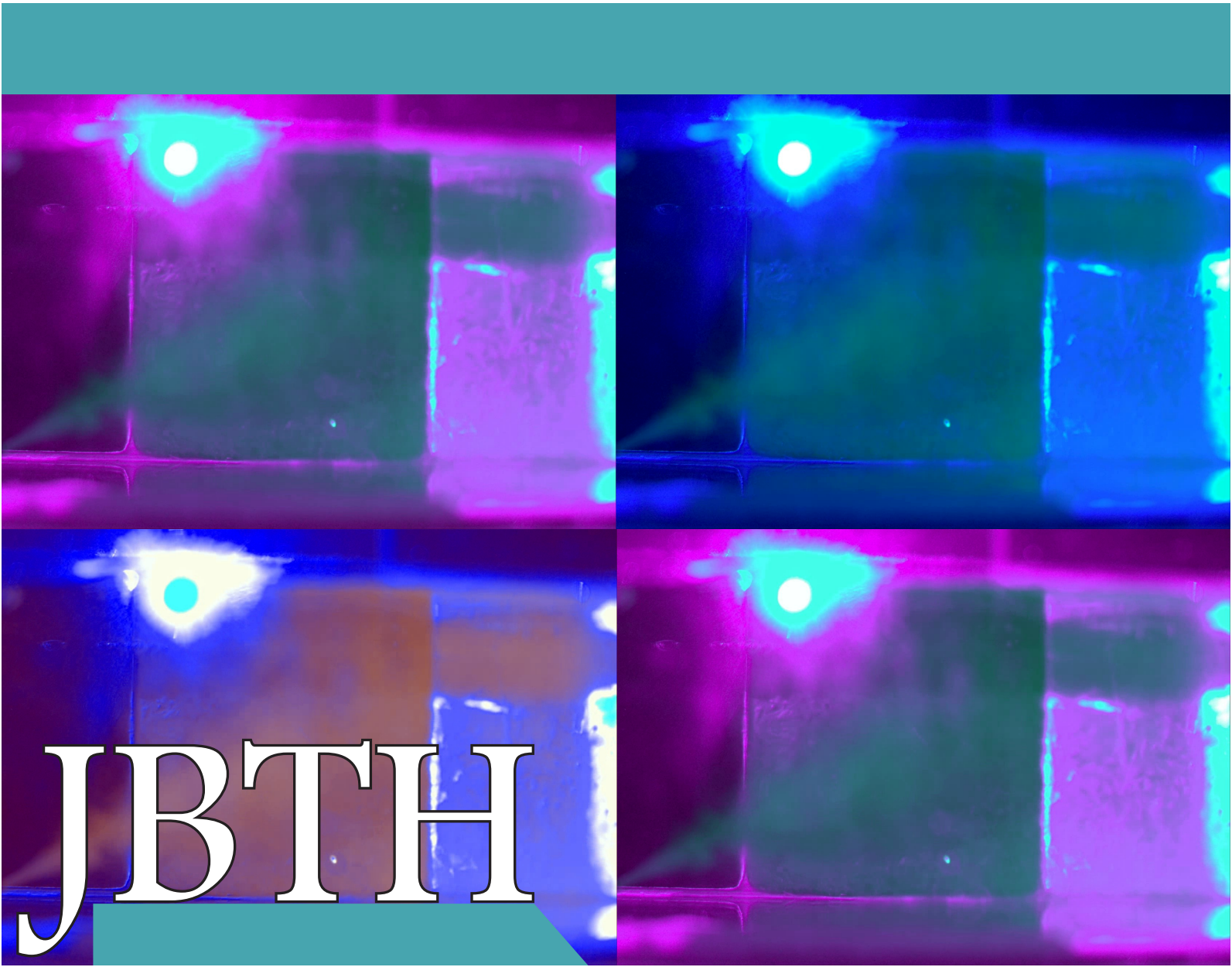

ISSN: 2764-5886 / e-ISSN 2764-622X

Volume 9 • Number 5 • May 2026

JOURNAL OF BIOENGINEERING TECHNOLOGIES AND HEALTH

An Official Publication of SENAI CIMATEC

PUBLISHED BY SENAI CIMATEC

Sistema FIEB | SENAI CIMATEC
PELO FUTURO DA INOVAÇÃO

May 2026
Printed in Brazil

JOURNAL OF BIOENGINEERING TECHNOLOGIES AND HEALTH

An Official Publication of SENAI CIMATEC

JOURNAL OF BIOENGINEERING TECHNOLOGIES AND HEALTH

Volume 9 • Number 5 **SUMMARY** *May 2026*

Original Articles

The Journal of Bioengineering, Technologies and Health (JBTH) is an official publication of the SENAI CIMATEC University (Serviço Nacional de Aprendizagem Industrial - Universidade Centro Integrado de Manufatura e Tecnologia). It is published montly (January to December) in English by SENAI CIMATEC University – Avenida Orlando Gomes, 1845, Piatã, Zip Code: 41650-010, Salvador-Bahia-Brazil; phone: (55 71) 3879-5501. The editorial offices are at SENAI CIMATEC University.

Editorial Office

Correspondence concerning subscriptions, advertisements, claims for missing issues, changes of address, and communications to the editors should be addressed to the Deputy Editor, Dr. Roberto Badaró, SENAI CIMATEC University (Journal of Bioengineering, Technologies and Health – JBTH) – Avenida Orlando Gomes, 1845, Piatã, Zip code: 41650-010, Salvador-Bahia-Brazil; phone: (55 71) 3879-5501; or sent by e-mail: jbth@fieb.org.br / jbth.cimatec@gmail.com.

Permissions

Postmaster

Send address changes to JBTH, Avenida Orlando Gomes, 1845, Piatã, Zip Code: 41650-010, Salvador-Bahia-Brazil.

Information by JBTH-SENAI CIMATEC University
Address: Avenida Orlando Gomes, 1845, Piatã, Zip Code: 41650-010, Salvador-Bahia-Brazil
Home-page: www.jbth.com.br
E-mail: jbth@fieb.org.br / jbth.cimatec@gmail.com
Phone: (55 71) 3879-5501 / 3879-5500 / 3879-9500

DOI:10.34178

ISSN: 2764-5886 / e-ISSN 2764-622X

COVER: Table 2. YOLO12n performance using index + G + B channel combinations as input (RGB as baseline). Unraveling Improvements in Underwater Leak Detection Using Color Channel Operations by Diego Perpétuo Andrade de Oliveira et al. J Bioeng. Tech. Health 2026;9(5):472.

A Comprehensive Survey on LDPC Code Design for CV-QKD

Mauro Queiroz Nooblath Neto[1]*, Guilherme Vergne de Oliveira[1], Micael Andrade Dias[1,2], Nelson Alves Ferreira Neto[1], Francisco Revson Fernandes Pereira[1], Valéria Loureiro da Silva[1]

[1]QuIIN – Quantum Industrial Innovation, Centro de Competência Embrapii Cimatec, SENAI CIMATEC; Salvador, Bahia, Brazil; [2]Department of Electrical and Photonics Engineering, Technical University of Denmark; Lyngby, Denmark

Continuous-Variable Quantum Key Distribution (CV-QKD) represents a promising technology for secure communication, but its practical implementation heavily relies on highly efficient information reconciliation (IR) to extract a secret key from correlated quantum data shared over noisy channels. Low-density parity-check codes (LDPC) have emerged as the state-of-the-art solution for this task due to their capacity-approaching performance. However, designing LDPC codes that perform reliably in the very low signal-to-noise ratio (SNR) regime of CV-QKD, while preserving practical implementation complexity, remains a major challenge. This work presents a comprehensive survey of LDPC code design methodologies for CV-QKD, with particular emphasis on three key structural classes: Quasi-Cyclic (QC-LDPC), Multi-Edge Type (MET-LDPC), and their hybrid form (QC-MET-LDPC).

Keywords: Quantum Key Distribution. Continuous-Variable. Low-Density-Parity-Check Codes. Information Reconciliation. Code Design. Quantum Communication.

Abbreviations: CV-QKD, Continuous-Variable Quantum Key Distribution; LDPC, Low-Density Parity-Check; IR, Information Reconciliation; QC-LDPC, Quasi-Cyclic Low-Density Parity-Check; MET-LDPC, Multi-Edge Type Low-Density Parity-Check; QC-MET-LDPC, Quasi-Cyclic Multi-Edge Type Low-Density Parity-Check; SNR, Signal-to-Noise Ratio.

A typical continuous variables quantum key distribution (CV-QKD) protocol consists of three main stages: quantum state transmission, information reconciliation (IR), and privacy amplification. In quantum state transmission, Alice sends a sequence of N very low-intensity coherent states to Bob, who performs detection and obtains a correlated, but not identical sequence. Discrepancies arise due to quantum channel noise, detection imperfections, and potential eavesdropping. Given the extremely low signal-to-noise ratio (SNR) inherent to these systems, the IR phase becomes particularly challenging. Its goal is to ensure that Alice and Bob share an identical and secure key by employing error-correcting codes — most notably, Low-Density Parity-Check (LDPC) codes, defined by sparse parity-check matrices H of size $(n - k)\times n$, with code rate $R_{code} = \frac{k}{n}$. In low-SNR regimes, very high redundancy is required to achieve reliable reconciliation, leading to large matrix dimensions (on the order of 106) and a significant computational burden during decoding. This complexity negatively impacts the performance of the Belief Propagation (BP) algorithm and limits the real-time secret key rate, posing a major challenge to the scalability of CV-QKD systems. Consequently, the design of LDPC code structures optimized for low-SNR and efficient hardware implementation is essential for advancing practical CV-QKD deployments.

This paper aims to provide an overview of the most relevant results and recent advancements in the field of CV-QKD systems, with a focus on LDPC code methods applied to IR techniques.

The structure of this paper presents the fundamentals of CV-QKD and reconciliation techniques; it describes LDPC codes and quasi-cyclic construction; it approaches about LDPC codes specifically designed for CV-QKD, including MET-LDPC codes and enonder/decoder architectures; it reviews practical applications and performance results; and concludes the paper with final remarks.

Received on 13 February 2026; revised 22 April 2026.

Address for correspondence: Mauro Queiroz Nooblath Netoa. Av. Orlando Gomes, 1845, Piatã. Zipcode: 40850-610 Salvador, Bahia, Brazil. E-mail: mauro.neto@fieb.org.br
.

J Bioeng. Tech. Health 2026;9(5):376-382

CV-QKD and Reconciliation

CV-QKD is a promising branch of quantum cryptography protocols, where information is encoded in the quadratures of coherent states of light, allowing the use of conventional optical receivers [1]. In contrast to discrete variable QKD (DV-QKD) protocols, the CV-QKD approach offers greater compatibility with current optical infrastructures, such as fiber-optic networks and integrated photonic components [2].

During the quantum stage of the protocol, the transmiter (Alice) sends to the receiver (Bob) a sequence of coherent states whose amplitudes are modulated according to a continuous Gaussian distribution. Bob, in turn, uses a detector (homodyne or heterodyne) to measure one or both quadratures of the received states. Due to the nature of the quantum channel, attenuation and noise effects, as well as possible eavesdropping (by Eve), the values obtained by Bob are only correlated with those sent by Alice, not identical [1].

To extract a common and secure key, an Information Reconciliation (IR) step is necessary, which consists of correcting errors between the correlated data using error-correcting codes. In long-distance CV-QKD, reconciliation must be performed efficiently even under extreme conditions, such as very low signal-to-noise ratios (SNR).

The reconciliation efficiency is expressed by a factor $\beta \in [0, 1]$, which represents how close the reconciliation process is to the ideal efficiency imposed by Shannon's limit. The higher the value of β, the higher the secret key generation rate, defined as Milicevic and colleagues defined [3]:

$$R_{key} = \beta I_{AB} - X_{BE} \quad (1)$$

where I_{AB} is the mutual information between Alice and Bob, and X_{BE} is the maximum information Eve can obtain about Bob's key. Therefore, the choice of reconciliation technique directly affects both security and practical viability. Among the existing techniques, the following, whose main characteristics are summarized in Table 1, stand out:

Slice Reconciliation: Maps continuous samples into multiple binary slices to apply binary codes at each layer [1].

Multilevel Coding / Multistage Decoding (MLC-MSD): It organizes bits into layers of decreasing reliability, applying codes with varying redundancy per level [1,4].

Multidimensional Reconciliation: It uses linear transformations, such as orthogonal rotations or Hadamard matrices, to maximize correlation efficiency between samples and enable the use of high-performance binary error-correcting codes [2,4,5]. Multidimensional reconciliation has become the most effective approach for low SNR regimes, such as those encountered in long-distance CV-QKD. This technique facilitates the use of efficient binary codes, such as LDPC, reducing the error rate (BER) and improving the key rate [1,2].

LDPC Codes

Low Density Parity Check (LDPC) codes are among the most promising strategies for

Table 1. Comparison of the main reconciliation techniques in CV-QKD.

Technique	Best for	SNR (dB)	Computational Complexity	Reconciliation Efficiency
Multidimensional	Long distances	Low (−20–0 dB)	High	High (≥ 95%)
MLC-MSD	Medium distances	Medium (−3–5 dB)	Medium	High (≥ 94%)
Slice Reconciliation	Short distances	High (> 5 dB)	Low	Medium (90–93%)

application in the Information Reconciliation (IR) stage, as they enable performance close to the Shannon limit and are widely employed in noisy communication systems. The parity-check matrix H can be represented by a bipartite graph known as Tanner graph, denoted by $\mathscr{G}$, composed of two sets of nodes: the variable nodes V_j, associated with the columns of the parity-check matrix, and the check nodes C_i, corresponding to the rows of matrix [6]. A connection between a variable node j and a check node i is established when the element $H(i,j) = 1$, indicating the existence of an edge between these nodes (Figure 1).

The number of edges connected to the vertices of $\mathscr{G}$ is referred to as the vertex degree. Its distribution is defined by a pair of polynomials, $\lambda(x) = \sum_i \lambda_i x^i$ and $\rho(x) = \sum_i \rho_i x^i$, where λ_i and ρ_i respectively denote the fraction of variable and check nodes of degree i in the Tanner graph $\mathscr{G}$ [6].

Quasi-Cyclic LDPC

The LDPC Quasi-cyclic codes (QC-LDPC) represents a structured LDPC code class, in which the parity-check matrix H is built from circulant blocks. In other words, permutations of the identity matrix are made from a base matrix B that indicates the number of rotations applied to each identity matrix. This structure allows a compact representation, facilitating efficient hardware implementation and significantly reducing the computational cost of encoding and decoding, which is essential for CV-QKD systems with large block sizes.

The matrix H can be represented by the base matrix B of dimensions $m_b \times n_b$, whose elements $b_{i,j} \in -1, 0, 1, 2,..., Q-1$ indicate the shift applied to an identity matrix of dimensions $Q \times Q$. Thus, the value -1 denotes a null block ($Q \times Q$ matrix of zeros), and the other values represent the number of positions in which the identity matrix should be circularly shifted to form the corresponding set [7].

This model allows the generation of large matrices using only the base matrix and the parameter Q, making QC-LDPC a highly scalable alternative. Moreover, the quasi-cyclic structure preserves the sparsity of the parity-check matrix, which is crucial for the good performance of the decoding algorithm.

Another advantage of the QC structure is its systematic encoding process based on the base matrix. The techinique involves generating the code-word divided into Q sized sets, replacing matrix multiplication operations by circular shifts (a characteristic of multiplication by a rotated identity matrix) [7].

LDPC Codes for CV-QKD

In the IR stage of CV-QKD systems, error correction is essential to ensure key agreement between Alice and Bob, given that quantum signals are highly susceptible to noise due to the low signal-to-noise ratio (SNR) of the channel [1]. LDPC codes are widely employed in this phase, and for scenarios involving extremely low SNR, new design approaches for these codes are

Figure 1. Tanner graph and its corresponding binary parity-check matrix.

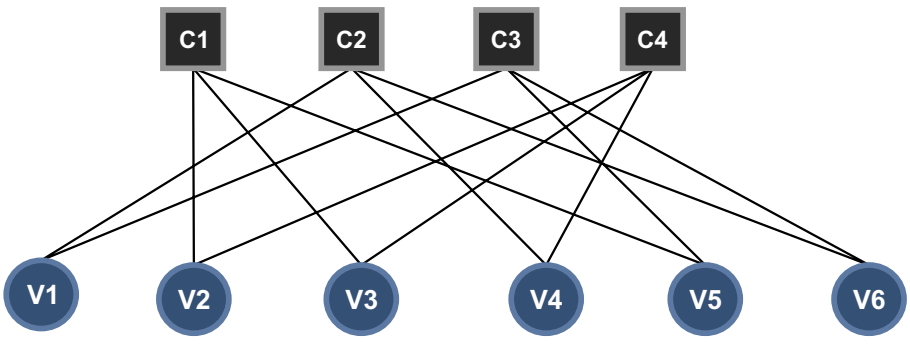

$$H = \begin{bmatrix} 0 & 1 & 1 & 0 & 1 & 0 \\ 1 & 0 & 0 & 1 & 0 & 1 \\ 1 & 0 & 0 & 0 & 1 & 1 \\ 0 & 1 & 1 & 1 & 0 & 0 \end{bmatrix}$$

required. In this context, Multi-Edge Type LDPC (MET-LDPC) codes stand out for their flexibility in tuning the degree distributions through multiple edge types in the Tanner graph, enabling optimization for low-rate regimes and performance close to the Shannon limit [2,5]. When combined with Quasi-Cyclic (QC) constructions, these codes allow for efficient implementations with reduced latency and computational complexity—features that are highly desirable for practical CV-QKD applications.

LDPC Multi-Edge Type

Multi-Edge Type LDPC (MET-LDPC) codes generalize both regular and irregular LDPC codes by introducing multiple edge types in the Tanner graph, allowing greater flexibility in defining the degree distributions of the nodes. This unified structure enables efficient modeling of codes with both uniform and non-uniform distributions, adapting them to varying channel conditions. A key advantage of MET-LDPC codes over conventional LDPC codes is their ability to achieve performance close to the Shannon limit, particularly in low-rate regimes such as Information Reconciliation (IR) in CV-QKD systems, where they operate robustly even under extremely low SNR conditions [8].

The formal description of a MET-LDPC code family is given by two multivariate polynomials:

$$\Omega(\vec{x}) = \sum_{d} \Omega_d \, x_1^{d_1} x_2^{d_2} \cdots x_t^{d_t} \tag{2}$$

$$\Psi(\vec{x}) = \sum_{d} \Psi_d \, x_1^{d_1} x_2^{d_2} \cdots x_t^{d_t} \tag{3}$$

where $\Omega(\vec{x})$ and $\Psi(\vec{x})$ describe the variable nodes and parity-check nodes, respectively. Unlike single-variable polynomials, as described in Section 1, these polynomials have multiple variables, each corresponding to a distinct edge type. The multivariate representation allows describing codes with t types of connections, characterized by degree vectors $[d_1, d_2, \ldots, d_t]$, where each component d_i indicates the number of sockets associated with edge type i. The coefficients Ω_d and Ψ_d thus denote the fractions of variable and check nodes exhibiting the corresponding connection profiles defined by the degree vector [8].

In Mani and colleagues [5], a MET-LDPC code is represented by the polynomials Ω and Ψ given by equations 4 and 5. These polynomials indicate that approximately 2.25% of the nodes have 2 sockets connected by edges of type 1 and 52 sockets connected by edges of type 2, with no sockets connected by edges of type 3, and so forth. Figure 2 illustrates the structure of the LDPC code family generated by these polynomials.

$$\Omega(r,\vec{x}) = 0.0225 r_1 x_1^2 x_2^{52} + 0.0175 r_1 x_1^3 x_2^{57} + 0.96 r_1 x_3 \tag{4}$$

Figure 2. Tanner graph corresponding to the MET-LDPC code specified by polynomials 4 and 5, with variable nodes depicted as circles and check nodes depicted as squares.

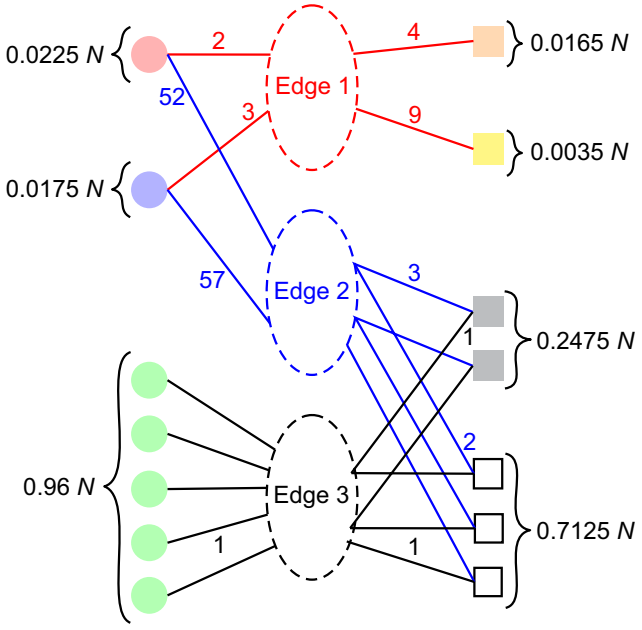

$$\Psi(\vec{x}) = 0.0165 x_1^4 + 0.0035 x_1^9 + 0.2475 x_2^3 x_3 + 0.7125 x_2^2 x_3 \tag{5}$$

Unlike the traditional Tanner graph, the structure of MET-LDPC codes features an additional layer of edge types, forming a cascaded architecture. In this configuration, the first edge type represents the irregular portion of the code, while the intermediate types connect this region to the final edges, which are in turn connected to

variable and check nodes with a single socket. This organization is crucial for error correction in very low SNR scenarios, ensuring improved decoding efficiency [5].

As described in Quasi-Cyclic LDPC, QC codes are defined by parity-check matrices constructed from a $q \times q$ array of cyclically shifted identity matrices and $q \times q$ zero matrices. The design of QC-MET-LDPC codes is performed by repeating the multi-edge random sampling process using a block length of $\frac{n}{q}$ instead of n to obtain a base Tanner graph $\mathscr{G}_B$. The base parity-check matrix HB is derived from $\mathscr{G}_B$ by replacing each nonzero element with a randomly chosen integer from the set $[0, q)$. The matrix H is then obtained from H_B by substituting each nonzero value i with an identity matrix I_i cyclically shifted by i positions [2].

Encoder and Decoder LDPC

Given a message $\vec{u}$ of length k, there are several ways to encode this message using a parity-check matrix H generated by an LDPC code of dimension $(n - k) \times (n)$. This encoding produces a code-word $\vec{c}$ of length n. Note that since $\vec{c}$ has length n, the encoding process essentially consists of adding redundancy of length $(n - k)$ to the message. Typically, this is achieved by constructing a generator matrix G from H. To obtain G, H is transformed into the standard systematic form H_{std} via a Gaussian elimination process, such that $H_{std} = [P|I]$, where P is the parity portion and I is an identity matrix. From H_{std}, the generator matrix is given by $G = [I|P^T]$, and G satisfies $GH_{std}^T = 0$. The codeword is then obtained as $\vec{c} = \vec{u}G^T$ [6].

In the decoding stage, the algorithm commonly used is Belief Propagation (BP), an iterative message-passing algorithm aimed at converging to a valid codeword $\vec{c}$ by updating probabilities between variable and check nodes over the Tanner graph. The most common variant of the BP algorithm is the Sum-Product algorithm. The scheme illustrated in Figure 3 details each step of this algorithm.

Figure 3. Steps of the Sum-Product Belief Propagation algorithm. (1) Message propagation from check nodes to variable nodes. (2) Backward message propagation from variable nodes to check nodes. (3) Estimates for the calculation of $\vec{c}$.

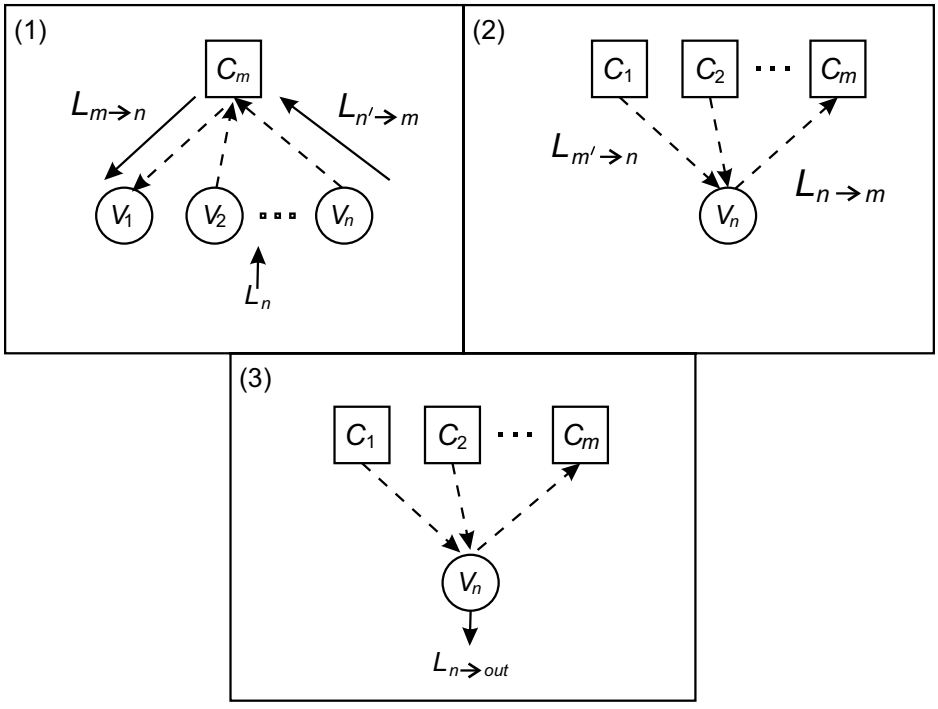

The decoding algorithm begins with step 1, in which the variable nodes receive the a priori log-likelihood ratios (LLRs) L_n from the BI-AWGN channel. Next, message passing is performed from the check nodes m to the variable nodes n, using the following equation:

$$L_{m\to n} = 2\text{arctanh}\left(\prod_{n'\in\mathcal{N}(m)\setminus n} \tanh\left(\frac{L_{n'\to m}}{2}\right)\right) \quad (6)$$

where $n' \in \mathcal{N}(m) \setminus n$ denotes the set of variable nodes connected to the check node m, excluding the node n that is currently receiving the message.

In step 2, message propagation occurs in the reverse direction, from check nodes to variable nodes. For each variable node n, the message sent to check node m is updated according to:

$$L_{n\to m} = L_n + \sum_{m'\in\mathcal{M}(n)\setminus m} L_{m'\to n}, \quad (7)$$

where $m' \in \mathcal{M}(n) \setminus m$ denotes the set of check nodes connected to the variable node n, excluding node m.

Step 3 corresponds to the generation of the initial estimate of the codeword after the first propagation iteration. For each variable node n, the output value is computed as

$$L_{n\to out} = L_n + \sum_{m'\in\mathcal{M}(n)} L_{m'\to n}, \quad (8)$$

and the hard decision of the corresponding bit estimation is carried out using the rule:

$$\hat{c}_n = \begin{cases} 0, & \text{if } L_{n\to\text{out}} > 0, \\ 1, & \text{otherwise.} \end{cases} \quad (9)$$

Practical Applications

Several studies have explored advanced methods to optimize the implementation of LDPC codes, aiming to maximize reconciliation efficiency, increase system throughput, and reduce the frame error rate in CV-QKD systems. Milicevic and colleagues [2] proposed the use of QC-MET-LDPC codes with a block length of 10^6 bits, enabling the reduction of decoding latency during key reconciliation over long distances. The GPU implementation demonstrated secret key generation rates of 4.10×10^{-7} bits per pulse for distances ranging from 100 km to 160 km, with throughput up to 8.03 times higher than the upper bound on secret key rate limit, effectively removing reconciliation as a bottleneck. Additionally, Mani and colleagues [5] extended the MLC-MSD scheme to reverse reconciliation in CV-QKD, identifying optimal coding rates over a wide range of SNRs (from –20 dB to 10 dB) and introducing G-EXIT charts as an analytical tool for evaluating MET-LDPC codes. The authors demonstrated asymptotic efficiencies exceeding 98% and highlighted the superior per formance of multidimensional reconciliation with d = 8 in extremely low SNR regimes. Finally, Jeong and colleagues [9] proposed a rate-compatible MET-LDPC coding scheme based on parity bit puncturing, enabling dynamic adaptation to channel quality using a single encoder/decoder pair. The scheme sig-nificantly reduces system complexity, eliminates the need for additional error-detection codes, and extends the usable SNR range by a factor of 1.44, with up to a 2.10-fold improvement in the secret key rate. This makes Information Reconciliation (IR) more efficient and robust for practical CV-QKD applications.

Conclusion

The research conducted led to the conclusion that MET-LDPC codes demonstrate superiority in extremely low SNRs, enabling the design of more efficient and adaptable reconciliation schemes under varying noise conditions. Concurrently, computational improvements of QC-LDPC solutions play a crucial role in reducing latency and increasing throughput, ensuring viable real-time implementations. These combined techniques, MET-QC-LDPC, can serve as a foundation for constructing codes applicable to various practical scenarios, including the optimization of IR in CV-

QKD systems operating at very low SNRs, thereby extending the range and efficiency of QKD on long-distance optical communications. Furthermore, the concept of adaptive rates may provide a solution for implementing robust CV-QKD systems.

Acknowlegement

This work was fully funded by the project LDPC Code Design for Information Reconciliation in CV-QKD Optimized for Hardware Implementation, supported by QuIIN – Quantum Industrial Innovation, the EMBRAPII CIMATEC Competence Center in Quantum Technologies. Financial resources were provided by the PPI IoT/Industry 4.0 program of the Brazilian Ministry of Science, Technology and Innovation (MCTI), under grant number 053/2023, in partnership with EM-BRAPII.

References

1. Yang S, Yan Z, Yang H, Wang Z, Liu Y, Wang X, et al. Information reconciliation of continuous-variable quantum key distribution: principles, implementations and applications. EPJ Quantum Technol. 2023;10(1):40.
2. Milicevic M, Feng C, Zhang LM, Kumar S, Elkouss D, Leverrier A, et al. Quasi-cyclic multi-edge LDPC codes for long-distance quantum cryptography. NPJ Quantum Inf. 2018;4(1):21.
3. Grosshans F, Grangier P. Continuous variable quantum cryptography using coherent states. Phys Rev Lett. 2002;88(5):057902.
4. Leverrier A, Alléaume R, Boutros J, Zémor G, Grangier P. Multidimensional reconciliation for a continuous-variable quantum key distribution. Phys Rev A. 2008;77(4):042325.
5. Mani H, Gehring T, Grabenweger P, Ömer B, Pacher C, Andersen UL. Multiedge-type low-density parity-check codes for continuous-variable quantum key distribution. Phys Rev A. 2021;103(6):062419.
6. Moon TK. Error correction coding: mathematical methods and algorithms. Hoboken: Wiley; 2005.
7. Ferreira Neto NA, Oliveira JRS, Oliveira WLA, Bittencourt JCN. VLSI architecture design and implementation of a LDPC encoder for the IEEE 802.22 WRAN standard. In: 2015 25th International Workshop on Power and Timing Modeling, Optimization and Simulation (PATMOS); 2015. p. 71-76.
8. Richardson T, Urbanke R. Multi-edge type LDPC codes. In: Proceedings of the IEEE International Symposium on Information Theory (ISIT); 2002.
9. Jeong S, Jung H, Ha J. Rate-compatible multi-edge type low-density parity-check code ensembles for continuous-variable quantum key distribution systems. NPJ Quantum Inf. 2022;8:6.

Automation of Patent Searches at INPI: A Web Scraping and Data Analysis Approach

João Alexandre Brito[1]*, Celso Barreto da Silva[2], Fabio Fonseca Barbosa Gomes[2]
[1]Startup Innovation Hub of SENAI CIMATEC University; [2]SENAI CIMATEC Uiversity, Postgraduation Department; Salvador, Bahia – Brazil

Patent searches are an essential step in technological development and innovation, but the traditional search process can be time-consuming and inefficient. This article presents PATENTIA, a system that automates patent searches at the National Institute of Industrial Property (INPI) using web scraping techniques and relational database data storage. The system allows the separation and analysis of patent data, presenting it in an organized way in a web interface developed with React and Node.js. In addition, the tool allows the export of results in Excel format, making it a useful resource for researchers, inventors, and companies. This study details the development of the tool, the challenges encountered, and the benefits of automation in the patent search process.
Keywords: Patent Search. Search Automation. Web Scraping. INPI. WIPO.

Patent research is a fundamental process for researchers, inventors, and companies seeking to assess the originality of an invention and ensure its legal protection. According to Souza and Almeida (2020) [1], access to information contained in patent databases is essential for the development of technological innovation. Similarly, Santos (2018) [2] emphasizes that the use of patent databases allows for strategic market and competitor monitoring. In Brazil, the main database for patent searches is the National Institute of Industrial Property (INPI), which provides information on patent applications and grants.

The traditional search process on the INPI [3] platform can be time-consuming and inefficient, requiring users to perform repetitive manual searches to obtain relevant information. As highlighted by Lima and colleagues (2019) [4], the large volume of data and the lack of advanced search tools hinder the analysis and extraction of relevant patent information. Oliveira and Mendes (2020) [5] point out that automating data collection and processing can significantly accelerate the retrieval of essential information.

Received on 12 February 2026; revised 18 April 2026.
Address for correspondence: João Alexandre Brito. SENAI CIMATEC University. Av. Orlando Gomes, 1845 - Piatã. Salvador, Bahia, Brazil Zipcode: 40650-010. E-mail: joao.brito@fieb.org.br.

J Bioeng. Tech. Health 2026;9(5):383-391

To address this issue, the present study proposes the automation of patent research through the tool PATENTIA. This solution is based on the use of web scraping—a technique for extracting data from the web—allowing for the automatic collection of information from INPI [3]. According to Silva and Ferreira (2021) [6], web scraping has been widely used to automate repetitive tasks involving large volumes of data, making previously slow processes more efficient. Likewise, Costa and Ribeiro (2022) [7] argue that the application of scraping techniques can drastically reduce the time spent collecting information from public databases.

PATENTIA aims to implement an intuitive web interface for patent searches, enabling users to perform queries, view organized information, and export results in Excel format for further analysis. According to Almeida (2021) [8], intuitive interfaces significantly enhance user efficiency when interacting with large data sets. Pereira (2020) [9] also emphasizes that visualization and data filtering tools allow for more objective and structured analyses, contributing to more assertive decision-making.

PATENTIA uses the Python programming language for automating the data collection process, Node.js for backend management, and the React language for the frontend, ensuring interactivity and usability of the system. According to Machado and Lopes (2022) [10], the combined

use of modern technologies such as Python and Node.js has enabled the creation of faster and more scalable solutions for information extraction and processing. Supporting this idea, Nogueira (2021) [11] argues that choosing frameworks like React provides more responsive and intuitive interfaces, enhancing the end-user experience.

In this context, the objective of this article is to present the development of the PATENTIA search tool, discuss the challenges of automating patent searches, and assess the impact of the tool on access to technological information available through INPI. The research is structured in sections detailing the methods used, the implementation of the tool, and the results obtained. As stated by Santos and Carvalho (2022) [12], the implementation of digital tools in patent knowledge management contributes to the optimization of industrial and academic processes. Thus, the PATENTIA solution represents an important step toward modernizing patent research in Brazil, as also emphasized by Vieira and Rocha (2023) [13], who highlight the positive impact of digitizing bureaucratic processes on research and technological innovation.

Theoretical Framework

Robotic Process Automation (RPA) emerges as an innovative solution for optimizing routine tasks, reducing human error, and increasing operational efficiency. According to Silva and colleagues (2023) [14], RPA enables companies to automate their most repetitive administrative processes, such as bill payments and report generation, freeing human resources for more strategic activities.

Furthermore, studies such as Freitas (2023) [15] highlight RPA's ability to integrate data from multiple systems, promoting a consolidated and reliable view of organizational processes. Thus, the application of RPA transcends sectors, being implemented in both corporate environments and governmental institutions, as emphasized by Souza and Almeida (2020) [1].

The databases of the National Institute of Industrial Property (INPI) and the World Intellectual Property Organization (WIPO) are fundamental sources of information for intellectual property analysis; however, they present challenges related to data volume and access complexity. The study by Silva and colleagues (2023) [14] points out that the INPI database is designed to support public queries but lacks advanced integration and visualization tools. Additionally, according to Santos and Carvalho (2023) [12], WIPO provides comprehensive patent classification and description resources, although the absence of automated processes still limits query efficiency. Integrating these databases with RPA technology, as advocated by Lima (2023) [16], can transform the user experience by enabling faster and more accurate access.

Data quality and reliability are critical factors for decision-making, especially in processes involving intellectual property. Silva and colleagues (2022) [14] emphasize that RPA application can mitigate errors caused by human intervention, promoting a more trustworthy data environment. Moreover, studies conducted by Costa (2023) [17] demonstrate that automation contributes to the validation and standardization of captured information, ensuring greater consistency. Finally, Oliveira (2023) [18] reinforces that the use of automated analysis tools significantly improves the accuracy and speed of data interpretation.

Data visualization is an essential element for understanding complex information, especially in scenarios involving large volumes of records. According to Freitas (2023) [15], interactive dashboards offer an efficient approach to presenting data, helping to identify patterns and relationships. Likewise, Santos and Carvalho (2023) [12] highlight that implementing graphical tools in intellectual property databases enables faster and more intuitive interpretation of results. Additionally, Lima (2023) [16] suggests that the use of visual elements, such as interactive maps, can enhance communication between different areas of an organization.

Data integration and time optimization are critical challenges that can be addressed through process automation. Costa (2023) [17] points out that using RPA for dynamic data querying provides a unified and centralized view, reducing information dispersion. Complementarily, the study by Oliveira (2023) [18] indicates that this centralization can reduce up to 40% of the time spent on manual queries. According to Santos e Carvalho (2023) [12], this agility enables greater focus on high-value activities, such as the strategic analysis of collected data.

Practical applications of RPA for intellectual property data analysis also include the possibility of creating search histories and pagination functionality, as demonstrated by Silva and colleagues (2023) [14]. These tools facilitate navigation through large volumes of records, allowing for quick retrieval of previously accessed information. Additionally, Santos e Carvalho (2023) [12] observe that search history promotes the reuse of data in future analyses, increasing productivity. Freitas (2023) [15] adds that proper pagination ensures a more efficient experience for the end user, eliminating performance bottlenecks during navigation.

These aspects, when integrated, provide a robust theoretical foundation for developing RPA-based solutions capable of significantly transforming how intellectual property databases are queried and analyzed. The combination of automation, efficient visualization, and data integration represents a significant advancement toward optimizing processes related to intellectual property.

Materials and Methods

The methodology employed in this study followed a structured scientific approach, encompassing essential steps to ensure the rigor, validity, and replicability of the results obtained during the development of the PATENTIA system. Initially, a systematic literature review was conducted to identify and understand the existing challenges in manual patent searches, providing a theoretical basis for the need for automation, as highlighted by authors such as Lima and colleagues (2019) [4] and Oliveira and Mendes (2020) [5].

The adopted scientific methodology included the clear formulation of the problem, definition of specific objectives, appropriate selection of technologies and tools, data collection and processing, implementation of the solution, execution of empirical tests and validations, as well as analysis and discussion of the results, as illustrated in Figure 1.

The development of the system was structured into the following methodological steps, as detailed in Figure 1:

Figure 1. Methodological diagram.

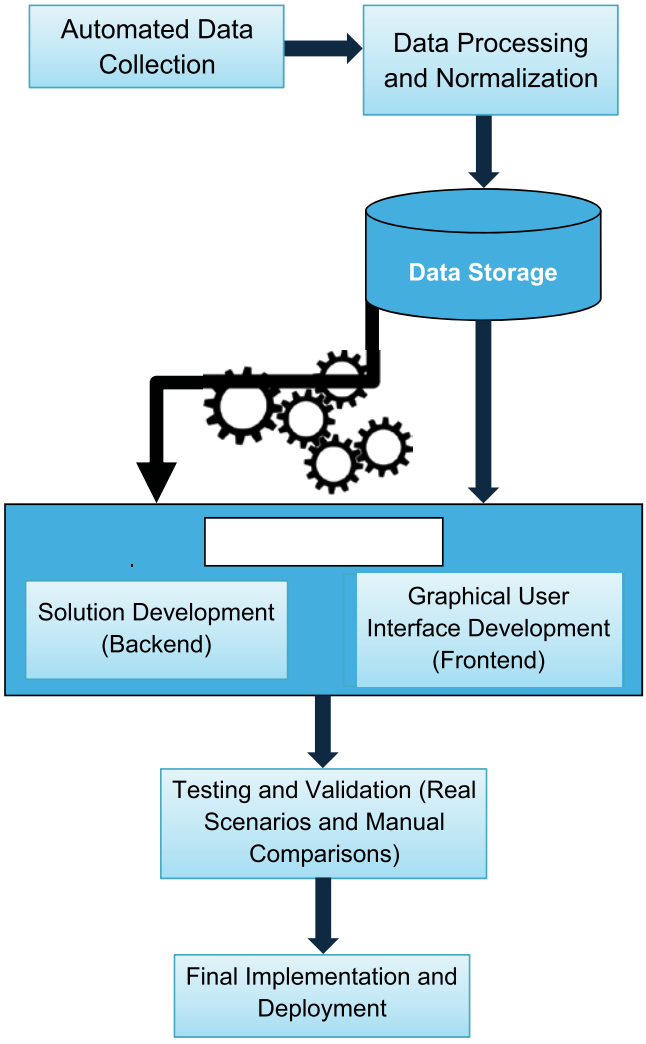

1. **Literature Review and Problem Definition:** Identification of issues and challenges related to manual patent searches through critical analysis of existing literature.
2. **Selection of Technologies and Tools:** Informed selection of modern and efficient technologies such as Python, Node.js, React, MySQL, Selenium, and Requests to meet the specific needs of the project.
3. **Automated Data Collection (Web Scraping):** Implementation of the Web Scraping technique using Python, Selenium, and Requests, ensuring robustness and efficiency in extracting data directly from the INPI database.
4. **Data Processing and Normalization:** Use of Python scripts to ensure the standardization, consistency, and quality of the collected data, eliminating duplicates and errors.
5. **Data Storage and Management:** Storage of processed data in a MySQL database, using Sequelize as the ORM framework to ensure performance and scalability.
6. **Backend and Frontend Development:** Construction of a robust and scalable platform with a backend developed in Node.js and an interactive frontend built with React, offering a user-friendly and functional interface.
7. **Testing and Validation:** Evaluation of the tool's accuracy and efficiency through empirical testing and systematic comparisons between manually and automatically obtained results.

What Problem Does This Project Solve

PATENTIA aims to address the limitations associated with manual patent searches within the database of the National Institute of Industrial Property (INPI). Currently, researchers and companies must manually access this database, perform repetitive queries, and extract information in an unstructured manner. According to INPI (2024) [3], conducting a patent search requires users to be familiar with classification codes and perform refined queries to obtain relevant results. Furthermore, Alvarez, Filgueiras, and Angeli (2023) [19] point out that identifying public domain patents in Brazil poses challenges due to the data structure and the need for repeated searches to locate specific information.

The PATENTIA system automates this process, enabling fast and accurate searches while organizing data in a user-friendly interface with export options to spreadsheets, making patent access and analysis significantly more effective.

According to Silva, Santos, and Silva (2021) [14], platforms such as Patentscope (WIPO), Espacenet (EPO), and BuscaWeb (INPI/BR) already offer free patent search tools, but the structure in which information is presented can still be improved to facilitate user analysis.

Comparative Analysis of Patent Databases

Patent searching is a crucial step in the process of innovation and technological development. Several databases are available to support researchers and companies in this task, each with specific features that can influence the efficiency and accuracy of the searches. Among the main patent databases are: Espacenet, Patentscope, Google Patents, Lens, Derwent Innovation Index, and Orbit Intelligence.

One of the main difficulties faced by users of these databases is the complexity involved in locating and interpreting the desired options and patents, as demonstrated in Figures 2 and 3 from the INPI database. This is partly due to the need for familiarity with specific classification codes and the requirement to conduct refined searches to obtain relevant results. Furthermore, patent descriptions may be ambiguous or generic, making the identification process more challenging. Alvarez and colleagues (2023) [19] emphasize that identifying public domain patents in Brazil faces difficulties due to the data structure and the need for repeated queries to find specific information.

Figure 2 presents the initial interface of the database provided by the National Institute of Industrial Property (INPI), which offers access to various categories related to industrial property,

such as trademarks, patents, industrial designs, geographical indications, computer programs, integrated circuit topographies, technology transfer, and patent-related technological information.

However, it is observed that this interface does not provide support elements or clear instructions to facilitate navigation and understanding for beginner or inexperienced users in intellectual property searches. This lack of guidance may hinder the research process, reinforcing the need for more intuitive and interactive alternative tools, such as the PATENTIA system.

Therefore, the standard INPI interface highlights the importance of solutions that enhance usability and accessibility, especially for audiences less familiar with the process of searching for and analyzing patents.

Figure 2. INPI database interface.

Source: Instituto Nacional de Propriedade Industrial (INPI) [3].

Figure 3. INPI database.

Source: Instituto Nacional de Propriedade Industrial (INPI) [3].

Each of the aforementioned databases has distinct features that can meet different user needs. For example, Espacenet, developed by the European Patent Office (EPO), offers free access to more than 90 million patent documents and is recognized for its user-friendly interface and comprehensive coverage (Figures 4, 5 and 6). Patentscope, maintained by the World Intellectual Property Organization (WIPO), also provides free access and includes advanced search functionalities, such as the ability to search for chemical sequences.

Google Patents integrates information from various databases and features a simplified interface, making it more accessible for less experienced users. Lens stands out by combining patent data with academic information, making it especially useful for research involving scientific innovation. On the other hand, Derwent Innovation

Figure 4. Interface of the ESPACENET database.

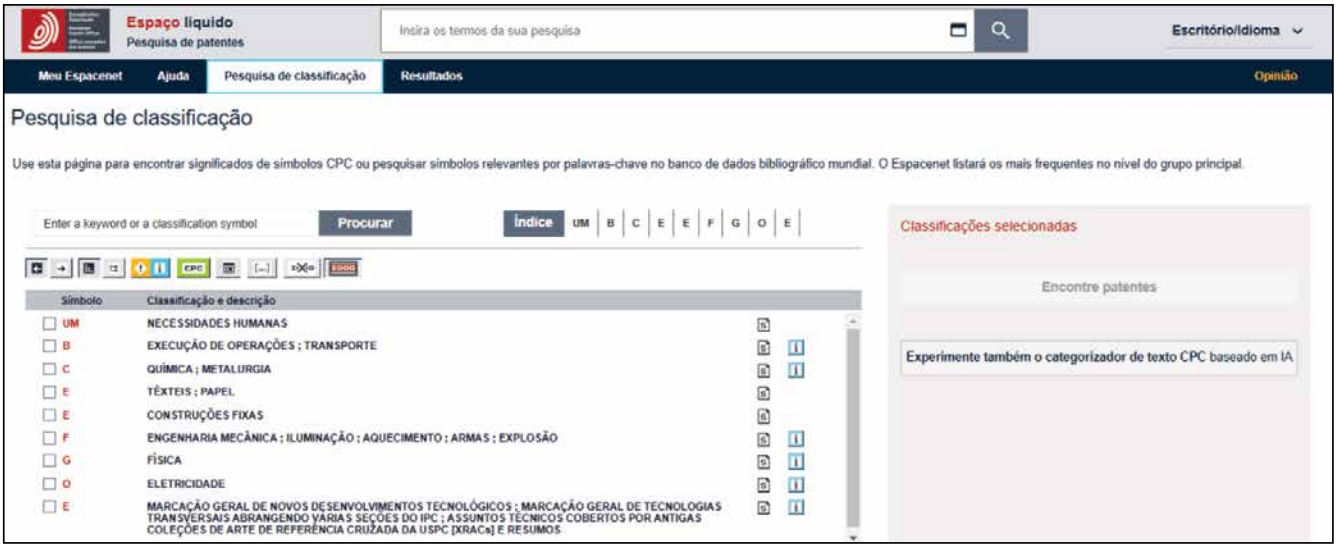

Source: ESPACENET (2025).

Figure 5. Classification-based search in the ESPACENETdatabase.

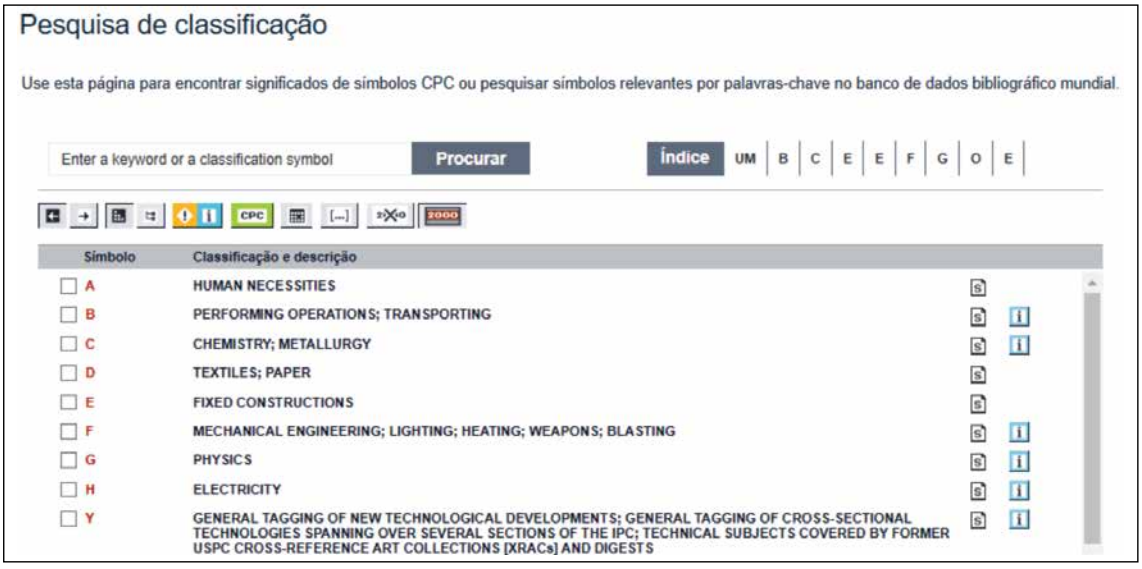

Figure 6. IPC code search in the ESPACENET database

Source: ESPACENET (2025).

Index and Orbit Intelligence are paid platforms that offer advanced data analysis and visualization tools. These platforms are widely used in corporate and academic environments for competitor monitoring and identifying technological partners.

Table 1 presents a comparison of the main features of these databases. The choice of the most suitable database will depend on the specific needs of the user, considering factors such as the depth of the research, available resources, and familiarity with the tools offered by each platform.

Results and Discussion

The implementation of the PATENTIA system enabled significant improvements in the process of patent search and data analysis. Among the main results observed, several stand out due to their impact on efficiency, accuracy, and usability. One of the key achievements was the standardization of the search process. The system ensures that every patent search follows the same structured steps, eliminating inconsistencies that may arise from manual searches. This uniformity contributes to greater reliability and repeatability of results, especially when dealing with large volumes of information.

Moreover, PATENTIA allowed an increase in the volume of data retrieved per search within a reduced time frame. Traditional patent queries often require manual access and filtering through multiple pages and parameters. With the automated web scraping and structured database integration, the system is capable of processing dozens of patent records in a fraction of the time previously required, significantly boosting productivity.

Another important result was the development of a timeline-based visualization for the retrieved data. Through a dynamic dashboard interface, users can visualize patent filings and trends across different time intervals. This feature enhances the strategic analysis of intellectual property landscapes, providing intuitive insights that support decision-making processes. The tool also features

Table 1. Comparison of the main patent database.

Database	Access	Coverage	Search Tools	Statistical Analysis
Espacenet	Free	Over 90 million patents	User-friendly interface, keyword search, and extensive classification; includes patent family analysis and global coverage	Limited
Patentscope	Free	International and national patents	Advanced search, including chemical sequences	Limited
Google Patents	Free	Integrates multiple databases	Simplified interface, keyword search	Limited
Lens	Free	Patents and academic literature	Keyword and classification search, integration with academic data	Moderate
Derwent Innovation Index	Paid	Extensive, with patent family analysis	Advanced search and analysis tools	Advanced
Orbit Intelligence	Paid	Comprehensive, with global coverage	Advanced tools for search, analysis, and data visualization	Advanced

an Excel export function, allowing users to generate spreadsheets with structured patent data. This makes it easier to conduct external analysis, share information with third parties, and incorporate the results into business or academic reports.

Furthermore, the system proved to be effective in reducing human error during the search and analysis stages. Manual searches are prone to data omissions, incorrect filtering, and transcription mistakes. By automating the entire pipeline—from data collection to presentation—PATENTIA minimizes these risks and ensures greater data integrity.

In addition to these main points, the architecture of PATENTIA, built using modern technologies such as Python, Node.js, and React, enabled the creation of a responsive and user-friendly interface, which proved to be a crucial element in improving the overall user experience.

Conclusion

This study presented the development and implementation of PATENTIA, a system designed to automate patent searches at the National Institute of Industrial Property (INPI) using web scraping techniques and modern web technologies. The solution addresses several inefficiencies associated with the traditional manual search process, offering a reliable, scalable, and user-friendly alternative for researchers, inventors, and organizations engaged in innovation.

The automation of the search process through standardized procedures ensures consistency and reduces dependency on user expertise, while significantly increasing the volume of data processed in less time. This improvement has a direct impact on productivity and strategic intelligence, particularly in R&D environments where timely access to information is essential for innovation and competitive advantage.

One of PATENTIA's most notable contributions is the transformation of complex and disorganized datasets into structured, easily interpretable information. The integration of a timeline-based visualization dashboard enables users to identify historical trends, monitor technological development, and anticipate market movements based on patent

activity. Additionally, the Excel export function enhances usability by enabling further analysis and data sharing across different platforms.

Another major impact of the system is the reduction of human error in data retrieval and processing. By automating repetitive and error-prone tasks, PATENTIA enhances the reliability of patent data and allows professionals to focus on higher-value activities, such as strategic planning and innovation design.

Furthermore, the project highlights the relevance of combining emerging technologies—such as Python for automation, React for intuitive user interfaces, and Node.js for backend processing—to create effective solutions for public data access. The modular and extensible architecture of PATENTIA also opens possibilities for future improvements, including integration with other patent databases (such as WIPO and EPO), implementation of AI-driven search optimization, and multilingual support.

In conclusion, PATENTIA represents a significant advancement in the way intellectual property data is accessed and used in Brazil. It offers not only technical innovation but also a strategic tool that democratizes access to patent information, promotes efficiency, and supports the broader goals of innovation and technological development. The solution has the potential to inspire further initiatives in digital transformation within the intellectual property domain, setting a new standard for transparency, accessibility, and intelligence in patent research.

References

1. Souza A, Almeida B. O acesso à informação em bases de patentes e seu impacto na inovação tecnológica. Rev Bras Inov. 2020;2:45-60.
2. Santos F. Monitoramento estratégico de mercado por meio da análise de patentes. Rev Est Propr Intelect. 2018;1:30-40.
3. Instituto Nacional da Propriedade Industrial (INPI). Guia prático para buscas de patentes. Rio de Janeiro: INPI; 2025. Available from: https://www.gov.br/inpi
4. Lima C, et al. Dificuldades de acesso a bases de dados de patentes: um estudo sobre o INPI. Cienc Tecnol. 2019;4:25-35.
5. Oliveira R, Mendes J. Automação e eficiência na coleta de dados de patentes. Rev Sist Intelig. 2020;2:50-65.
6. Silva D, Ferreira P. Aplicações de web scraping na recuperação de dados científicos. Rev Cienc Dados. 2021;3:60-75.
7. Costa T, Ribeiro A. Redução do tempo na coleta de dados em bases públicas através de scraping. Rev Tecnol Aplic. 2022;1:45-55.
8. Almeida S. Interface de usuário e eficiência na navegação de grandes volumes de dados. Rev Exp Usuário. 2021;2:75-85.
9. Pereira H. Ferramentas de visualização e filtragem de dados para análise estruturada. Inform Aplic. 2020;1:50-60.
10. Machado F, Lopes M. Tecnologias modernas na degradação e processamento de informações. Rev Bras Comput. 2022;2:85-95.
11. Nogueira G. Desenvolvimento de interfaces responsivas para visualização de dados. Interfaces Intelig. 2021;1:100-110.
12. Santos A, Carvalho L. Ferramentas digitais na gestão do conhecimento em patentes. Gest Conhecimento. 2022;3:115-125.
13. Vieira M, Rocha E. O impacto da digitalização nos processos burocráticos da inovação. Rev Bras Inov Tecnol. 2023;4:85-95.
14. Silva FM, Santos RA, Silva RC. Patentscope (WIPO), Espacenet (EPO), BuscaWeb (INPI/BR): ferramentas de busca de patentes gratuitas. Rev Tecnol Soc. 2021;17(41):125-139. Available from: https://periodicos.utfpr.edu.br/rts/article/view/14478
15. Freitas L. Dashboards interativos para visualização de dados complexos. Tecnol Visualização. 2023;3:77-89.
16. Lima C. Integração de RPA em bases públicas. Rev Bras Cienc Dados. 2023;4:90-103.
17. Costa R. Automação e confiabilidade em sistemas de propriedade intelectual. Rev Inov Digit. 2023;5:40-52.
18. Oliveira R. Padronização e validação de dados em sistemas automatizados. Rev Sist Intelig. 2023;3:50-65.
19. Alvarez LO, Filgueiras R, Angeli R. Desafios na identificação de patentes em domínio público no Brasil. Cad Prospec. 2023;16(4):1292-1308. Available from: https://www.revistas.ufba.br/index.php/nit/article/view/51958

A Proposal for Applying Bio-inspired Optimization Algorithms: A Comparative Study of Genetic Algorithms and Particle Swarm Optimization for Sensor Selection

Daniel do Carmo Silva Ribeiro[1]*, Henrique Nunes Teixeira[1], Tiago Menezes de Oliveira[1], Fillipe Valente Braz[2], Tiago Silva e Silva[2], Samara Maria Assunção de Souza[2]

[1]Federal University of Bahia, DEEC, Salvador, Bahia; [2]Federal University of Recôncavo da Bahia, CETENS,Feira de Santana, Bahia, Brazil

This paper presents an application proposal and a comparative study between two bio-inspired optimization algorithms: Genetic Algorithms (GA) and Particle Swarm Optimization (PSO). The main objective is to demonstrate the effectiveness of these algorithms in selecting a subset of sensors, aiming to minimize the variance of the collected data. Through the analysis of results from two distinct datasets, this work explores the convergence characteristics, final population distribution, and the profile of the sensors selected by each algorithm. The results indicate that while both algorithms are capable of finding satisfactory solutions, GA tends to achieve better optimization values (lower standard deviation), whereas PSO demonstrates faster convergence. This study contributes to the understanding of the capabilities and limitations of each approach in problems of feature selection and sensing systems optimization.

Keywords: Genetic Algorithms. Particle Swarm Optimization. Sensor Selection. Bio-inspired Optimization. Variance Analysis.

Abbreviations: GA, Genetic Algorithms. PSO, Particle Swarm Optimization.

Optimization is a fundamental field in various areas of science and engineering, seeking to find the best solutions for complex problems, often with a vast search space. In scenarios where traditional analytical methods prove to be unfeasible or inefficient, metaheuristics, inspired by natural phenomena, emerge as powerful alternatives. Among these, bio-inspired algorithms, which mimic biological and behavioral processes, have gained prominence due to their ability to handle non-linear, multimodal, and high-dimensional problems [1].

Among the most established metaheuristics for solving complex problems, Genetic Algorithms (GA) and Particle Swarm Optimization (PSO) stand out. GA emulates the evolutionary process and principles of genetics, exploring the search space through operators such as selection, crossover, and mutation to converge towards the fittest solutions [1]. In turn, PSO models the collective intelligence of flocks or swarms, where particles adjust their trajectories based on individual experience and the global knowledge of the swarm [1,2].

The robustness of these approaches makes them ideal for solving combinatorial optimization challenges, such as sensor selection. This problem consists of identifying an optimal subset from a larger set of sensors, aiming not only for system efficiency—through the reduction of costs, complexity, and energy consumption—but also for improving the quality and reliability of the acquired data [1,2]. Minimizing data variance, for example, is a frequently adopted optimality criterion, as a reduced standard deviation suggests greater consistency and precision in measurements [3,4].

In this context, the present article details an application and a comparative analysis of GA and PSO in the sensor selection problem for variance minimization. The study evaluates the advantages and disadvantages of each metaheuristic in terms of convergence speed, final solution quality, and the characteristics of the selected sensor subset.

The paper was organized in topics to explores the theoretical foundations of Genetic Algorithms and Particle Swarm Optimization, respectively; describes the research methodology and the datasets

Received on 23 January 2026; revised 30 March 2026.

Address for correspondence: Daniel do Carmo Silva Ribeiro Rua Sucupió, Residencial Betaville. Camaçari – BA, Brazil Bahia, Brazil. Zipcode: 42825-016. E-mail: pedro.souza@aln.senaicimatec.edu.br.

J Bioeng. Tech. Health 2026;9(5):392-402

used; presents and discusses the experimental results; and consolidates the conclusions, highlighting the main contributions of the study and pointing out directions for future research.

Original Contribution and Novelty

This work fills a gap by offering a comparative analysis focused on variance minimization for sensor selection, a critical aspect for data reliability not extensively covered in prior studies [1,3].

A key novelty is the detailed justification for algorithm parameters, enhancing reproducibility. Furthermore, a dedicated discussion on limitations and practical implications provides a holistic view often over-looked. The qualitative analysis of selected sensor profiles reveals distinct search strategies, offering unique insights for designing sensor systems.

Genetic Algorithms (GA)

Principles

Genetic Algorithms (GAs) are a class of optimization algorithms inspired by the principles of natural selection and biological genetics, as proposed by Charles Darwin. They operate on a population of candidate solutions (individuals), which evolve over generations through genetic operators such as selection, crossover, and mutation [1].

- **Initial Population:** The process begins with the creation of an initial population of individuals, usually generated randomly. Each individual represents a potential solution to the problem at hand [1].
- **Fitness Function:** A fitness function is used to evaluate the quality of each individual in the population. The higher the fitness, the better the solution [1].
- **Selection:** Individuals with higher fitness have a greater probability of being selected for reproduction, passing their characteristics on to the next generation. Common methods include roulette wheel selection and tournament selection, among others [1].
- **Crossover:** Two individuals (parents) are combined to generate new individuals (offspring) by exchanging genetic material. This allows for the recombination of features from good solutions [1].
- **Mutation:** Small, random changes are introduced into the genes of individuals. Mutation helps to maintain genetic diversity within the population and prevents the algorithm from getting stuck in local optima [1].
- **Replacement:** The new generation of individuals replaces the old population, and the process repeats for a predefined number of generations or until a stopping condition is met. Elitism is a strategy that ensures the best individual from the current generation survives to the next [1].

Applications

Genetic Algorithms are widely applied in a variety of fields due to their ability to explore complex search spaces and find optimal or near-optimal solutions for optimization, search, and learning problems [1]. Some notable applications include:

- **Optimization:** Solving combinatorial optimization problems (such as the Traveling Salesperson Problem), function optimization, engineering design, network and system optimization.
- **Machine Learning:** Feature selection, model parameter optimization (e.g., neural networks), rule learning.
- **Engineering:** Circuit design, industrial process optimization, route planning, resource allocation, and global localization of robots [1].
- **Finance:** Portfolio optimization, market forecasting.
- **Biology and Medicine:** DNA sequence analysis, drug discovery, modeling of biological systems.

Advantages and Disadvantages

Advantages

- **Robustness:** Ability to handle complex, non-linear problems with multiple local optima,

as demonstrated in challenging localization scenarios [1].
- **Implicit Parallelism:** They explore multiple regions of the search space simultaneously through their population [1].
- **No Reliance on Gradient Information:** They do not require the objective function to be differentiable or continuous.
- **Flexibility:** They can be applied to a wide variety of problems with few modifications.
- **Find Global Solutions:** They exhibit a good trade-off between computational cost and exploration/exploitation capabilities, tending to find global solutions [1].

Disadvantages

- **Computational Cost:** They can be computationally expensive, especially for large populations and many generations [1].
- **Parameter Definition:** The choice of parameters (population size, crossover and mutation rates) can be challenging and significantly impact performance [1].
- **Slow Convergence:** Although robust, they may take many generations to converge to the optimal solution.
- **Fine-Tuning:** They can be slow at fine-tuning the solution in the later stages of optimization.
- **Encoding:** The problem representation (the individual's encoding) can be complex for some types of problems.

Principles

Particle Swarm Optimization (PSO) is an optimization metaheuristic inspired by the social behavior of bird flocks or fish schools. Proposed by Kennedy and Eberhart in 1995 [5], PSO is a population-based algorithm where each candidate solution (particle) moves through the search space, adjusting its trajectory based on its own experience (personal best position) and the experience of the swarm (global best position) [1,2].

- **Particles:** Each particle represents a potential solution in the search space and has a position and a velocity [2].
- **Personal Best Position (pBest):** Each particle keeps a record of the best position it has ever reached in the search space, along with its corresponding fitness value [1,2].
- **Global Best Position (gBest):** The swarm as a whole keeps a record of the best position found by any particle in the swarm, along with its corresponding fitness value [1,2].
- **Velocity and Position Update:** The velocity of each particle is updated based on three components: its inertia (previous velocity), the cognitive component (attraction to its personal best position), and the social component (attraction to the global best position). The new position of the particle is then calculated by adding the velocity to the current position [1,2].

Applications

PSO is known for its simplicity of implementation and its effectiveness on a variety of optimization problems, especially in continuous domains. Its applications include:
- **Function Optimization:** Finding the minima or maxima of non-linear mathematical functions [1].
- **Engineering:** Control system design, antenna optimization, route planning, resource allocation, and global localization of robots [1,2].
- **Signal Processing:** Adaptive filtering, pattern recognition.
- **Machine Learning:** Training neural network weights, feature selection, model parameter tuning, and in particle filters for robot localization [2].
- **Finance:** Portfolio optimization.

Advantages and Disadvantages

Advantages

- **Simplicity:** Easy to understand and implement, with few parameters to adjust.

- **Computational Efficiency:** Generally faster than other evolutionary algorithms for certain types of problems, reducing the number of particles needed compared to approaches like particle filters [2].
- **No Reliance on Gradient Information:** Like GAs, they do not require the objective function to be differentiable.
- **Good Exploration Capability:** Exhibits a good trade-off between computational cost and exploration/exploitation capabilities [1].

Disadvantages

- **Premature Convergence:** Tendency to converge prematurely to local optima in complex and multi-modal problems.
- **Parameter Sensitivity:** Performance can be sensitive to the choice of parameters (inertia weight, cognitive and social coefficients).
- **Difficulty with Discrete Problems:** Originally designed for continuous problems, it may underperform on discrete problems without specific adaptations.
- **Fine-Tuning:** It can have difficulty fine-tuning the solution in the later stages of optimization, and its precision may be limited without additional techniques [2].

Materials and Methods

We employed a methodology for the application and comparison of Genetic Algorithms (GA) and Particle Swarm Optimization (PSO) to the sensor selection problem. The main objective is to identify a subset of sensors that minimizes the variance of the collected data, ensuring the consistency and quality of the measurements.

Problem Definition

The problem addressed consists of selecting a fixed number of sensors from a larger set in order to optimize a specific metric. In this study, the optimization metric is the minimization of the variance of the data collected by the selected sensors. Variance is a measure of the dispersion of data around the mean; therefore, a lower variance value indicates greater homogeneity and reliability in the sensor readings.

Formally, given a set of N sensors and a desired number of K sensors to be selected ($K < N$), the problem is to find the subset of K sensors such that the variance of the data collected by these K sensors is the smallest possible. The objective function (or fitness function, in the context of bio-inspired algorithms) is defined as the negative of the variance, since optimization algorithms generally seek to maximize fitness. Thus, maximizing the negative of the variance is equivalent to minimizing the variance. This type of optimization problem is common in various areas of robotics and autonomous systems, where localization and sensing are crucial.

Datasets

For the evaluation of the algorithms, two real-world datasets from sensor readings were used. The files, named `scan.csv` and `scan(1).csv`, contain multiple columns, of which only those prefixed with `ranges_` were considered. Each column that follows the `ranges_*` pattern represents the readings of a specific sensor over time. The use of two distinct datasets allowed for the evaluation of the robustness and generalization of each algorithm's performance in different scenarios.

Algorithm Configuration

Genetic Algorithm (GA)

The GA was configured based on literature recommendations and preliminary tests. A population of 50 individuals evolved over 100 generations, a setup that balanced diversity and computational cost, ensuring convergence without excessive processing. A mutation rate of 0.1 was chosen to maintain genetic variability and prevent

premature convergence to local optima. The number of sensors to select was fixed at 10, as per the problem definition.

Particle Swarm Optimization (PSO)

The PSO was configured with 30 particles and 50 generations, leveraging its known rapid convergence. This setup proved sufficient for reaching stable solutions efficiently. The inertia weight (w=0.5) balanced exploration and exploitation, while cognitive (c1=1.5) and social (c2=1.5) coefficients were set to equally weigh individual and collective knowledge, fostering a robust search. The number of sensors to select was also 10.

Evaluation Metrics

To compare the performance of the algorithms, the following metrics and analyses were used:

- **Convergence of the Best Standard Deviation:** Convergence plots were generated to visualize how the best standard deviation (lowest variance) evolves over the generations for each algorithm and dataset. This allows for the analysis of the optimization's speed and stability.
- **Distribution of Standard Deviation in the Final Population/Swarm:** Box plots were used to analyze the distribution of standard deviation values of the solutions in the final population (GA) or final swarm (PSO). This provides insights into the diversity and quality of the solutions found.
- **Sensor Profile of the Best Solution:** Sensor profile plots were generated to visualize the average readings of the sensors selected by the best solution found by each algorithm. This helps to understand which sensors were considered most relevant for minimizing variance and how their readings behave.

Through this methodology, the aim is to provide a comprehensive and comparative analysis of the performance of GA and PSO in optimizing sensor selection, contributing to the choice of the most suitable approach in different application contexts.

Results and Discussion

This section presents and discusses the results obtained from the application of the Genetic Algorithm (GA) and Particle Swarm Optimization (PSO). The analysis focuses on the convergence of the algorithms, the fitness distribution of the final solutions, and the profile of the selected sensors. Two distinct datasets were used, hereafter referred to as Dataset A (`scan_2019-05-07-17-40-30`) and Dataset B (`scan_2019-05-07-15-54-45`), providing a basis for comparing their performances.

Convergence Analysis

The convergence graphs (Figures 1 to 4) illustrate the evolution of the best standard deviation value found by each algorithm over the generations. For Dataset A, the GA demonstrated a reduction in standard deviation from approximately 2.27 to 2.03 over 100 generations, showing a gradual and stable convergence. Similarly, for Dataset B, the GA converged from 2.22 to 1.97. In both cases, the GA's convergence curve exhibits discrete steps, indicating significant improvements in certain generations, followed by periods of stabilization.

In contrast, the PSO, executed for 50 generations, demonstrated faster convergence. For Dataset A, the standard deviation was reduced from 2.30 to 2.14. In the case of Dataset B, the convergence was from 2.23 to 2.15. The convergence speed of PSO is a notable characteristic, attributed to its nature of a guided search by the swarm's global best experience. However, it is observed that, despite the accelerated convergence, the GA achieved slightly lower standard deviation values, suggesting a superior ability to find higher-quality solutions in terms of variance minimization, given a larger number of iterations.

Figure 1. Convergence history of the best standard deviation for GA (Dataset A).

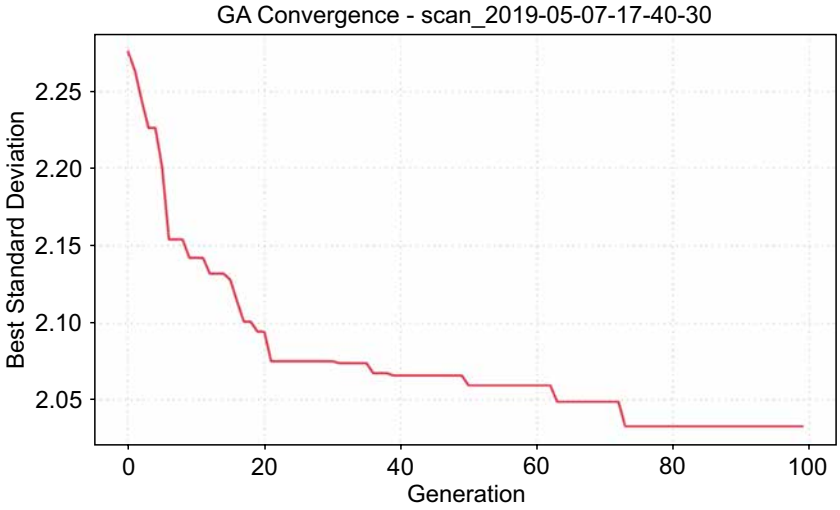

Figure 2. Convergence history of the best standard deviation for GA (Dataset B).

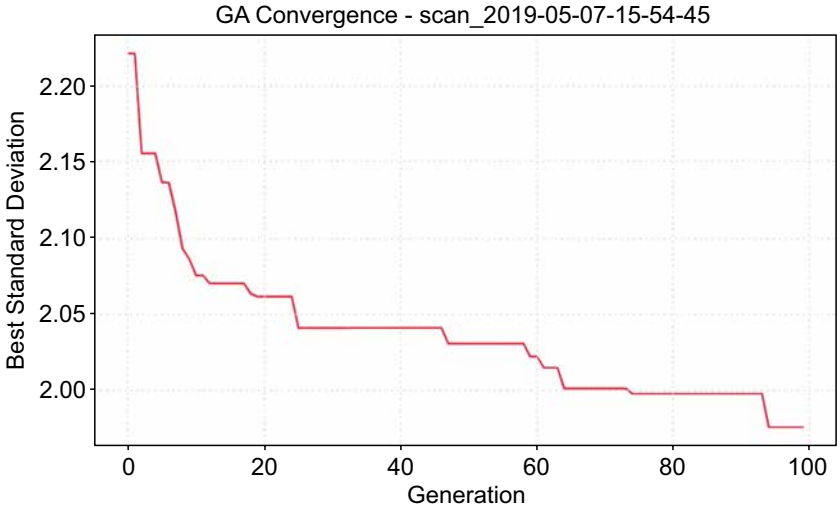

Figure 3. Convergence history of the best standard deviation for for PSO (Dataset A).

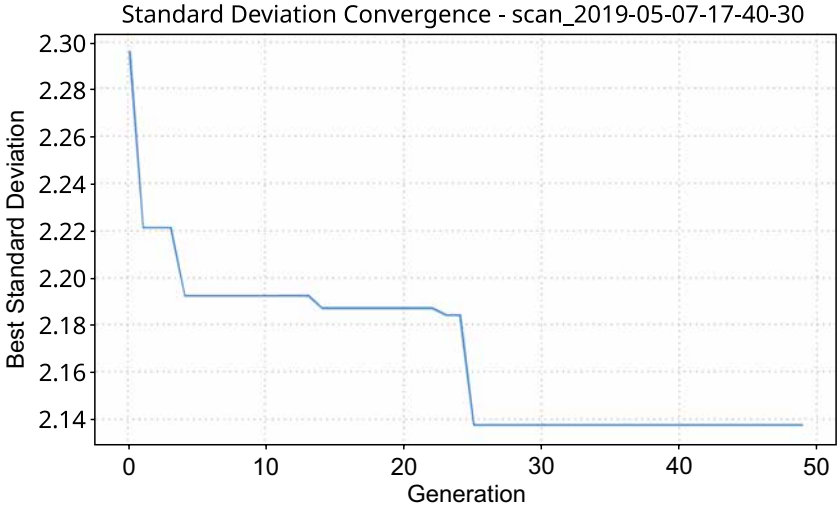

Figure 4. Convergence history of the best standard deviation for for PSO (Dataset B).

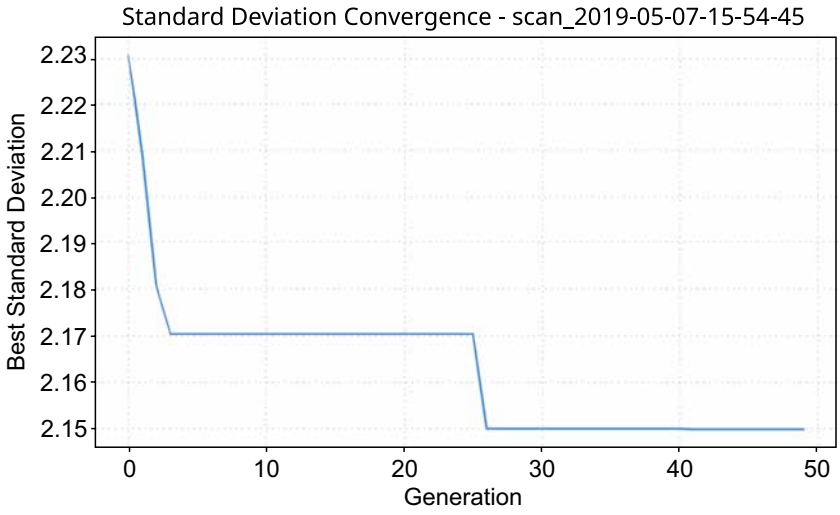

Limitations and Practical Implications

This study has limitations, including parameter sensitivity and the use of a single optimization metric (variance). The scalability to larger sensor networks was not exhaustively tested. The sensor selection was static, whereas dynamic environments might require adaptive strategies.

Practically, the results guide algorithm choice: GA is preferable for applications prioritizing data quality, while PSO excels when rapid solutions are critical. This work demonstrates that sensor subset selection can optimize resources (cost, energy) and improve data reliability, offering a foundation for advanced, adaptive sensing systems.

Fitness Distribution in the Final Popula-tion/Swarm

The box plots (Figures 5 to 8) provide a view of the distribution of standard deviation values of the solutions in the final population (GA) and the final swarm (PSO). For the GA, in Dataset A, most solutions had a standard deviation concentrated between 2.15 and 2.20, with an outlier at 2.30. In Dataset B, the distribution was slightly wider, ranging between 2.15 and 2.25.

For PSO, the standard deviation distribution in the final swarm for Dataset A was concentrated between 2.35 and 2.42. In Dataset B, the distribution varied between 2.32 and 2.40, with an outlier at 2.52. The analysis of the plots reve-als that both algorithms generated outliers, but the GA, in general, produced solutions with a lower average standard deviation and a more compact distribution, indicating gre-ater consistency in solution quality. The PSO, on the other hand, showed a distribution at slightly higher values and, in some cases, which might indicate greater diversity in the swarm, but also less convergence to high-quality solutions across all particles.

Selected Sensor Profile

The sensor profile graphs (Figures 9 to12) illustrate the indices of the sensors selected by the best solution of each algorithm, as well as their respective average readings.

For the GA, in Dataset A, the selected sensors were: `110, 177, 180, 181, 202, 209, 222, 223, 224, 225`. In Dataset B, the chosen sensors were: `149, 175, 183, 188, 190, 191, 194, 196, 208, 210`.

We observed that the GA tended to select sensors with numerically close indices, suggesting that the optimization sought a cohesive set to minimize the variance of the readings.

For the PSO, in Dataset A, the selected sensors were: `64, 80, 101, 116, 118, 163, 165, 168, 182, 194`. In Dataset B, the sensors were: `156, 159, 182, 195, 197, 216, 284, 323, 388, 431`.

Figure 5. Box-plot of the standard deviation distribution in the final population for GA (Dataset A).

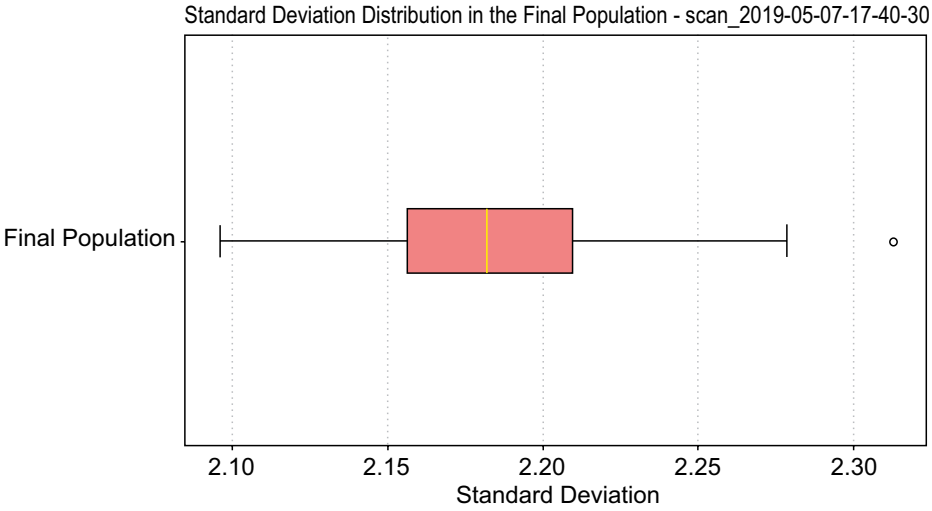

Figure 6. Box-plot of the standard deviation distribution in the final population for GA (Dataset B).

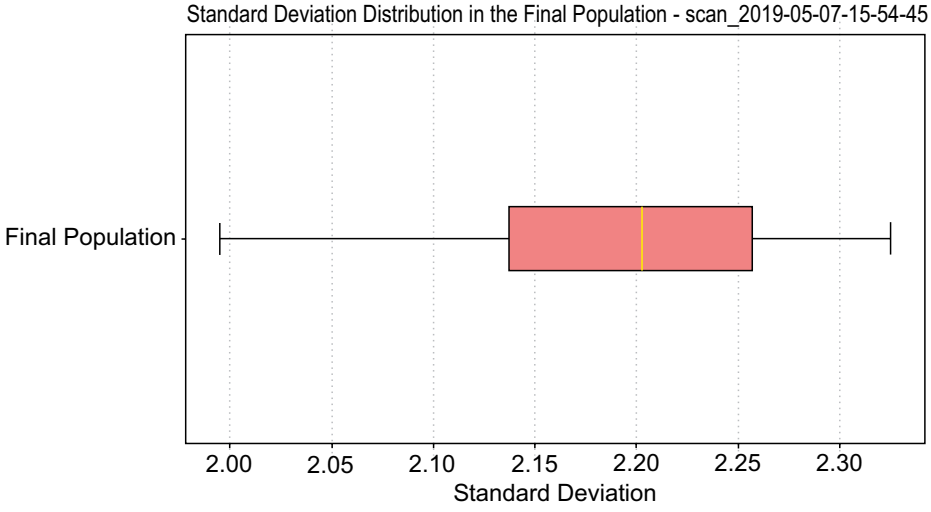

Figure 7. Box-plot of the standard deviation distribution in the final population for PSO (Dataset A).

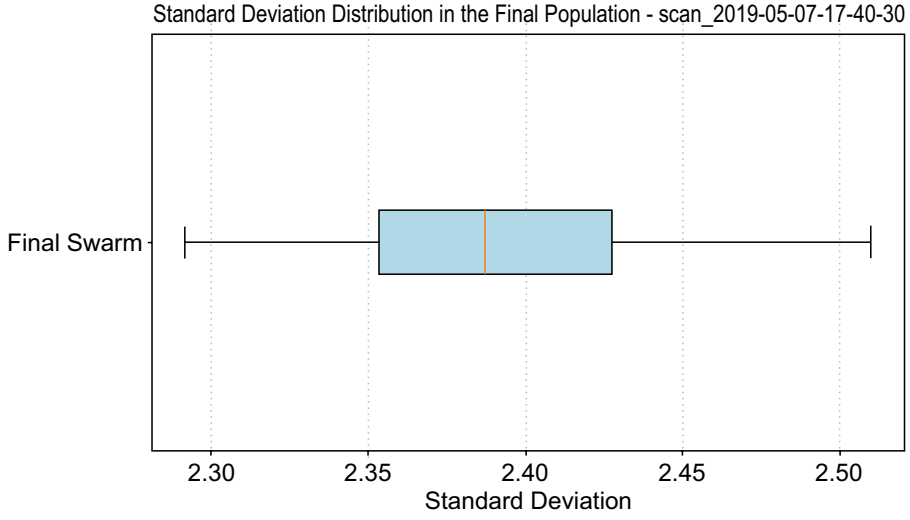

Figure 8. Box-plot of the standard deviation distribution in the final population for PSO (Dataset B).

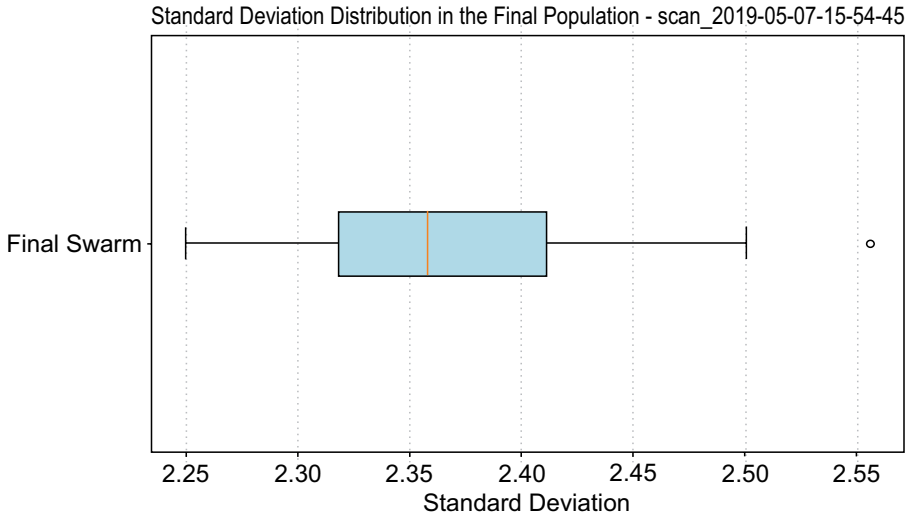

Figure 9. Sensor profile of the best solution for GA (Dataset A).

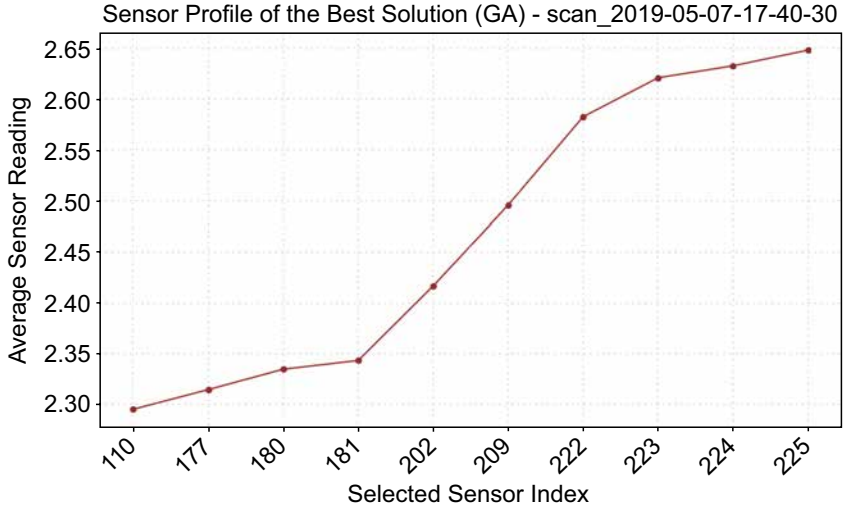

Figure 10. Sensor profile of the best solution for GA (Dataset B).

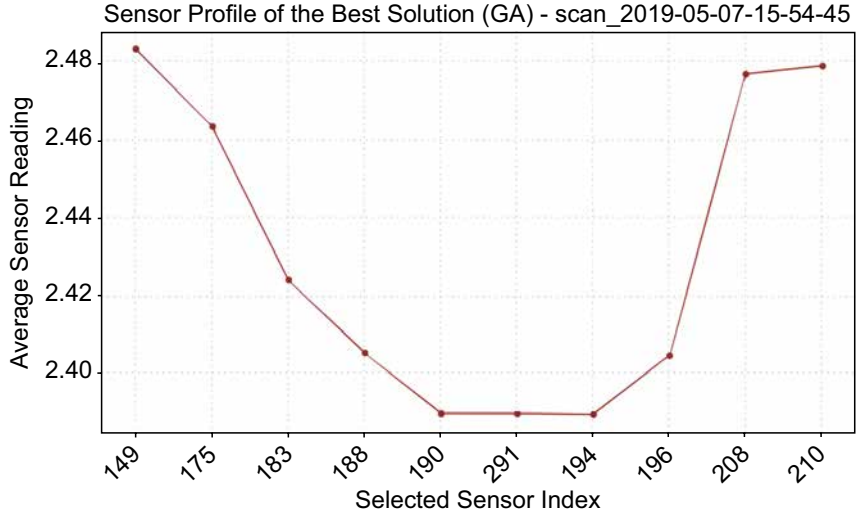

Figure 11. Sensor profile of the best solution for PSO (Dataset A).

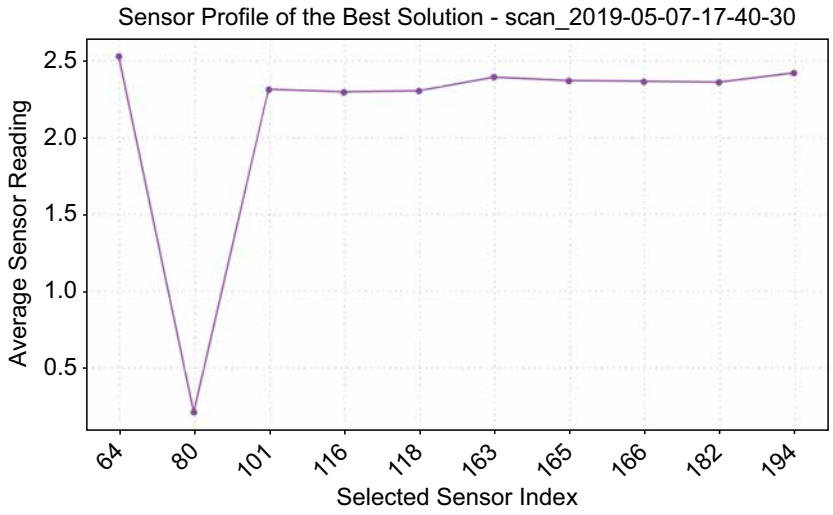

Figure 12. Sensor profile of the best solution for PSO (Dataset B).

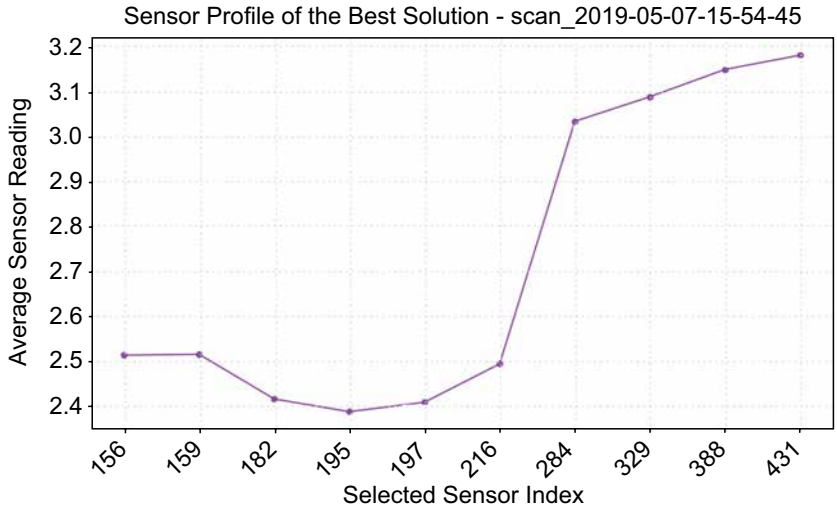

Unlike the GA, the PSO selected sensors with more scatte-red indices in the search space. This may indicate a broader exploration, but it does not necessarily result in a cluster of sensors with homogeneous characteristics, which is the objective of variance minimization.

Overall Comparison

In terms of performance, the GA demonstrated a superior ability to find solutions with a lower standard deviation, resulting in a more effective optimization for the proposed problem. Its convergence, although slower, was more sta-ble and consistent. On the other hand, the PSO stood out for its convergence speed, reaching satisfactory solutions in a smaller number of generations. However, the quality of the PSO solutions, on average, was slightly inferior to that of the GA, and the fitness distribution of the final swarm was more dispersed.

The choice of the most suitable algorithm will depend on the specific requirements of the application. If the pri-ority is the quality of the solution and robustness in opti-mization, the GA may be more indicated. If convergence speed is a critical factor, PSO may be preferable, even if it implies a slightly less optimized solution. The

difference in the selected sensor profiles also suggests that each algo-rithm explores the search space differently, which can be an advantage in problems where solution diversity is desirable.

Conclusion

This work presented a comparative study between GA and PSO for sensor selection, focusing on data variance minimization. The results demonstrated that GA, despite slower convergence, achieved superior solutions with lower standard deviation, indicating greater effectiveness in opti-mizing data quality. PSO, on the other hand, excelled in convergence speed, quickly reaching satisfactory solutions, though of slightly lower quality.

The analysis of sensor profiles revealed distinct selec-tion patterns: GA favored cohesive sensor clusters, while PSO selected more dispersed sensors, reflecting different search strategies. This trade-off between solution quality (GA) and convergence speed (PSO) is a key takeaway. The choice of algorithm should depend on application-specific needs: prioritize optimality with GA or rapid deployment with PSO.

Future work could explore hybrid approaches combi-ning the strengths of both algorithms and investigate their application in dynamic environments with multi-objective optimization criteria.

References

1. Carvalho JLC, Farias PCMA, Simas Filho EF. Global localization of unmanned ground vehicles using swarm intelligence and evolutionary algorithms. J Intell Robot Syst. 2023;107:45. doi:10.1007/s10846-023-01813-6.
2. Zhang Q, Wang P, Bao P, Chen Z. Mobile robot global localization using particle swarm optimization with a 2D range scan. In: Proceedings of the 2017 International Conference on Robotics and Automation; 2017. doi:10.1145/3175603.3175618.
3. Sobreira H, Costa CM, Sousa I, Rocha L, Lima J, Farias PCMA, et al. Map-matching algorithms for robot self-localization: a comparison between perfect match, iterative closest point and normal distributions transform. J Intell Robot Syst. 2020;93:533-546. doi:10.1007/s10846-017-0765-5.
4. Menines MS, Entringer AMM, Silva LA, Sá FB, Izabel VH, Vassallo RF. Detection and localization of mobile robots in intelligent spaces using artificial neural networks. [Publication details unavailable].
5. Kennedy J, Eberhart R. Particle swarm optimization, Proceedings of ICNN'95 - International Conference on Neural Networks, Perth, WA, Australia, 1995, pp. 1942-1948 vol.4, doi: 10.1109/ICNN.1995.488968.

Data Acquisition and Communication in CNC Machine Tools for PdM

Marcus Vinicius Ramos Figueiredo[1]*, Arthur Adriano Mendes Machado[2], Herman Augusto Lepikson[1,2]
[1]Federal University of Bahia, Mechatronic Graduation Program; [2]SENAI CIMATEC University, Salvador, Bahia, Brazil

In addition to the traditional requirements of quality and productivity, new production paradigms also demand fault prognosis and diagnosis capabilities that classical maintenance methods do not provide. In this scenario, the application of predictive maintenance emerges as a viable alternative. Predictive maintenance is a technique that uses monitoring systems to analyze the condition of assets, based on data collected from sensors, to prevent or avoid failures. By estimating the future condition of machine components, maintenance costs can be reduced, operating time can be increased, and maintenance tasks can be optimized. Despite these advantages, the technique is not yet widely adopted within the manufacturing sector because it requires sensing and data processing resources that make its implementation costly. To facilitate the implementation of this technique in the manufacturing sector, a low-cost hardware for data acquisition was proposed. Based on the system's components, an architecture for communicating the collected data and an application model were proposed, which allow for the visualization of this data and serve as a basis for implementing predictive algorithms for fault detection and anomaly prediction. After implementation on a demonstration machine, the system is expected to be capable of collecting machine data in real-time, enabling the identification of faults and anomalies, thereby reducing downtime and costs. This adds benefits to various organizational levels, such as at the operational level, through the reduction of unplanned stops and increased safety. In the maintenance and process sector, it facilitates a transition from preventive to proactive methods. In terms of strategic results, it leads to the reduction of operational costs and an increase in the reliability and predictability of production.
Keywords: CNC Machine Tools. Predictive Maintenance. MQTT. Monitoring Systems.

The manufacturing industry represents a highly relevant sector for the economic development of many countries [1], becoming a target of research, development, and innovation (RDI) actions aimed at strengthening the competitiveness of both companies and countries in the segment. The incentive to adopt new technologies, along with new production demands, transforms traditional manufacturing into smart manufacturing, evolving from mass production to customized production [2,3].

Monostori and colleagues [3] explain that smart manufacturing is a paradigm that optimizes resource allocation, featuring real-time analysis, intelligence, refinement, and agile perception of the real-time status of the market and customers. This means that processes are constantly monitored by sensors and connected systems that apply artificial intelligence and machine learning algorithms to learn from the collected data, analyzing data in real-time, which enables the early detection of failures, the automatic adjustment of production parameters, and the continuous improvement of process and product quality control. In this way, smart manufacturing reduces waste, costs, and increases operational efficiency.

This new paradigm demands from production systems not only the traditional requirements of quality and productivity but also requirements for fault prognosis and diagnosis. In this context, traditional maintenance processes become insufficient as they are not capable of detecting failures in advance, thus favoring the application of predictive maintenance.

Predictive maintenance (PdM) uses condition-based monitoring systems that identify significant fluctuations and variations in variables and signals based on sensor data, to prevent or avoid failures [4]. This means that the future behavior/condition of machine components can be approximated, which will help to optimize maintenance tasks [5]

Received on 11 February 2026; revised 27 April 2026.
Address for correspondence: Marcus Vinicius Ramos Figueiredo.Av. Milton Santos, s/nº - Ondina. Salvador, Bahia, Brazil. Zipcode: 40170-110. E-mail: mvictim7@gmail.com.

J Bioeng. Tech. Health 2026;9(5):403-409

that can be performed before failures occur, during periods of inactivity, or lower equipment demand.

Therefore, the implementation of PdM is a vital requirement for the manufacturing sector, where increasing productivity and product quality are constant objectives. These advantages can be of great value for an important piece of manufacturing equipment, the CNC machine tool

Dependent on the CNC's operational conditions, the production rate and the quality of processed products are directly affected by improvements in the machine's operational conditions. Thus, increasing the reliability of this equipment can bring great benefits to the sector.

However, despite its advantages, the manufacturing industry has been discouraged from implementing such maintenance practices due to the high associated investment. Predictive maintenance requires additional expenses, such as sensors and the development of computational algorithms for data analysis [6]. To facilitate the implementation of PdM in the manufacturing sector, a low-cost hardware for data acquisition, a communication architecture for the collected data, and an application model for analyzing this data will be proposed.

This work is organized as follows: This section presented an introduction addressing the context, the problem description, the research objectives, and a justification for the topic's relevance. The second section will describe the components and procedures used for the construction of the hardware, propose a communication architecture model for integration between the hardware's constituent devices, and an application model for processing and visualizing the collected data. The third section will discuss the expected results from the method's implementation. Finally, the fourth section will provide final considerations on the method's implementation and the next steps.

Materials and Methods

To develop the proposed method, the critical components to be monitored were first identified through a literature review. These include: the condition of the machining tool, as monitored by Hesser and Bernd, [7], Goodall and colleagues [8], Zhu [9], or Qianzhe and colleagues [2], and Ramírez and colleagues [10]. The spindle bearing, by Lee and colleagues [5], and Thoppil and colleagues [11]. The servomotors for the x and z axes, the ball screw bearing, the turret, the spindle, and the coolant, by Thoppil and colleagues [11]. The model was proposed for a ROMI Discovery 4022 vertical machining center, shown in Figure 1.

Figure 1. ROMI Discovery 4022 vertical machining center.

For the equipment in question, the tool, the spindle, and the spindle motor will be monitored. Based on the components to be monitored, the sensors could be defined and a hardware for monitoring could be proposed. Based on the elements that constitute the system, the protocols for the integration of all entities could be defined. Then, an application for processing and visualizing the collected data was proposed.

Hardware for Data Acquisition

Based on the components to be monitored, the sensors and devices for the construction of the hardware responsible for acquiring data from the machine tool were defined. These elements are presented in Table 1.

Table 1. Hardware components.

Component	Quantity
Altus XP 340 PLC	1
Allen-Bradley 1606 XLE Power Supply	1
Altus PH-3500 Multifunction Meter	1
BALLUFF BCM R15E-002-DI00, 5-S4 Condition Monitoring Sensor	2
Altus ET2 – 0800 Switch	1
TURCK TBEN-L5-8IOL IO-Link Master Module	1
Current Transformer	3

The Table 1 presents the elements used for the construction of the system. Each element has a specific function, which are:

Power Meter – For measuring the current, power, and voltage data of the spindle motor, a power meter can be used (in this case, an Altus PH-3500) which has as its main features: a 16- column by 4-line liquid crystal display (LCD), capable of displaying up to 64 characters on the screen, a built-in Ethernet interface, and support for MQTT.

Programmable Logic Controller (PLC) –For the proposed system, the Altus XP 340 programmable logic controller was used as a communication interface. Its main features include: low cost, compact design, a 32-bit ARM processor, 16 inputs, 16 digital transistor outputs, 5 V/I analog inputs, 2 three-wire analog inputs, 4 analog outputs, 1 Ethernet port, 1 RS- 485 serial port, and support for a web server tool that allows the creation of supervision screens without the use of Supervisory Control and Data Acquisition (SCADA) systems. Additionally, the PLC is compatible with major communication protocols, including MQTT, OPC UA, MODBUS, PROFINET, among others.

Vibration Sensor – For monitoring the vibrations of the tool and the spindle, the BALLUFF BCM R15E-002-DI00, 5-S4 condition monitoring sensor was used. Its main features are: an operating voltage of 24Vdc, operating current <15 mA, vibration measurement in the time domain with a frequency range of 2…1800 Hz (±10 %), 2…2500 Hz (±3 dB), contact temperature with a measurement range of -25...+70 °C, and an IO-Link communication interface.

Switch – To allow communication via Ethernet between the various connected devices, a switch can be used. The Altus ET2 – 0800 was chosen, which features: 8 fast Ethernet ports, a 448 kb memory buffer, and an IP30 protection rating.

Power Supply – The devices that are part of the hardware require a constant 24 V supply. For this, a power supply with such capacity must be used; the chosen one was the Allen Bradley 1606 – XL power supply.

RS-232 to USB Serial Converter – As the machine's data output is of the RS-232 type, an RS-232 to USB serial converter can be used so that the CNC command data can be transmitted to the PLC.

IO-Link Master Module – To enable communication between the BALLUFF condition

monitoring sensor and the Altus PLC, the TURCK TBEN-L5-8IOL IO-Link master module must be used. Its features include: an operating voltage of 24 Vdc, operating current <300 mA, and it operates with PROFINET, EtherNet/IP, and Modbus TCP Server protocols.

Current Transformer (CT) – For the power meter to be used for measuring the motor's data, current transformers must be used. This is because the power meter has a current measurement range limited to 10 A, while the spindle motor's current is 25 A.

From the definition of the hardware and the knowledge of the protocols supported by each component, a communication architecture for the acquisition, processing, and visualization of the collected data could be proposed.

Communication

Based on criteria such as latency, reliability, availability, scalability, interoperability, ease of implementation, and cost, a three-layer communication architecture was proposed. They are:

Data Acquisition Layer

This is the direct interface with the physical process. It is divided into three fronts:

- **CNC Data Collection:** Data will be collected via an RS-232 to USB converter cable. A computer will act as an intermediary, physically connecting to the CNC through the USB converter to read the serial data and then use a script to publish this information on the local network via the MQTT protocol. In this way, the Altus XP 340 PLC can subscribe to the corresponding MQTT topic and receive the CNC data over the Ethernet network, integrating it efficiently with the rest of the monitoring system.
- **Electrical Data Collection:** Electrical data will be collected by the power meter, connected directly to the Altus ET2-0800 Switch via an Ethernet cable. The following protocols can be used:
  - MQTT (Recommended for Analysis): The power meter can act as an MQTT client, publishing data asynchronously to a broker.
  - Modbus TCP (Recommended for Control): The PLC can act as a Modbus master and query the power meter at regular intervals to obtain real-time data for control logic or local interlocking.
- **Vibration and Temperature Data Collection:** Vibration data will be collected by the Balluff BCM Sensor with an IO-Link interface. The sensor is connected via a standard IO-Link cable to the TURCK TBEN-L5-8IOL IO-LinK Master Module. The sensor communicates with the master via IO- Link. The IO-Link Master, in turn, connects to the Altus ET2-0800 Switch via an Ethernet cable.

Communication and Local Processing Layer

In this layer, the data is concentrated in the PLC and processed locally. It has the following structure:

- **Local Network:** The Altus ET2-0800 Switch creates the local Fast network, interconnecting the PLC, the IO-Link Master, and the Power Meter.
- **Communication with the IO-Link Master:**
  - Protocol: PROFINET. The Altus XP 340 PLC will act as the PROFINET Controller, and the TURCK IO-Link Master as the PROFINET Device. This is a high-performance, deterministic communication, ideal for obtaining vibration and temperature data with low latency.
- **Data Aggregation in the PLC:**
  - The PLC receives vibration/temperature data from the IO-Link Master via PROFINET.
  - The PLC receives electrical data from the Power Meter (via Modbus TCP or by subscribing to a local MQTT topic).
  - The PLC receives command data from the CNC over the Ethernet network.

- **Edge Processing:** The PLC can perform pre-processing to carry out several functions, such as synchronization, temporal alignment of data from different sources, calculation of simple indicators, issuing alerts, generating immediate alarms, and local supervision. The embedded web server tool in the PLC can be used to create simple supervision screens, accessible by any browser on the local network, for quick diagnostics without the need for a SCADA system.

Supervision and Analysis Layer

This layer is responsible for transforming raw data into intelligence for predictive maintenance. It is composed of:

- **Gateway to the Cloud:** The Altus XP 340 PLC acts as the gateway. After aggregating and synchronizing the data, it prepares it for sending.
- **Sending Protocol:** MQTT is the protocol for communication with the cloud/corporate systems. It is lightweight, secure, and efficient in networks with possible instability. The PLC must format the data from all sources into a single message.
- **Destination Infrastructure:**
  - MQTT Broker: The PLC will publish this message to a specific topic in an MQTT Broker. This broker can be on a local server or on a cloud service.
  - Consumers: Various systems can subscribe to this topic to receive real-time data, such as Databases, Analysis Platforms, and Dashboards.

With the definition of the communication architecture, an application model for the consumption and visualization of data can be established.

Data Processing and Visualization

An application was proposed to consume and process the collected data, allowing for the visualization of the machine's behavior in real- time. The application has the following structure:

Data Source: MQTT Broker

The application architecture integrates with the communication architecture. The Altus XP 340 PLC publishes a consolidated message to a topic in the MQTT Broker, which is the entry point for all real-time data.

Ingestion and Storage: Telegraf + InfluxDB

To move data from the broker to the database efficiently, Telegraf is used:

- **Telegraf:** It is a lightweight collection agent, part of the InfluxDB ecosystem. Telegraf is configured to subscribe to the MQTT topic where the PLC publishes the data. It collects each message, converts it to the optimized InfluxDB format, and inserts it into the database in real-time.
- **InfluxDB:** It will contain buckets (like databases) for the raw machine data and for the results generated by the analysis platform.

Analysis and Intelligence

The analysis platform interacts with InfluxDB in a continuous cycle that has the following structure:

- **Data Reading:** A Python script queries InfluxDB to obtain historical data that can be used to train Machine Learning models. It can also query recent data to make real-time predictions.
- **Insight Generation:** The model processes the data and generates new information, such as a machine Health Index, anomaly detection, and failure prediction.
- **Recording the Results:** The script writes these new insights back into InfluxDB, in a separate bucket.

Visualization Layer: Grafana

Grafana can be used as a visualization tool, as it has native and high-performance integration with InfluxDB. It connects to InfluxDB and allows for the creation of interactive dashboards.

The proposed model allows for real-time monitoring of the asset, facilitating the analysis of indicators and the creation of predictions about the machine's health.

Results and Discussion

The proposed method was based on establishing the critical variables to be monitored in a CNC machine tool to propose a hardware for monitoring and communicating this data. A communication architecture was developed to integrate the connected devices, enabling the development of an application that allows for real-time monitoring of the asset, in addition to the possibility of using the collected data to create an operational history that can be used for building and training machine learning algorithms for failure prediction and anomaly detection.

After the hardware implementation, it will be possible to monitor the process in real-time, providing data for more assertive decision- making regarding operational and maintenance aspects. This culminates in benefits such as a reduction in the number of unplanned downtimes, a reduction in operating costs, an increase in overall equipment effectiveness, and greater reliability and predictability of production.

Conclusion

The development of a low-cost methodology for monitoring CNC machine tools that allows for the application of predictive maintenance techniques is of great value to the manufacturing sector. The results obtained impacted various organizational levels, such as the operational level, through the reduction of unplanned downtimes and increased safety. In the maintenance and process sector, it facilitates a transition from preventive to proactive maintenance methods. In strategic results, it leads to a reduction in operational costs and an increase in the reliability and predictability of production.
The next steps consist of validating the method, which will occur with its implementation on a demonstration machine located at the Advanced Manufacturing Plant (PMA) of SENAI CIMATEC. For this, the hardware will be installed on the machine, and based on the collected data, the application responsible for monitoring and failure prediction can be developed.

Acknowledgement

The authors express their acknowledgment to UFBA and CNPQ for providing the scholarship funding for this project, and to the Advanced Manufacturing Laboratory of SENAI CIMATEC for supplying technical staff and physical infrastructure for the project's development.

References

1. Haraguchi N, Cheng CFC, Smeets E. The importance of manufacturing in economic development: Has this changed?. World Dev [Internet]. 2017;93:293–315. Available from: https://doi.org/10.1016/j.worlddev.2016.12.013
2. Qianzhe Q, Wang J, Ye L, Gao R. Digital twin for machining tool condition prediction. Procedia CIRP [Internet]. 2019;81:1388-1393. Available from: https://doi.org/10.1016/j.procir.2019.04.049
3. Monostori L, Kádár B, Bauernhansl T, Kondoh S, Kumara S, Reinhart G, et al. Cyber-physical systems in manufacturing. CIRP Annals - Manufacturing Technology [Internet]. 2016;65:621–641. Available from: https://doi.org/10.1016/j.cirp.2016.06.005
4. Vanraj, Goyal D, Saini A, Dhami SS, Pabla BS. Intelligent predictive maintenance of dynamic systems using condition monitoring and signal processing techniques — a review. In: International Conference on Advances in Computing, Communication, & Automation (ICACCA). 2016. p. 1–6.
5. Lee WJ, Wu H, Yun H, Kim H, Jun MBG, Sutherland JW. Predictive maintenance of machine tool systems using artificial intelligence techniques applied to machine condition data. Procedia CIRP [Internet]. 2019;80:506-511. Available from: https://doi.org/10.1016/j.procir.2018.12.019

6. Thoppil NM, Vasu V, Rao CSP. Failure mode identification and prioritization using FMECA: A study on computer numerical control lathe for predictive maintenance. J Fail Anal and Preven [Internet]. 2019;19:1153–1157.
7. Hesser DF, Markert B. Tool wear monitoring of a retrofitted CNC milling machine using artificial neural networks. Manufacturing Letters [Internet]. 2019;19:1-4.
8. Goodall P, Pantazis D, West A. A cyber physical system for tool condition monitoring using electrical power and a mechanistic model. Computers in Industry [Internet]. 2020;118:103223. Available from: https://doi.org/10.1016/j.compind.2020.103223
9. Zhu K. A cyber-physical production system framework of smart CNC machining monitoring system. IEEE/ASME Transactions on Mechatronics [Internet]. 2018;PP:1-1. Available from: https://doi.org/10.1109/TMECH.2018.2834622
10. Ramírez IZ, Daviu JAA, Hernandez MT, Rios RAO. Cutting tool wear monitoring in CNC machines based in spindle-motor stray flux signals. IEEE Transactions on Industrial Informatics [Internet]. 2020;PP:1-1. Available from: https://doi.org/10.1109/TII.2020.3022677
11. Thoppil NM, Vasu V, Rao CSP. On the criticality analysis of computer numerical control lathe subsystems for predictive maintenance. Arab J Sci Eng [Internet]. 2020;45:5259–5271.

Trajectory Planning for Manipulators on Mobile Bases and in Dynamic Environments, Using Adaptive Models

Anderson Queiroz do Vale[1]*, Herman Augusto Lepikson[1,2]
[1]Federal University of Bahia, Mechatronics Department; [2]SENAI CIMATEC University, GETEC Department, Salvador, Bahia, Brazil

This study addresses the challenges of trajectory planning for mobile manipulators whose base moves continuously during capture tasks. The main difficulty lies in adapting planning algorithms to dynamic scenarios, where base displacement compromises motion accuracy and efficiency. Traditional algorithms, developed for static or predictable environments, are unsuitable for unpredictable base movements. Key challenges include recalculating trajectories in real time to maintain safety and efficiency, while considering embedded systems' computational constraints and the need for rapid responses to avoid collisions and optimize manipulation. To overcome these issues, approaches must integrate dynamic data and generate feasible trajectories regardless of base position. This work proposes adapting and evaluating two widely used motion planning algorithms: Rapidly-exploring Random Tree (RTT) and Real-Time Adaptive Motion Planning (RAMP). Both will be modified to account for base displacement, ensuring safe and efficient trajectories. Adjustment strategies will be embedded into the planning process, enabling algorithms to react dynamically to environmental and base position changes. Implementation will occur in a simulated environment, with a manipulator on a mobile base interacting with dynamically modeled objects. Experiments will assess accuracy, response time, and robustness. Expected outcomes include improved adaptation to base variations, reduced execution times, and enhanced object capture performance. These optimizations aim to advance real-world applications of mobile manipulators in industrial and assistive robotics.

Keywords: Mobile Manipulator. Dynamic Path Planning. Manipulator. ROS.

Mobile manipulators represent an emerging and crucial research area in robotics, combining the mobility of mobile robots with the manipulation capabilities of robotic arms. This integration enables these systems to perform a wide range of complex tasks in diverse environments, ranging from industrial applications to domestic services.

These robots have been widely adopted in various sectors, such as manufacturing, smart food services, daily assistance, and healthcare. Their broad applicability stems from their versatility and ability to manipulate objects, characteristics that make them suitable for different tasks such as pushing, pulling, and transporting.

The growing popularity of these robots can be attributed to their ability to meet specific demands, providing adaptable and effective solutions for a wide range of tasks and applications [1]. The capability to avoid obstacles in real time is of vital importance for the efficient completion of tasks in challenging environments, where complex and constantly changing obstacles are present [2]. This is achieved through the use of advanced environmental perception sensors, which enable rapid detection, and effective algorithms, which ensure agile responses to objects and adverse conditions. In this way, this set of technologies guarantees not only safety but also operational success in challenging environments.

Collaborative robots that are or have arms enable interaction between humans and robots in shared workspaces. To date, their applications have been limited to structured and static environments, usually for specific tasks. In industrial contexts, robot trajectory planning is still generally performed offline. To ensure autonomous and safe operations, it is imperative to use online motion planners capable of readjusting the robot's trajectory in the face of unexpected obstacles or variable

Received on 20 February 2026; revised 18 April 2026.
Address for correspondence: Anderson Queiroz do Vale. Av. Orlando Gomes, 1845, Piatã, Salvador, Bahia, Brazil. Zipcode: 41650-010. E-mail: anderson_qdv@hotmail.com.

J Bioeng. Tech. Health 2026;9(5):410-416

goals [3]. Therefore, the implementation of real-time motion planners is essential to expand the application of collaborative robots in dynamic industrial scenarios, enabling more adaptive and safer operations in interaction with humans.

Other significant application of mobile manipulators lies in their integration with underwater vehicles, representing one of the primary research areas for scientists. This field requires investigation due to the complexity of the underwater vehicle–manipulator interaction, which involves coupled motion and parameter uncertainties [4]. According to the authors, these vehicles have begun to play an important role in underwater activities, including, but not limited to, seabed exploration, oil-related operations, and military and scientific investigations.

Mobile manipulators have been employed in various applications that would traditionally require multiple fixed-base robots or large-scale robotic systems. This capability is enabled by the mobility of the mobile base. However, the mobile base also introduces redundancy to the system, making the motion planning of the mobile manipulator more challenging [5].

As previously mentioned, mobile manipulators represent a highly versatile and promising technology, with applications spanning various sectors, from manufacturing to underwater operations. Their success is driven by the ability to deliver adaptable and effective solutions for a wide range of tasks and environments. However, persistent challenges, such as dynamic trajectory planning and real-time interaction with obstacles and variable goals, continue to demand ongoing innovation and research.

The need for online motion planners capable of adjusting manipulator trajectories in response to environmental changes and base displacements is essential to ensure autonomous and safe operations, particularly in industrial and collaborative contexts. Furthermore, the integration of manipulators with underwater vehicles opens new frontiers for exploration and discovery in marine environments, enhancing the precision of object retrieval and valve manipulation under maritime disturbance conditions.

This research examines existing models in the literature, focusing on promising approaches and techniques aimed at improving the efficiency of dynamic trajectory computation for manipulators, with the goal of increasing autonomy and safety in mobile manipulator operations. By addressing these challenges in a collaborative manner, it becomes possible to assess and compare the different models proposed, identifying those that yield the best results in object retrieval and transportation tasks within dynamic environments and with constant base displacement, while seeking algorithmic improvements and optimization in dynamic tasks. This comparative evaluation is crucial to highlight the most effective approaches, presenting both strengths and weaknesses to guide future research and developments in the field of continuously moving mobile manipulators. In this way, the sharing of knowledge and experience can foster innovation and drive advances toward more sophisticated and efficient solutions to the challenges faced by these robotic systems.

This research aims to employ dynamic trajectory planning models for mobile manipulators, with an emphasis on performing object pick-and-place tasks between two points while the robot's base is in continuous motion during operation. Based on the results obtained, a comparative analysis of the techniques will be conducted. The study seeks to identify the most effective methods and propose advancements in the development of strategies that enhance the adaptability and efficiency of these systems in industrial and collaborative environments.

In this research, several stages will be carried out to complete the study:

1. Analyze existing trajectory planning techniques in the literature for mobile manipulators, with emphasis on online approaches and their applicability in dynamic environments;
2. Compare the effectiveness of dynamic trajectory planning models in terms of performance in object retrieval and transportation tasks within

dynamic environments and with constant manipulator base displacement;
3. Develop an evaluation methodology to test the robustness of mobile manipulators in dynamic and collaborative environments, considering displacement variables and external interferences;
4. Implement and test real-time trajectory planning techniques adapted for mobile manipulators, focusing on improving operational accuracy and safety;
5. Conduct simulated experiments using robotic manipulators on mobile bases to assess the feasibility of the models in real-world scenarios;
6. Analyze experimental results and qualitative observations, identifying strengths and limitations of each trajectory planning model.

The research is motivated by the complexity of operating robotic manipulators in dynamic environments, in which their mobile base is subject to displacements during the execution of specific tasks.

This situation is frequently observed in various practical applications, such as object manipulation in spaces shared with humans, operations on the seafloor, where the base is in constant motion, or in industrial environments where autonomous load transportation is required.

In this context, it is essential to investigate and compare different trajectory planner models, considering not only the dynamics of the mobile base but also the presence of dynamic obstacles. The inclusion of such obstacles, simulating the presence of people or moving objects within the manipulator's operating area, introduces a realistic challenge to the analysis, enabling an accurate assessment of conditions encountered in practical environments.

Through a comparative analysis of trajectory planner models found in the literature, the aim is not only to identify their advantages and limitations but also to gain insights into their ability to estimate dynamic trajectories efficiently and accurately, ensuring acceptable execution times and effective adaptation to dynamic scenarios.

Mobile Manipulators

The structure of mobile manipulators consists of multifunctional mechanical arms equipped with grippers or claws, enabling them to handle objects with precision and flexibility, along with integrated sensor subsystems [6]. These devices are complemented by locomotion systems, which may include wheels, thrusters, tracks, or even legs, providing the capability to move across uneven terrain and operate in challenging environments (Figure 1).

Mobile manipulators use their bases as approach vehicles to perform tasks. For the trajectory computation to be successfully executed, these bases must remain stable, that is, free from disturbances or displacements during operation. This requirement arises from the fact that manipulator trajectory planning algorithms consider the base as a fixed reference. Consequently, any displacement in the base's position may introduce errors into the trajectory calculation or require recalculating it, which can increase operation time and reduce energy efficiency.

Trajectory Planning Algorithms for Mobile Manipulators

Trajectory planning algorithms for robotic manipulators are computational methods used to determine the path or sequence of movements that a manipulator must follow to reach its final target. The primary goal of these algorithms is to ensure that the manipulator moves accurately and optimally, while adhering to the constraints of the operating environment, considering factors such as obstacles, the robot's physical limitations, and dynamic environmental conditions. This study addresses two trajectory planning algorithm methods: RRT and RAMP.

RRT

The RRT method is a sampling-based trajectory planning approach widely employed in dynamic

Figure 1. Structural models of bases for mobile manipulators [9,10].

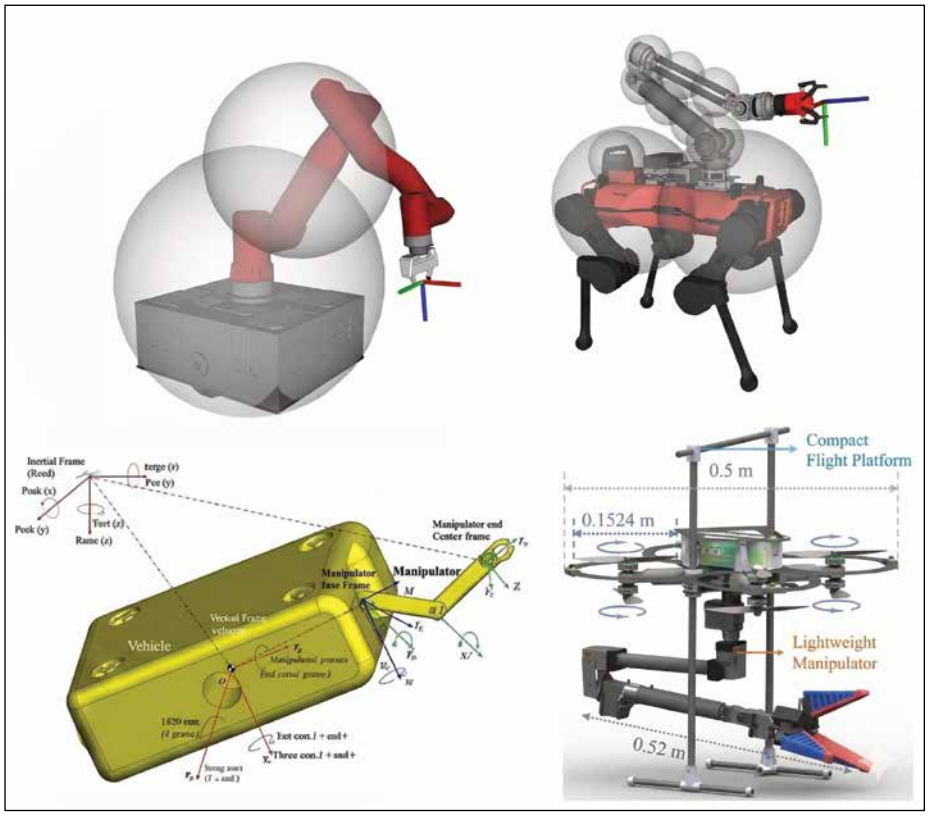

trajectories for robotic manipulators with multiple degrees of freedom operating in complex environments [7]. This algorithm is grounded in principles of optimal control theory, nonholonomic planning, and random path strategies, with its core concept consisting of the progressive expansion of a search tree from an initial state [8]. This expansion occurs through the application of control inputs over small time intervals, enabling transitions to new states. Each node in the tree corresponds to a state, while the directed edges represent the inputs applied to connect consecutive states. Upon reaching the target region, the tree structure defines an open-loop trajectory that connects the initial point to the goal. Figure 2 shows the path generated by the RRT algorithm.

RAMP

RAMP is an adaptive real-time motion planner developed for robotic manipulators [11]. According to the authors, the RAMP methodology is based on concepts of randomized and optimized planning, operating in a parallel and continuous manner, thereby eliminating several disadvantages of traditional approaches. The RAMP method represents complete trajectories in the configuration-time (CT) space and continuously refines them during simultaneous planning and execution. Unlike sequential or incremental approaches, which only provide the final trajectory upon completion of the process, RAMP can quickly generate a valid trajectory and improve it as needed to meet global real-time planning requirements. It allows for the flexible integration of multiple optimization criteria, such as minimizing energy and time or maximizing manipulability, directly in the continuous CT space, avoiding the constraints imposed by graph-based representations. Furthermore, its parallel architecture maintains multiple trajectories active simultaneously, enabling instant adjustments and, when necessary, drastic changes to respond to environmental variations.

Figure 2. Structural models of bases for mobile manipulators [7].

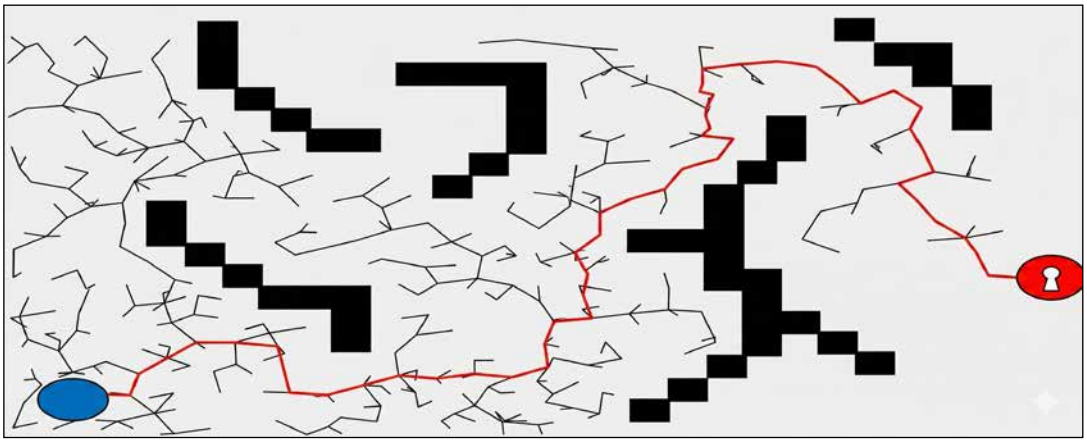

The approach is also highly adaptable, continuously adjusting trajectory search and optimization in response to new conditions. Since planning and execution occur in parallel, the robot can follow viable portions of a trajectory while new alternatives are generated to bypass infeasible regions. The method supports partially specified goals, allowing different trajectories to terminate at distinct locations within the same target region. In redundant robots, such as mobile manipulators, RAMP leverages redundancy by representing trajectories as loosely coupled redundant variable paths, thereby maximizing collision avoidance and meeting multiple optimization objectives simultaneously.

Perception

A simple yet robust alternative for object detection is the use of fiducial markers. The literature presents various types and formats of these markers [12]. In this work, the AprilTag was chosen due to its greater robustness to occlusions and distortions, as well as its lower incidence of false detections [12]. However, the main source of error in AprilTag pose estimation is related to the camera's angular rotation [13], which will not pose a challenge in this study, as the camera will not undergo any rotation. The structure of the AprilTag, for example, consists of black outer borders and internal patterns composed of white squares, which facilitates differentiation through various topologies, as illustrated in Figure 3, which shows an example application.

Proposed Model for Mobile Manipulator Trajectory Planning

The proposed model consists of three main components: (1) a hierarchical control system,

Figure 3. Illustrative example of an AprilTag [14].

responsible for managing the manipulator's movements, ensuring path supervision to prevent collisions, and guaranteeing that the final objective is achieved safely; (2) a dynamic trajectory planning algorithm, designed to enable the manipulator to capture the object even during continuous base movement, adapting trajectories in real time as needed; and (3) a sensing module, tasked with identifying the object's relative position with respect to the base and providing essential information for system operation, as illustrated in Figure 4.

Conclusion

This study presented two path planning methods, RRT and RAMP, for mobile manipulators performing pick-and-place tasks while operating on continuously moving bases. The proposed model, integrating a hierarchical control system, a non-adaptive and adaptive real-time planning algorithm, and a sensing module using AprilTags, demonstrated the feasibility of accurate and efficient manipulation in dynamic environments.

The RRT is widely recognized for its efficiency in exploring high-dimensional state spaces, a feature that makes it suitable for trajectory planning in robotic manipulators. As previously noted, this algorithm can rapidly identify feasible paths in complex environments, which is particularly relevant in scenarios that demand immediate responses. However, its original formulation does not account for variations in the environment, requiring the tree to be reconstructed whenever changes occur. To address this limitation, the algorithm will be modified to allow new replanning whenever alterations to the final goal arise.

The RAMP, in turn, was designed for dynamic scenarios, enabling simultaneous planning and execution. This method generates partially feasible trajectories almost immediately, refining them continuously based on real-time sensory data. Furthermore, it supports the integration of multiple optimization criteria, such as reducing execution time, improving energy efficiency, and enhancing manipulability, thereby ensuring robust performance even under adverse conditions. Thus, while RRT and its variants provide speed in exploring the search

Figure 4. Diagram of the proposed model for real-time object manipulation.

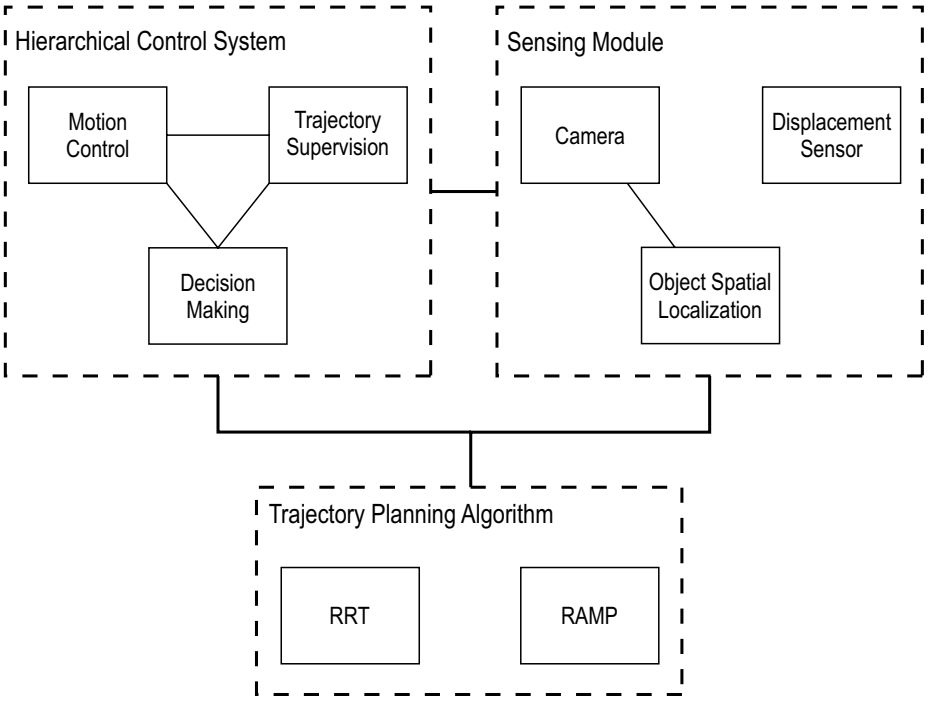

space, RAMP distinguishes itself by its continuous adaptability, making it particularly suitable for tasks performed in collaborative environments or under constant perturbations.

Future research will focus on implementing the model, optimizing processing time, expanding sensor integration, and conducting real-world experiments to further validate and refine the proposed approach.

Acknowledgement

We express our sincere gratitude to Professor Dr. Herman for his indispensable guidance, constructive feedback, and constant encouragement throughout the development of this research.

References

1. Wang G, et al. Development of a search and rescue robot system for the underground building environment. J Field Robot. 2023;40(3):655-683.
2. Wang G, et al. Reactive mobile manipulation based on dynamic dual-trajectory tracking. Robot Auton Syst. 2024;172:104589.
3. Gafur N, et al. Dynamic path planning and reactive scheduling for a robotic manipulator using nonlinear model predictive control. In: Proceedings of the 30th Mediterranean Conference on Control and Automation (MED); 2022. p. 604-611.
4. Mohan S, Kim J, Singh Y. A robust task space position tracking control of an underwater vehicle manipulator system. ACM Int Conf Proc Ser. 2015.
5. Nguyen QN, Pham QC. Planning optimal trajectories for mobile manipulators under end-effector trajectory continuity constraint. In: Proceedings of the IEEE International Conference on Robotics and Automation (ICRA); 2024. p. 14356-14362.
6. You Y, et al. Design and implementation of mobile manipulator system. In: Proceedings of the IEEE Annual International Conference on CYBER Technology in Automation, Control, and Intelligent Systems (CYBER); 2019. p. 113-118.
7. Wei K, Ren B. A method on dynamic path planning for robotic manipulator autonomous obstacle avoidance based on an improved RRT algorithm. Sensors (Basel). 2018;18(2).
8. LaValle SM, et al. Rapidly-exploring random trees: progress and prospects. In: Algorithmic and Computational Robotics: New Directions. 2001. p. 293-308.
9. Mittal M, et al. Articulated object interaction in unknown scenes with whole-body mobile manipulation. In: Proceedings of the IEEE/RSJ International Conference on Intelligent Robots and Systems (IROS); 2022. p. 1647-1654.
10. Liu Q, et al. A compact aerial manipulator: design and control for dexterous operations. J Intell Robot Syst. 2024;110(2):1-20.
11. Vannoy J, Xiao J. Real-time adaptive motion planning (RAMP) of mobile manipulators in dynamic environments with unforeseen changes. IEEE Trans Robot. 2008;24(5):1199-1212.
12. Kalaitzakis M, et al. Fiducial markers for pose estimation: overview, applications and experimental comparison of the ARTag, AprilTag, ArUco and STag markers. J Intell Robot Syst. 2021;101:1-26.
13. Abbas SM, et al. Analysis and improvements in AprilTag-based state estimation. Sensors (Basel). 2019;19(24):5480.
14. Pfanne M, et al. Fusing joint measurements and visual features for in-hand object pose estimation. IEEE Robot Autom Lett. 2018;3(4):3497-3504.

Sodium Bicarbonate and Citric Acid as Blowing Agents in Polymer Composites with Recycled Textiles: An Alternative to Azodicarbonamide

Marcus Vinicius Badaró de Oliveira Ribeiro[1]*, Adriano Puglia Lima[1], Maria Luiza Marques Rapold Souza[2], Pollyana da Silva Melo[1]

[1]SENAI CIMATEC University; Salvador, Bahia, Brazil

The study evaluated the influence of sodium bicarbonate (SB) combined with citric acid (CA) as a blowing agent in polymeric compounds produced from recycled polymer and textile waste, comparing its performance with the conventional agent azodicarbonamide (ADC). The compounds were processed in a thermokinetic mixer (DRAISS Homogenizer), and the specimens were prepared by hydraulic press molding, using formulations with 5% and 10% of each blowing agent. Density measurements showed that the SB + CA combination, at a 10% concentration (FCSB10), achieved a 19.29% reduction in density compared to the non- expanded reference, surpassing the applications with azodicarbonamide. Although ADC was slightly more effective at lower concentrations (5%), the combined sodium bicarbonate and citric acid system demonstrated expansion without the need for initiators and without exposure to toxicological risks. The results indicate that this system may be a viable and sustainable alternative to ADC for producing expanded polymers, although adjustments in processing parameters and optimization are still required.

Keywords: Polymer Waste. Textile Waste. Blow Agent. Citric Acid. Sodium Bicarbonate.

Expanded polymers play a significant role in various industrial applications, from packaging and automotive components to thermal and acoustic insulators [1]. Properties such as low density, high strength-to-weight ratio, and excellent energy absorption capacity are achieved by creating a cellular structure within the polymer matrix [1,2]. This process is often carried out with the aid of chemical blowing agents, which decompose under heating to release gases and form the desired cellular morphology [2].

Processing with chemical blowing agents employs the same equipment used in conventional extrusion and utilizes up to 10% by weight of the foaming agent. This process requires precise temperature control and preferably uses a screw with a mixing section [3]. The blowing agent decomposes in the plasticization zone, and when the product is released from the die, expansion occurs to form a cellular material. Typically, the density of foams produced by this method is above to 0.25 g/cm³. The decomposition residues of chemical blowing agents can adversely affect material properties, as they act as fillers [3].

Among the available blowing agents, azodicarbonamide (ADC) has been widely used for decades due to its high gas-yielding efficiency and ability to generate homogeneous, closed-cell structures in a wide range of polymers, such as PVC, polyethylene, and rubbers [2,4]. Its high decomposition temperature approximately 200°C can be adjusted with activators to match the polymer's processing temperature, which has established ADC as a standard additive in the plastics processing industry [5].

However, concerns regarding its use are associated with the byproducts generated during thermally induced decomposition [5,6]. Studies shown that ADC may produce potentially harmful compounds, such as semicarbazide (SEM), particularly in food- contact applications due to its toxicity, as well as the release of urea and carbon monoxide, raising additional occupational and environmental safety concerns [5–8]. Workers exposed to azodicarbonamide exhibited a higher prevalence of respiratory symptoms (coughing, wheezing, chronic bronchitis) and airway irritation, suggesting direct adverse effects from

Received on 20 March 2026; revised 25 April 2026.

Address for correspondence: Marcus Vinicius Badaró de Oliveira Ribeiro. Av. Orlando Gomes, 1845, Piatã, Salvador, Bahia, Brazil. Zipcode: 41650-010. E-mail: marcus.oliveira@fieb.org.br; marcus.vinicius.badaro@gmail.com.

J Bioeng. Tech. Health 2026;9(5):417-422

the compound or its decomposition byproducts [9–11].

The growing demand for safer and more sustainable materials and processes, researchers have sought viable alternatives to azodicarbonamide that perform the same function without generating toxic residues [2]. Promising alternatives have emerged in systems based on sodium bicarbonate (SB), due to its ability to release carbon dioxide (CO_2) when heated, and citric acid, which decomposes to release gases that assist in cellular structure formation [12].

Several researchers have demonstrated the feasibility of using citric acid (CA) and sodium bicarbonate (SB) as blowing agents in various polymeric matrices, highlighting their significant advantages over azodicarbonamide, particularly in terms of safety and environmental profile [13–15].

Being an exothermic agent, azodicarbonamide operates at higher temperatures (170–200 °C), whereas the SB/CA mixture is endothermic and composed of substances classified as non-toxic and non- hazardous. This eliminates concerns related to handling hazardous chemicals and mitigates environmental impacts [16]. Furthermore, SB and CA masterbatches release a substantial amount of gas (water vapor and CO_2) upon reaction, within a broad temperature range (160–210 °C) compatible with many polymers, enabling the production of high-quality foams at low loadings (1–2 wt%) [16].

This combination of safety, efficient performance, and reduced environmental risk positions the sodium bicarbonate/citric acid system as a superior and more sustainable alternative to traditional blowing agents such as azodicarbonamide.

Extensive studies highlight the critical need to optimize processing conditions, temperature and heating rate, to maximize expansion efficiency and final material properties. Achieving consistent performance across different polymer matrices remains a technical challenge.

Within this framework, the present study aims to investigate the effect of sodium bicarbonate combined with citric acid in recycled polymer waste applications, with direct comparison to azodicarbonamide for producing expanded polymer sheets. This research seeks to contribute to developing safer and more sustainable solutions for the expanded polymer industry.

Materials and Methods

Materials

The study was used a waste-derived polymer compound, from polymer waste and textile waste, as the matrix material, incorporating two different chemical blowing agent systems for comparison: (1) azodicarbonamide and (2) citric acid combined with sodium bicarbonate.

Methods

The samples of the polymer compound were prepared from the formulations contained in Table 1.

In a thermokinetic mixer (Figure 1, MH-Equipment model MH-1000), following initial processing parameters of 800 RPM at low rotation speed with temperature starting from 100°C for feeding the materials (polymer waste, textile waste, and blowing agents). The rotation speed was then increased to approximately 1800-2500 RPM for mixing and homogenization of the formulation, while controlling the mixing temperature until reaching values between 150-160°C to preserve the compound integrity. Upon reaching the designated temperature while maintaining high rotation speed, the composite was maintained for a predetermined time interval to ensure compound homogeneity.

The molten mass was transferred to a rectangular plate mold mounted on a hydraulic press (Advanced brand, Figure 2) with a 4-ton capacity, preheated to 160°C. The mass was pressed to shape the plate, followed by pressure release to allow expansion while maintaining contact with the heating plates for 30 minutes

Table 1. Composition of expanded recycled composite.

Composition	PWTW	FAZ5	FAZ10	FCSB5	FCSB10
Polymer Waste + Textile Waste	100%	95%	90%	95%	90%
Azodicarbonamide	-	5%	10%	-	-
Citric Acid	-	-	-	2%	4%
Sodium Bicarbonate	-	-	-	3%	6%

Figure 1. Thermokinetc mixer (DRAISS homogenizer).

to enable thermal decomposition of the blowing agents. After 30 minutes, the press was turned off and cooled by natural convection, as the hydraulic press lacked a forced cooling mechanism.

Experimental Characterization

Density Properties

Density testing was performed using a analytical balance, DSL910 (F) (Figure 3), which applies Archimedes' principle of buoyancy and displacement to determine density in grams per cubic centimeter.

To perform this test, the preparation of specimens with similar dimensions was carried out. Then, a determined volume of anhydrous

Figure 2. Hydraulic press.

Figure 3. Analytic balance DSL910.

alcohol with density 0.8165 g/cm³ is added to the container and placed on the balance. The test is performed in two stages. In the first stage, the analytical balance precisely measures the mass (m) of the specimen in air. In the second stage, the specimen was immersed in the anhydrous alcohol, displacing a volume of alcohol equal to its own volume, and by Archimedes' principle, the balance measures the apparent weight of the immersed specimen. The difference between the dry weight and immersed weight (which corresponds to the buoyancy force) is used to calculate the volume of the specimen through Archimedes' principle. Finally, the density of the specimen is calculated by dividing its mass by the determined volume.

Results and Discussion

The density evolution of the materials as a function of different blowing agent additions and their respective quantities is presented in Figure 4.

These results are also presented in Table 2, which allows comparison of the distinct behaviors regarding compound expansion and density reduction.

Figure 4. Density behavior graphics.

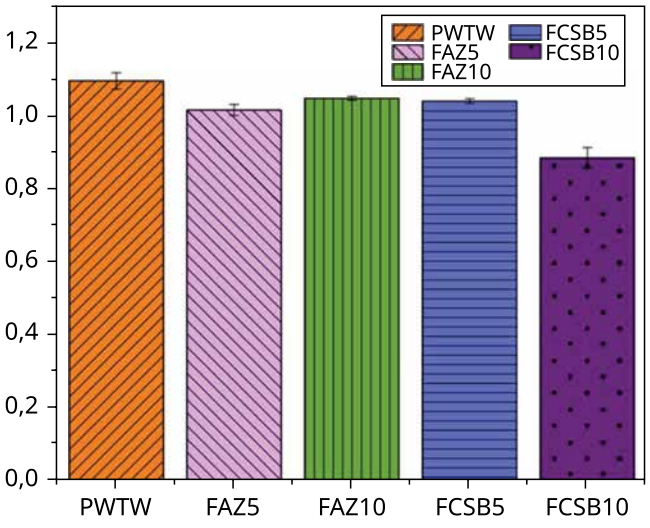

The comparative performance of formulations containing azodicarbonamide (FAZ) and citric acid combined with sodium bicarbonate (FCSB), at concentrations of 5% and 10% for density reduction, relative to the non-expanded reference composite (PWTW), revealed distinct responses to the expansion process.

Comparative analysis indicated that the FCSB10 formulation achieved the highest density reduction among the conditions studied, with a decrease of 19.29% relative to the reference. This result contrasts with the performance of FAZ5 and FAZ10, which exhibited comparatively modest reductions of 7.30% and 4.36%, respectively. For the FCSB- based composites, increasing the concentration from 5% to 10% markedly enhanced expansion performance, with density reductions of 5.07% and 19.29%, respectively. In contrast, the FAZ- based composites displayed an inverse trend, with reductions decreasing from 7.30% at 5% concentration to 4.36% at 10%, suggesting the presence of an optimal concentration threshold for this blowing agent.

The direct comparison between materials at the same concentration revealed that FAZ5 was 2.40% more effective than FCSB5, whereas at 10% concentration, the relationship was sharply reversed, with FCSB10 outperforming FAZ10 by 15.62%. This phenomenon indicates that additional factors in their mechanisms of action influence the expanded matrix in different ways, with FCSB exhibiting a performance pattern dependent on higher concentrations within the studied parameters.

It is well established that the effectiveness of azodicarbonamide is directly linked to the use of temperatures above 200 °C or to the presence of initiators that lower the component's thermal

Table 2. Density result.

Form.	PWTW	FAZ5	FAZ10	FCSB5	FCSB10
Mean SD	1,0941 ±0,0223	1,0143 ±0,0151	1,0464 ±0,0050	1,0386 ±0,0066	0,8830 ±0,0283

decomposition temperature [5]. However, the optimal temperature for this condition is not applicable to the material investigated in this study. Furthermore, no initiators were employed in this work, as the objective was to identify a potential substitute for azodicarbonamide.

The results obtained converge with the data reported in the literature. Sadik and colleagues [13] developed low-density polyethylene (LDPE) masterbatches containing AC, BS, or their combination, evaluating their thermal decomposition kinetics. Their findings showed that BS follows first-order kinetics, releasing CO_2 and H_2O between 100–180 °C, whereas AC decomposes in two stages (160–270 °C), forming intermediates such as aconitic acid and maleic anhydride. The combination of both agents resulted in distinct decomposition stages, enabling better control of expansion at the high heating rates typical of injection molding processes [13].

Vorawongsagul and colleagues [14] employed SB as a blowing agent in PLA/PBS composites reinforced with cellulose fiber, produced by extrusion and injection molding. The decomposition of SB generated closed-cell structures with reduced density and enhanced mechanical and thermal properties, demonstrating particular suitability for food packaging applications [14].

In addition, Bettelli and colleagues [15] investigated citric acid as a multifunctional additive in wheat gluten applications, combining it with ammonium bicarbonate. In this study, AC simultaneously acted as a crosslinking agent and plasticizer, producing low-density foams with high porosity and predominantly closed- cell structures [15]. This contrasts with the findings of Sadik and colleagues [13], who demonstrated that AC and SB mixtures in masterbatches enable expansion kinetics coupled with well- defined decomposition stages for each component. Taken together, these studies highlight the versatility of CA and SB in applications requiring precise control of expansion, reinforcing their potential as sustainable alternatives to conventional blowing agents [13].

Gouissem and colleagues 16] highlighted that the density results confirmed the efficiency of combining citric acid (CA) and sodium bicarbonate (SB) when compared to the traditional blowing agent azodicarbonamide. While CA alone reduced the density by up to 43% and SB by approximately 48.6%, their mixtures at optimized proportions, particularly the 60/40 ratio, promoted a synergistic effect, achieving reductions close to 50% and leading to finer, more uniform, and regular cell structures. These findings demonstrate that the CA/SB combination not only results in lower densities than those obtained individually but also offers structural advantages over azodicarbonamide-based systems, especially in terms of sustainability and environmental profile [16].

Therefore, the data suggests that the selection of the most suitable material is highly dependent on the concentration used and warrants further investigation into the interactions between the materials and the production parameters applied for the development of optimized formulations. Even with the positive response observed for FCSB, the underlying physicochemical mechanisms behind the observed differences, the behavior of additional parameters, and processing conditions, such as molding, temperature, cost- effectiveness, as well as collateral properties of the formulations should be further explored.

Conclusion

The results indicated that the combination of sodium bicarbonate with citric acid shows potential to replace azodicarbonamide as a blowing agent. In this study, 10% concentrations were shown to achieve lower densities than the composites containing azodicarbonamide. Although ADC proved to be slightly more efficient than CA combined with SB at 5% concentrations, the significant advantage of the latter at higher concentrations, without the need for initiators and without the associated risks of azodicarbonamide,

suggests that this material could serve as a viable substitution alternative. Nevertheless, the use of this expansion system still requires adjustments and optimizations in both formulations and preparation methods, to better understand the potential for greater expansion and to reduce concentration levels, thereby optimizing costs.

For future research, it is essential to investigate specimen molding methodologies, the influence of mold temperature, forming pressure, and strategies to optimize the quantity of chemical agents, with the aim of improving the expansion performance of the developed composites.

Acknowledgement

The authors gratefully acknowledge the Materials Characterization Laboratory at SENAI CIMATEC for providing access to the equipment, and ECOLOY for supplying the waste materials used in this study.

Reference

1. Krishnan VG, Fiorucci L, Sarbu A, Drenckhan-Andreatta W. Characterizing the foaming process of polymers: review of experimental methods. Adv Colloid Interface Sci. 2025;344:103579.
2. Jin FL, Zhao M, Park M, Park SJ. Recent trends of foaming in polymer processing: a review. Polymers (Basel). 2019;11(6):953.
3. Rabello M. Aditivação de polímeros. São Paulo: Artliber; 2000.
4. Lendvai L, Degosy G, Jakab SK, Fekete I. Foam injection molding of poly(lactic acid) with azodicarbonamide-based chemical blowing agent. Eng Proc. 2024;79(1):44.
5. Guo RL, Liu SH, Lu YM. Investigation of how pressure influences the thermal decomposition behavior of azodicarbonamide. J Loss Prev Process Ind. 2023;83:105062.
6. Krutko I, Danylo I, Kaulin V. Kinetics of azodicarbonamide decomposition in the presence of an initiator for obtaining solid foams. Voprosy Khimii i Khimicheskoi Tekhnologii. 2019;(1):26-34.
7. Wu S, Feng Y, Chen S, Zhao Y, Li C, Deng J, et al. A novel strategy for the detection of semicarbazide in crustaceans by modified QuEChERS coupled with hydrophilic interaction liquid chromatography–tandem mass spectrometry. Foods. 2025;14(3):541.
8. Xing L, Sun W, Sun X, Peng J, Li Z, Zhu P, et al. Semicarbazide accumulation, distribution and chemical forms in scallop (Chlamys farreri) after seawater exposure. Animals (Basel). 2021;11(6):1500.
9. Whitehead LW, Carson ML, Ward EM, Boswell RT, Wolfe RA. Respiratory symptoms associated with the use of azodicarbonamide foaming agent in a plastics injection molding facility. Am J Ind Med. 1987;11(1):83-92.
10. Suojalehto H, Malo JL, Cullinan P. The classification of azodicarbonamide (ADCA) as a respiratory sensitiser: adding to the weight of evidence. Regul Toxicol Pharmacol. 2018;94:330-1.
11. Kupczewska-Dobecka M, Konieczko K, Jurewicz J. Effect of occupational exposure to ADCA on the incidence of allergic respiratory reactions: a literature review. Med Pr. 2024;75(5).
12. Murphy J, editor. Additives for plastics handbook. Oxford: Elsevier; 2001.
13. Sadik T, Pillon C, Carrot C, Reglero Ruiz JA. DSC studies on the decomposition of chemical blowing agents based on citric acid and sodium bicarbonate. Thermochim Acta. 2018;659:74-81.
14. Vorawongsagul S, Pratumpong P, Pechyen C. Preparation and foaming behavior of poly(lactic acid)/poly(butylene succinate)/cellulose fiber composite for hot cups packaging application.Food Packag Shelf Life. 2021;27:100608.
15. Bettelli MA, Hu Q, Capezza AJ, Johansson E, Olsson RT, Hedenqvist MS. Effects of multifunctional additives during foam extrusion of wheat gluten materials. Commun Chem. 2024;7:75.
16. Gouissem L, Benmekideche A. Contribution to the expansion of low-density polyethylene by the use of chemical blowing agents based on sodium bicarbonate and/or citric acid. Polym Sci Ser A. 2021;63(5):542-55.

Analysis of the Influence of ISR with TiO_2 Addition on the Compressive Strength and Durability of Structural Self-Compacting Concrete Associated with Porosity

Pedro Victor Correia e Reis[1]*, Marianna Luna Sousa Rivetti[1], Nilson Santana de Amorim Júnior[1], Pedro Manoel Moreira Novaes Santos[2]

[1]SENAI CIMATEC University, Civil Construction; Salvador, Bahia; [2]CIVIL Group; Simões Filho, Bahia, Brazil

In the contemporary global landscape, efforts to reduce energy consumption and mitigate the carbon footprint associated with products and human activities have intensified, with the construction industry emerging as one of the most environmentally impactful sectors due to its substantial consumption of natural resources and significant waste generation. Among the sustainable strategies under investigation, the reuse of industrial or mining residues through their incorporation into construction materials has gained particular relevance. Within this framework, the present study evaluates the utilization of industrial solid residue (ISR) generated during TiO_2 extraction for pigment production as an additive in cementitious matrices, aiming both to ensure the environmentally responsible disposal of this waste and to harness the photocatalytic potential of the residual TiO_2. Specifically, the research investigates the incorporation of 15% ISR into structural self-compacting concrete (fck ≥ 30 MPa), assessing its influence on key physical and mechanical properties, with emphasis on apparent porosity, water absorption, and axial compressive strength. Experimental results revealed marked increases in water absorption (12.03% for ISR vs. 6.73% for REF), void index (24.23% vs. 14.56%), and capillary absorption (1.71 g/cm² vs. 0.86 g/cm²), alongside a reduction in compressive strength (31.32 MPa vs. 32.61 MPa). These findings indicate that ISR incorporation significantly modifies the concrete microstructure, promoting greater capillary pore formation and diminishing mechanical performance. While the resulting material complies with applicable technical standards, the observed microstructural changes underscore the need for further durability investigations to fully ascertain the long-term implications for service life and structural performance.

Keywords: Self-Compacting Concrete. Absorption. Axial Compression. Residue. Porosity.

Abbreviations: ISR, Industrial Solid Residue, REF, Reference.

In the current international context, strategies aimed at minimizing energy consumption and the carbon footprint generated by goods and human activities are expanding. The construction industry plays a significant role in the global environmental scenario, accounting for a considerable share of natural resource consumption and waste generation [1]. Population growth and the high demand for construction have resulted in large volumes of waste and increased exploitation of natural resources. In this scenario, sustainable solutions have gained prominence, particularly the reuse of industrial waste by incorporating it into, or converting it into, construction materials. The utilization of such environmental liabilities—materials that would otherwise be landfilled or improperly disposed of, leading to environmental pollution—is of paramount importance and is considered in determining the carbon footprint and energy consumption of products [2,3].

Based on this premise, the incorporation of Industrial Solid Residue (ISR), generated during the TiO_2 extraction process for pigment production, into a cementitious matrix aims not only to ensure proper disposal of this environmental liability but also to harness the photocatalytic potential of the residual TiO_2 that could not be recovered from the ore, thereby rendering the resulting product photocatalytic.

This approach holds significant importance for the construction sector [4,5].

In this study, the influence of adding 15% ISR to a structural self-compacting concrete will be

Received on 15 February 2026; revised 20 April 2026.

Address for correspondence: Pedro Victor Correia e Reis. Avenida Orlando Gomes, 1845 - Piatã. Salvador, Bahia, Brazil. Zipcode: 41650-010. E-mail: pedro.victor@fbest.org.br.

J Bioeng. Tech. Health 2026;9(5):423-429

evaluated, with the objective of analyzing how the incorporation of the residue into the cementitious matrix may affect the physical and mechanical properties of the concrete.

Materials and Methods

Materials

ISR – Unreacted Ore

The industrial solid residue containing titanium dioxide (ISR) used in this study is presented as a pulverized solid with irregular particle size distribution, as shown in Figure 1. For concrete production, the residue was employed in its natural form, without undergoing any additional grinding process.

Figure 1. Titanium dioxide residue.

The particle size distribution indicates a broad distribution of particles in the sample, with an average size of 22.334 µm (micrometer). The particle volume distribution according to particle size was obtained, indicating the percentage of particle size present in the sample, where 10% of the particles are smaller than 2.687 µm, 50% are smaller than 16.381 µm, and 90% are smaller than 47.281 µm. The results show that the average diameter of the residue is less than 75 µm.

The particle size distribution of the residue was established using a PSA 1190L laser particle size analyzer from Anton Paar Brasil. To analyze particle size distribution, the residue had to be dispersed in ethyl alcohol.

Laser particle size analysis is a technique based on the sedimentation of suspended particles. This method uses light absorption to accurately measure the particle size of the material, providing a detailed understanding of particle size distribution.

Fine Aggregate

The fine aggregate consists of natural quartz sand, with a fineness modulus of 1.56 mm and a maximum particle size of 2.36 mm, sourced from deposits in Barra de Pojuca, Camaçari/BA, as illustrated in Figure 2.

Figure 2. Fine sand.

For concrete production, the sand was used in a dry state after oven-drying to ensure the absence of moisture. In industrial-scale production, where the sand is exposed to ambient conditions, it is recommended that moisture content be determined and controlled, and the water present in the sand be compensated for in the concrete mix.

Coarse Aggregate

The coarse aggregate used is crushed stone, with a characteristic maximum particle size of 12.5 mm (commonly referred to as “brita 0”), as shown in Figure 3.

Figure 3. Brita 0.

Cement

The cement used in this study was CP V-ARI RS produced according to the parameters stipulated by ABNT NBR 16697:2018 (Portland Cement – Requirements) [6] (Figure 4).

Figure 4. CP V-ARI RS.

CP V-ARI (High Early Strength Portland Cement) is a type of Portland cement specially formulated to provide high early strength. It is widely used in constructions requiring rapid formwork removal or when accelerating the project schedule is desired. This cement achieves high mechanical strength at early ages due to its high clinker content and low limestone filler addition.

Admixture

The admixture used in this study was a superplasticizer (Figure 5), classified as a normal setting admixture for Portland cement concrete. It is a liquid substance composed of polycarboxylates, which are macromolecules employed as high-efficiency dispersants in cementitious matrices. These compounds reduce the material's viscosity and minimize the amount of water used in the mix by up to 45%.

Figure 5. Superplasticizer admixture.

The superplasticizer has a specific gravity of approximately 1.070 g/cm³ and acts through surface adsorption and steric separation effects on Portland cement particles during its hydration process.

Its primary advantage in relation to self-compacting concrete, the focus of this research, is the ability to adjust its dosage to meet stringent requirements for flowability, workability retention, and the reduction of cement and water consumption in the mixture.

Water

The mixing water used in the concrete production was sourced from the public supply network of Empresa Baiana de Água e Saneamento S.A. (Embasa).

Methods

Physical Properties

Determination of Absorption, Voids and Specific Gravity

The water absorption, void index, and specific gravity tests are conducted with the objective of evaluating the porosity and density of cementitious matrix materials such as concrete. These parameters are essential for understanding the durability and strength of the material.

The water absorption test in this study was performed according to the procedure described in ABNT NBR 9778:2005 (Hardened mortar and concrete – Determination of water absorption, void index, and specific gravity) [7], from which the values of Water Absorption (Equation 1), Void Index (Equation 2), and Real Specific Gravity (Equation 3) are obtained. The Bel Mark electronic scale, model K-200001, with a resolution of +0.1, was used to verify the mass of the test specimens.

Where:

$$A = \frac{m_{sat} - m_s}{m_s} \times 100 \quad (1)$$

m_{sat} = saturated mass after soaking (g);

m_s = dry mass (g).

Where:

$$Iv = \frac{m_{sat} - m_s}{m_{sat} - m_i} \times 100 \quad (2)$$

m_i = mass of the saturated sample immersed in water.

$$\rho_r = \frac{m_s}{m_s - m_i} \quad (3)$$

For the execution of the test, the specimens, at 28 days of curing, were initially placed in an oven at a temperature of 105 ± 2ºC. After 72 hours, the dry mass of the specimens was determined. Subsequently, the specimens were immersed in water at room temperature (23 ± 2ºC) for a period of 72 hours, after which their immersed mass was determined using a hydrostatic balance. Afterwards, the specimens were removed from the water, the excess surface moisture was wiped off with an absorbent cloth, and their mass was determined again, corresponding to the saturated condition. The oven used was the DL Type A.C, manufactured by Labomax.

Determination of Water Absorption by Capilarity

The capillary water absorption test was conducted to determine whether the porosity values obtained are directly related to the presence of capillary pores within the concrete structure, a crucial factor in assessing how material porosity affects durability and strength [8].

In this study, the test was performed according to the procedure described in ABNT NBR 9779:2012 (Hardened mortar and concrete – Determination of capillary water absorption) [9]. The results obtained from the test include capillary water absorption (Equation 6) and the height of internal capillary rise, which was measured following the diametral compression failure of specimens, in accordance with ABNT NBR 7222:2011 [10], after completing the partial immersion phase of the samples in water. The tests were conducted using an HD-150T servo-controlled press, manufactured by CONTENCO, with a maximum capacity of 150 tons-force and a resolution of 10 kgf.

$$C = \frac{m_{sat} - m_s}{S} \quad (6)$$

Where:

C = water absorption by capillarity;

S = cross-sectional area.

For the capillary water absorption test, the specimens, after 28 days of curing, were dried in an oven at a temperature of 105 ± 5ºC until a constant mass was achieved. Subsequently, the samples were cooled in a desiccator until reaching room temperature, and the initial dry mass was determined.

In the following step, the specimens were placed in trays containing a water layer of 5 ± 1 mm, ensuring that only the lower surface remained in contact with the water. During the test, the specimens were removed at predetermined time

intervals (3 min, 6 min, 15 min, 30 min, 1 h, 2 h, 3 h, 4 h, 6 h, 24 h and 48 h), the excess surface water was wiped off with an absorbent cloth, and the mass corresponding to each interval was measured.

Compressive Strength

The axial compressive strength of the concrete was evaluated in accordance with the standard ABNT NBR 5739:2018 – Concrete – Compression test of cylindrical specimens [11].

This procedure is essential for verifying the concrete's compliance with design specifications, ensuring that the material possesses the required load-bearing capacity.

The compressive strength, represented by the strength limit (fc), is quantified as the ratio between the maximum applied load (P_{max}) and the cross-sectional area (A) of the specimen, as expressed in Equation 7.

$$f_c = \frac{P_{máx}}{A} \quad (7)$$

Prior to testing, the specimens underwent capping on their upper and lower surfaces. This treatment was necessary to ensure the parallelism and flatness of the loading faces, promoting uniform stress distribution during the test.

Results and Discussion

Physical Properties

Absorption, Voids and Specific Gravity

After testing, the concrete containing the TiO_2 residue absorbed nearly twice the amount of water, in percentage terms, compared to the reference concrete, as illustrated in the graph in Figure 7. It is also notable that this factor influences the void index percentage, which is considerably higher in the 15% ISR mix than in the REF. These results are consistent with the literature [12,13]. However, the mix with residue addition exhibited a specific gravity 5.14% higher than that of the reference. The specific gravity values obtained through this test are not absolute, as they do not account for the impermeable pores present in the cementitious matrix product under evaluation [14,15].

Figure 7. Water absorption by immersion, void index, and specific gravity.

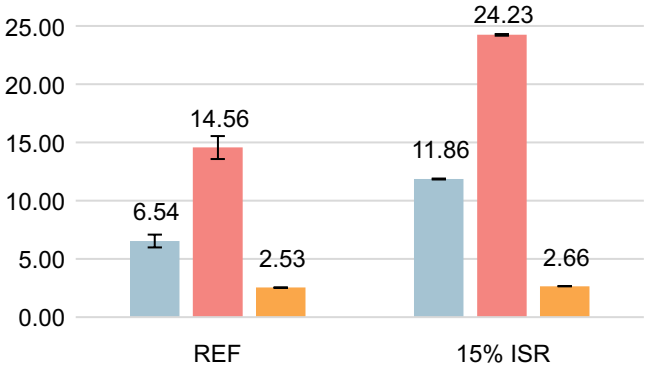

Water Absorption by Capillarity

The capillary absorption test demonstrated that the addition of 15% ISR results in a greater presence of capillary pores compared to the reference concrete, with an absorption value of 1.71 g/cm² after testing, whereas the REF exhibited 0.86 g/cm².

To confirm this result, graphs were generated from the absorption values, as shown in Figure 8, which illustrate the absorption behavior of each concrete and the trend line indicating the likely material response. It is notable from the generated graphs that the coefficient of the equation describing the behavior of the 15% ISR is significantly higher than that of the REF, which is consistent with the literature [16].

Compressive Strength

In the comparative analysis of the axial compressive strength test results of the mixes (Figure 9), it is observed that the incorporation of the residue leads to a reduction in the compressive strength of the concrete. This finding is

Figure 8. Absorption by capillarity – a) REF; b) 15% ISR.

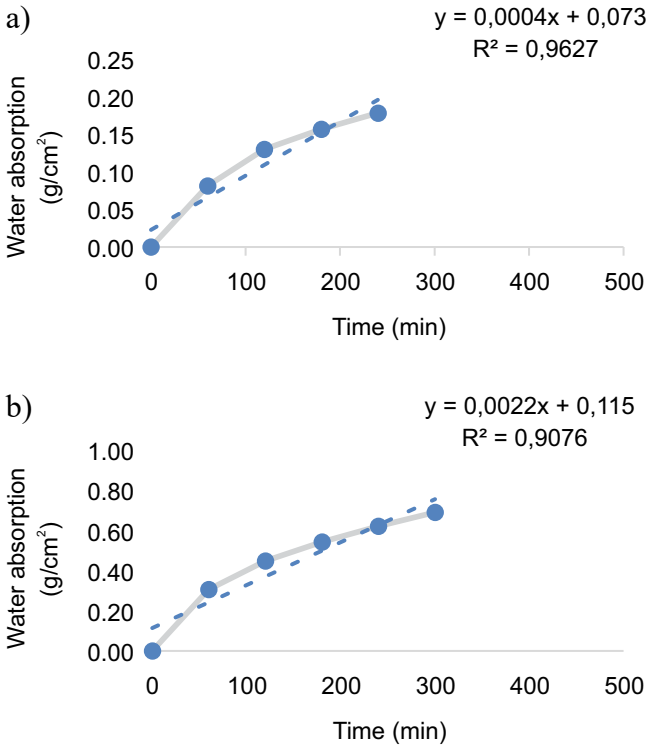

consistent with the previously presented physical characterization test results, as typically, the greater the amount of interconnected pores in concrete, the lower the quantity of cementitious matrix, which consequently decreases its compressive strength [17,18].

Another factor contributing to the notable reduction in compressive strength of the 15% ISR mix is likely associated with the higher content of solid particles in the system, which reduces the space available for the formation of hydration compounds, thereby decreasing the hydration reaction rate of the cementitious matrix [19].

The concrete with 15% residue addition, although exhibiting the lowest strength among the tested samples (31.37 MPa), still meets the minimum requirement established by ABNT NBR 6118:2023 [20], which specifies 30 MPa for applications in reinforced and prestressed concrete structural elements.

Figure 9. Axial compressive strength of concretes.

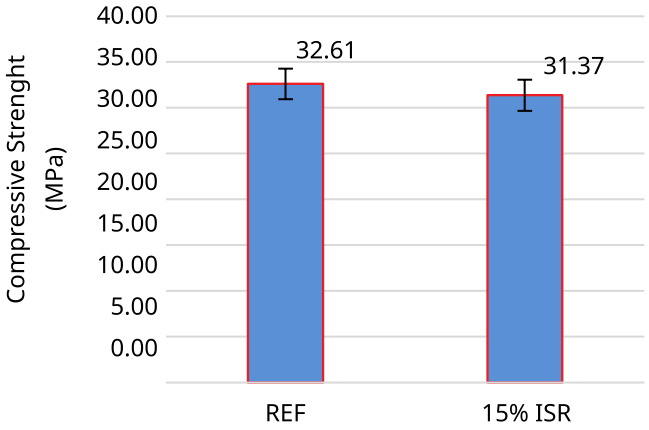

Conclusion

The present study evaluated the performance of self-compacting concretes incorporating titanium dioxide industrial solid residue (ISR), considering their properties in both fresh and hardened states. The results demonstrate that the addition of this residue significantly alters the physical and mechanical characteristics of the concrete, leading to an increase in capillary porosity and a consequent reduction in axial compressive strength. Based on the conducted analyses, there is a clear need to perform additional durability tests to estimate the material's service life. Although the concrete meets the normative requirements for compressive strength despite the reduction, evaluating its durability is essential to determine its long-term performance.

References

1. Gibson RK. The green building revolution. London: Routledge; 2018.
2. Ige OE, Olanrewaju OA, Duffy KJ, Obiora C. A review of the effectiveness of life cycle assessment for gauging environmental impacts from cement production. J Clean Prod. 2021;324:129213.
3. Santos PMN, Lied EB, Trevisan AP, Mprejon CFM. Evaluation of the reuse potential of industrial waste from TiO_2 production as aggregate for concrete manufacturing. In: 13th International Solid Waste Forum; 2022; São Paulo, Brazil.
4. Andrade Neto JS, Amorim Junior NS, Mariani BB, Albuquerque D, Ribeiro DV. Characterization of waste

from the production of titanium dioxide (UOW) for reuse in other processes. J Solid Waste Technol Manag. 2021;47(3):590-600.
5. Albuquerque DDM, Andrade JS, Amorim NS, Ribeiro DV. Properties of coating mortars containing waste from TiO_2 production (MNR). Cerâmica. 2019;65:340-50.
6. Associação Brasileira de Normas Técnicas. ABNT NBR 16697: Cimento Portland — Requisitos. Rio de Janeiro: ABNT; 2018.
7. Associação Brasileira de Normas Técnicas. ABNT NBR 9778: Argamassa e concreto endurecidos – Determinação da absorção de água, índice de vazios e massa específica. Rio de Janeiro: ABNT; 2005.
8. Medeiros-Junior RA, Munhoz GS, Medeiros MHF. Correlations between water absorption, electrical resistivity, and compressive strength of concrete with different pozzolan contents. Rev ALCONPAT. 2019;9(2):152-66.
9. Associação Brasileira de Normas Técnicas. ABNT NBR 9779: Argamassa e concreto endurecidos – Determinação da absorção de água por capilaridade. Rio de Janeiro: ABNT; 2012.
10. Associação Brasileira de Normas Técnicas. ABNT NBR 7222: Execução de revestimentos de argamassa. Rio de Janeiro: ABNT; 2011.
11. Associação Brasileira de Normas Técnicas. ABNT NBR 5739: Concreto – Ensaio de compressão de corpos de prova cilíndricos – Método de ensaio. Rio de Janeiro: ABNT; 2018.
12. Dong JF, Wang QY, Guan ZW. Structural behaviour of recycled aggregate concrete filled steel tube columns strengthened by CFRP. Eng Struct. 2013;48:532-42.
13. Verian KP, Ashraf W, Cao Y. Properties of recycled concrete aggregate and their influence in new concrete production. Resour Conserv Recycl. 2018;133:30-49.
14. Silva PR, Brito J. Experimental study of the porosity and microstructure of self-compacting concrete (SCC) with binary and ternary mixes of fly ash and limestone filler. Constr Build Mater. 2015;86:101-12.
15. Coutinho JS. Improvement of the durability of concrete by treatment of the moulding [thesis]. Porto: Faculty of Engineering, University of Porto; 1998.
16. Zhang SP, Zong L. Evaluation of relationship between water absorption and durability of concrete materials. Adv Mater Sci Eng. 2014;2014:1-8.
17. Conceição ALSF, Mariani BB, Reis PVC, Santana ISA, Santos PMMN, Rivetti MLS. Properties of self-compacting concrete with the incorporation of titanium dioxide (TiO_2)-rich residue. In: Proceedings of the 65th Brazilian Concrete Congress (CBC 2024); 2024; Salvador, Brazil. Salvador: IBRACON; 2024.
18. Rivetti MLS, Mariani BB, Santos HCM, Garcez AP, Reis PVC, Santos PMMN. Properties of self-compacting concrete with the incorporation of titanium dioxide (TiO_2)-rich residue – Part 2. In: Proceedings of the 66th Brazilian Concrete Congress (CBC 2025); 2025; Salvador, Brazil. Salvador: IBRACON; 2025.
19. Scrivener K, Juilland P, Monteiro PJM. Advances in understanding hydration of Portland cement. Cem Concr Res. 2015;78(Pt A):38-56.
20. Associação Brasileira de Normas Técnicas. ABNT NBR 6118: Projeto de estruturas de concreto – Procedimento. Rio de Janeiro: ABNT; 2023.

An Intelligent Data Platform for Older Adults Health Monitoring Using Wearable Technologies

Lucas de Freitas Gomes[1]*, Raimar Barbosa Santos[1], Arlindo Bastos de Miranda Neto[1], João Vitor Silva Mendes[2], Herman Augusto Lepikson[1,2]

[1]SENAI CIMATEC University, GETEC Department; [2]Federal University of Bahia, Mechatronics Department; Salvador, Bahia, Brazil

The aging of the global population has intensified the demand for innovative and sustainable healthcare strategies. Wearable technologies stand out as a promising alternative to enable real-time monitoring, early detection of clinical changes, and the promotion of autonomy and well-being among the older adults. This study presents a proposal for an integrated data platform aimed at monitoring elderly health through wearable devices. The proposed architecture comprises biometric sensors, secure wireless connectivity, intelligent data processing using machine learning algorithms, and interactive dashboards for decision-making. Through a comprehensive literature review and analysis of current applications, the platform was designed to ensure interoperability with healthcare systems, compliance with data protection laws, and usability for older adults. The results point to the potential of wearable technologies to support preventive, personalized, and population-based care models. Future challenges include issues of data integration, user acceptance, cost-effectiveness, and regulatory frameworks. The implementation of such platforms may contribute significantly to transforming the current healthcare model into a more inclusive, proactive, and data-driven system.

Keywords: Wearable Devices. Elderly Health. Health Monitoring. Digital Health. Integrated Platform. Preventive Care.

The accelerated growth of the elderly population represents one of the greatest challenges in contemporary public health. According to data from the World Health Organization (WHO), the global population aged 60 and over will reach approximately 2 billion by 2050, more than double the total recorded in 2020 [1]. This highlights the urgent need for strategies focused on healthy aging.

Current healthcare systems face problems such as overburdened services, high hospital costs, and a shortage of professionals for long-term care. In response, digital technologies, such as wearable devices are increasingly being adopted. These devices allow for the continuous and non-invasive collection of physiological data. Devices like smartwatches, wristbands with biometric sensors, and clothing with sensory fabrics have been used to measure heart rate, blood pressure, body temperature, blood oxygenation, and patterns of sleep and physical activity. The integration of this data with systems based on the Internet of Things (IoT), Artificial Intelligence (AI), and clinical decision support platforms is consolidating a new paradigm of care – proactive, remote, and person-centered [2].

The use of these technologies is especially promising in providing healthcare for the elderly population, as it enables the early detection of critical events, the monitoring of chronic diseases, and the promotion of autonomy and well-being. However, despite these advancements, there are still gaps concerning system interoperability, the reliability of the data collected, and the privacy of users' sensitive information.

Considering this, this article aims to present a proposal for an integrated data platform to monitor the health of the elderly based on wearable technologies. The proposal stems from a technical and scientific review of the state-of-the-art of existing devices, sensors, and systems, and moves forward to build an architecture that supports continuous care, with a focus on quality of life, safety, and healthcare efficiency based on intelligent analysis.

Received on 25 February 2026; revised 23 April 2026.
Address for correspondence: Lucas de Freitas Gomes. Av. Orlando Gomes, 1845 - Piatã, Salvador – BA – Brazil, Zipcode: 41650-010. E-mail: lucas.gomes@fieb.org.br.

J Bioeng. Tech. Health 2026;9(5):430-435

Theoretical Framework

The evolution of wearable technologies over the past few decades has driven profound transformations in how individuals interact with their health. Initially designed as devices for sports performance or personal automation, wearables have become integrated into the digital health ecosystem, assuming a central role in data-driven care models, prevention, and remote care [3].

In general, wearable devices are equipped with sensors, wireless connectivity, and embedded processing systems, enabling the continuous collection of physiological data such as heart rate, temperature, blood oxygenation, body posture, physical activity, and sleep patterns, among others [4].

The scientific literature presents several taxonomies for these devices. Wearables applied to health can be classified into three categories: (i) sensors for continuous monitoring, (ii) devices for detecting critical events (such as falls and seizures), and (iii) systems to support clinical diagnosis [5]. In addition, Guk and colleagues [2] highlights the emergence of integrated platforms based on artificial intelligence algorithms, capable of interpreting large volumes of data and providing personalized and predictive responses.

The integration of these devices with the Internet of Medical Things (IoMT) and telehealth platforms has broadened their applicability, especially in supporting the management of chronic conditions like hypertension, diabetes, arrhythmia, and respiratory diseases. Akinwande and colleagues [6] present a conceptual framework where sensors interact with mobile gateways, cloud, and clinical systems, promoting a continuous cycle of data acquisition, processing, storage, and analysis.

In addition to traditional sensors, recent research has demonstrated the growing use of advanced and flexible materials, such as graphene, to create ultrathin, skin-adherent devices (e-skin) [7].

The concept of AAL (Ambient Assisted Living) also reinforces the importance of wearable technology in the context of population aging. AAL proposes smart environments where sensors, mobile devices, and algorithms cooperate to promote safety, comfort, and independence for older adults or individuals with reduced mobility [8].

Based on these models and advancements, wearable technologies hold a strategic position for the creation of digital platforms that connect users, caregivers, healthcare professionals, and managers in a data ecosystem geared towards clinical decision-making and personalized care.

Wearable Technologies and Health Applications

The application of wearable technologies in the healthcare field has evolved beyond basic monitoring to encompass advanced functionalities, including the prediction of critical events, rehabilitation support, quality of life assessment, and personalized therapeutic management. The most used sensors in wearables include accelerometers, gyroscopes, heart rate sensors, photoplethysmography (PPG), electrocardiography (ECG), temperature sensors, and electrochemical biosensors. These sensors can detect and record physiological variables with high accuracy, providing essential data for realtime or retrospective analysis [9].

Studies show that wearable devices have great potential in monitoring chronic diseases. Patients with heart failure, for example, can use sensor-equipped wristbands and vests to identify variations in heart rate or respiratory patterns, enabling early interventions [10]. In the case of elderly individuals with Alzheimer's or Parkinson's, wearables have been used for tracking mobility, episodes of disorientation, and fall detection, allowing caregivers or medical teams to be alerted immediately [11].

Furthermore, wearables are being incorporated into telehealth and remote physiotherapy, with sensors integrated into clothing and accessories that assist in the correct performance of exercises, post-operative recovery, and adherence to personalized therapeutic plans.

Companies and startups have played a central role in the innovation of this market. Silvertree, for example, develops smart wristbands for the elderly that combine GPS tracking, fall detection, and emergency communication. Hinge Health, in turn, offers digital solutions for musculoskeletal rehabilitation through motion sensors and personalized algorithms [12]. Philips has developed clinical-grade biosensors for hospital and home use, focusing on monitoring patients with acute or chronic conditions, and integrating with electronic health platforms [13].

In the context of the elderly, these applications still face challenges related to acceptance, ergonomics, technological understanding, and connectivity. Nevertheless, studies show that when properly implemented, wearables promote a greater sense of security, a reduction in hospitalizations, and an improvement in quality of life [14].

Proposal for an Integrated Platform for Elderly Monitoring

Based on scientific evidence and observed technological advancements, we propose an integrated digital platform for the continuous and intelligent health monitoring of the elderly using wearable technologies. This platform aims to support both self-care and the work of caregivers and healthcare professionals, with a focus on prevention, early detection of adverse events, and personalized care.

The platform's architecture is shown in Figure 1, based on four main layers: (1) wearable sensors, (2) connectivity and data collection, (3) intelligent processing and analysis, and (4) visualization and decision-making.

- **Wearable sensors:** These include devices such as wristbands, smartwatches, chest straps, and skin patches equipped with sensors for heart rate, blood pressure, oxygen saturation (SpO_2), temperature, and movement. Such sensors must be lightweight, comfortable, energy-efficient, and calibrated for geriatric profiles.
- **Connectivity and data collection:** The sensors communicate with local gateways (such as smartphones or home hubs) via Bluetooth Low Energy (BLE), ZigBee, or Wi-Fi. These gateways organize the data, apply compression, and transmit it to cloud servers with security and end-to-end encryption.

Figure 1. Proposed architecture of the wearable-based elderly health monitoring platform.

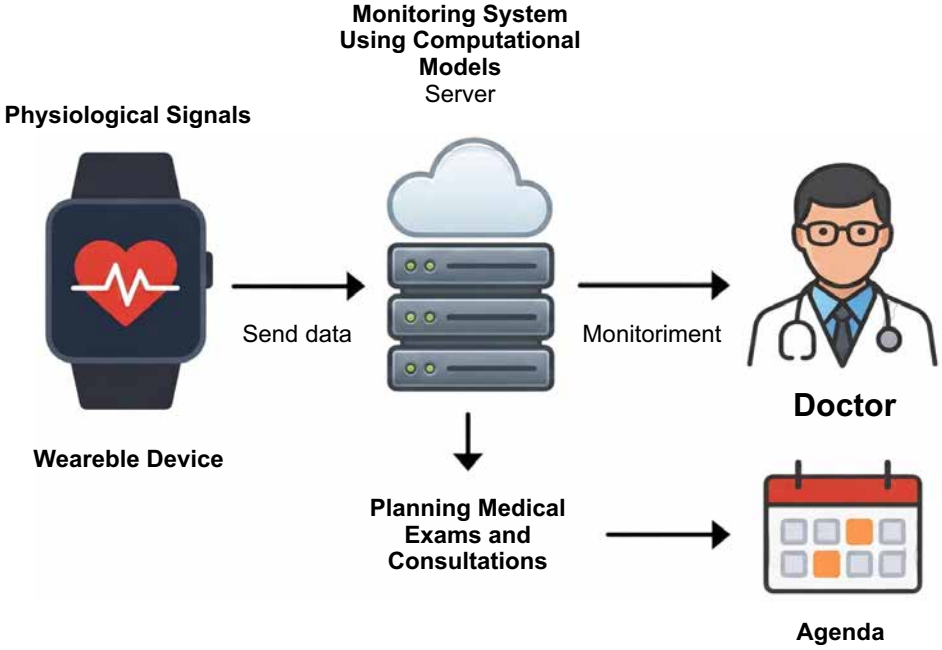

- **Intelligent processing and analysis:** The received data is stored in a secure database and processed by machine learning algorithms. These algorithms identify patterns, detect anomalies, generate automatic alerts, and make predictions based on individual history and risk profiles.
- **Visualization and decision-making:** The analysis results are presented on dashboards accessible via an application (for the user and caregiver) and a web platform (for healthcare professionals). The visualizations include trends, health alerts, emergency notifications, care plans, and comparisons with population standards.

This platform stands out by integrating continuous and heterogeneous data into a system that learns from each user's behavioral patterns, enabling the automatic sending of alert messages in situations such as a sudden increase in blood pressure, risk of falling, prolonged absence of movement, or variation in heart rate. Furthermore, the platform can send monthly health reports to family members, government, or institutions, promoting greater engagement and transparency in care, clearly aligned with data protection regulations.

The platform also incorporates interoperability features with public health systems, such as electronic health records based on HL7 and FHIR standards, expanding its potential for integration with clinics, primary care units, and hospitals. This creates an ecosystem where clinical intelligence is fed back with real-world daily data, optimizing medical decisions and reducing preventable hospitalizations.

As a use case, consider an elderly person living alone who uses a smartwatch connected to a dermal biosensor. The device continuously monitors blood pressure, heart rate, and mobility. If the system detects a fall followed by immobility, an alert is sent to the monitoring center and the registered caregiver. If the patient is at risk, the system can automatically trigger emergency services and share relevant clinical data.

The proposal's distinct advantage also lies in its capacity for population analysis. By aggregating and anonymizing data, public administrators can identify epidemiological patterns in specific regions (e.g., blood pressure spikes, syncope episodes), guiding public policies and health surveillance actions.

The project also provides for the use of best practices in information security, with compliance with the General Data Protection Law (LGPD), multifactor authentication, profile-based access control, and auditing of access logs.

Challenges and Future Prospects

Despite significant advances in integrating wearable technologies into healthcare, especially for the elderly, several challenges still limit their widespread, sustainable, and safe adoption. These challenges are related not only to the technological infrastructure but also to social, economic, regulatory, and cultural barriers.

Interoperability and Integration with Healthcare Systems

One of the main challenges with wearable device solutions is the lack of communication between them and healthcare systems. Many of these solutions use proprietary, non-open data formats, which hinders integration with electronic health records and other systems. To address this, the adoption of standards such as HL7 FHIR is essential to ensure that healthcare professionals [15] can efficiently utilize sensor data.

Privacy, Security, and Legal Compliance

The constant collection of sensitive data by wearable devices raises legitimate concerns about privacy and security. Information such as location, heart rate, sleep, movement patterns, and biometric data must be protected from unauthorized access. The General Data Protection Law (LGPD) in Brazil, as well as international regulations like

Europe's General Data Protection Regulation (GDPR) and the U.S. Health Insurance Portability and Accountability Act (HIPAA), require robust mechanisms for access control, explicit consent, encryption, and auditing [16].

Studies show that digital literacy and user-centered design focused on the elderly are determining factors for the acceptance of technology in sensitive contexts such as healthcare [17].

Usability and Acceptance Barriers

Another critical factor relates to device usability. For wearables to be effective in elderly populations, factors such as ergonomics, interface legibility, ease of charging, comfort during prolonged use, and simplicity of handling must be considered.

In a systematic review, it was observed that the acceptance of wearables among the elderly strongly depends on factors like perceived usefulness, trust in the technology, and available technical support [17].

Financial Sustainability and Scalability

The cost of wearable devices, as well as the infrastructure for connectivity, cloud storage, and technical support, still represents a barrier to their large-scale implementation. Although prices are gradually decreasing, public and private healthcare programs are still reluctant to invest in medium and long-term solutions without robust evidence of cost-benefit [18].

Cost-effectiveness studies, such as those conducted by Wang and colleagues [19], show that the use of wearables can reduce preventable hospitalizations and improve the management of chronic diseases, but their effectiveness depends on the quality of the data collected, user adherence, and integration with structured clinical workflows.

Future Perspectives

The outlook for the coming years is promising. Devices are expected to become even more miniaturized, autonomous, and multifunctional, incorporating new sensors, sustainable energy sources (such as flexible solar cells), 5G connectivity, and integration with virtual assistants.

The use of Artificial Intelligence and predictive models based on real-world data will enable systems to predict critical conditions even before visible symptoms appear. The consolidation of integrated platforms will also enable health managers to use aggregated data to guide epidemiological decisions and real-time preventive actions.

Furthermore, the advancement of technologies like Blockchain can ensure greater reliability in the traceability and integrity of medical data, facilitating secure sharing among different institutions and professionals [20].

As a result, wearable technologies are expected to take on a prominent role not only as monitoring tools but as central instruments in a new paradigm of care that is predictive, personalized, participatory, and population-based.

Conclusion

Population aging poses a major challenge to healthcare. Therefore, innovative strategies are needed to ensure the quality of life, autonomy, and safety of the elderly. In this scenario, wearable technologies emerge as a promising solution for continuous health monitoring, aiding in clinical decision-making and disease prevention.

This article proposes an integrated platform to monitor the health of older adults through wearable devices, using physiological sensors, secure connectivity, intelligent data processing, and intuitive visualization tools. This ecosystem aims to be useful for both patients and healthcare professionals.

The integration of these devices into public and private health strategies could transform care, making it proactive, data-driven, and focused on prevention and personalized service. However, the success of this implementation requires overcoming challenges related to interoperability,

data privacy, usability for the elderly population, and the economic viability of the solutions.

In summary, wearable technologies, combined with integrated and user-centered platforms, offer not only a new model of care but also a strategic opportunity to transform the healthcare system, making it more inclusive, intelligent, and prepared for the challenges of the 21st century.

References

1. World Health Organization. Decade of healthy ageing: baseline report. Geneva: World Health Organization; 2021.
2. Guk K, Han G, Lim J, Jeong K, Kang T, Lim EK, et al. Evolution of wearable devices with real-time disease monitoring for personalized healthcare. Nanomaterials (Basel). 2019;9(6):813. doi:10.3390/nano9060813.
3. Bonato P. Wearable sensors and systems: from enabling technology to clinical applications. IEEE Eng Med Biol Mag. 2010;29(3):25-36.
4. Majumder S, Mondal T, Deen MJ. Wearable sensors for remote health monitoring. Sensors (Basel). 2017;17(1):130.
5. Pantelopoulos A, Bourbakis NG. A survey on wearable sensor-based systems for health monitoring and prognosis. IEEE Trans Syst Man Cybern C Appl Rev. 2010;40(1):1-12.
6. Islam SMR, Kwak D, Kabir MH, Hossain M, Kwak KS. The Internet of Things for health care: a comprehensive survey. IEEE Access. 2015;3:678-708.
7. Akinwande D, Kim DH, Lu N, Rogers JA. Graphene electronic tattoos for biometric monitoring: opportunities and challenges. ACS Nano. 2017;11(9):8853-9. doi:10.1021/acsnano.7b03261.
8. Rashidi P, Mihailidis A. A survey on ambient-assisted living tools for older adults. IEEE J Biomed Health Inform. 2013;17(3):579-90.
9. Patel S, Park H, Bonato P, Chan L, Rodgers M. A review of wearable sensors and systems with application in rehabilitation. J Neuroeng Rehabil. 2012;9:21.
10. Reddy RK, et al. Mobile Heart Health: project highlighting the use of wearable devices for early detection of cardiac events. J Med Internet Res. 2020;22(10):e19138.
11. Hayes TL, Larimer N, Adami A, Kaye JA. Unobtrusive assessment of activity patterns associated with mild cognitive impairment. Alzheimers Dement. 2008;4(6):395-405.
12. Howarth J. Wearable startups to watch [Internet]. Exploding Topics; 2024 [cited 2026 Jun 18]. Available from: https://explodingtopics.com/blog/wearable-startups
13. Sharp N. Wearable medical devices transforming patient care [Internet]. ESCATEC Blog; 2024 [cited 2026 Jun 18]. Available from: https://www.escatec.com/blog/wearable-medical-devices
14. Mercer K, Li M, Giangregorio L, Burns C, Grindrod K. Acceptance of commercially available wearable activity trackers among adults aged over 50 and with chronic illness: a mixed-methods evaluation. JMIR Mhealth Uhealth. 2016;4(1):e7.
15. Mandel JC, Kreda DA, Mandl KD, Kohane IS, Ramoni RB. SMART on FHIR: a standards-based, interoperable apps platform for electronic health records. J Am Med Inform Assoc. 2016;23(5):899-908.
16. Brasil. Lei nº 13.709, de 14 de agosto de 2018. Lei Geral de Proteção de Dados Pessoais (LGPD) [Internet]. Brasília (DF): Presidência da República; 2018. Available from: http://www.planalto.gov.br
17. Peek STM, Wouters EJM, van Hoof J, Luijkx KG, Boeije HR, Vrijhoef HJM. Factors influencing acceptance of technology for aging in place: a systematic review. Int J Med Inform. 2014;83(4):235-48.
18. Giansanti D. Investigating wearable health monitoring systems: state of the art and future challenges. Sensors (Basel). 2020;20(20):5717.
19. Wang L, et al. A systematic review of cost-effectiveness of digital health interventions in cardiovascular disease. J Med Internet Res. 2021;23(2):e24007.
20. Vazirani AA, O'Donoghue O, Brindley D, Meinert E. Implementing blockchain for efficient health care: systematic review. JMIR Med Inform. 2020;8(2):e13549.

Evaluation of the Bioactive Compounds Present in Peanut Skin (*Arachis hypogaea* L.) for Antioxidant and Antifungal Activity

Letícia de Lima Santos Ferreira[1]*, Clidejane Oliveira Bastos Ribeiro[1], Elivandra de Oliveira Simão[1], Felipe de Oliveira Aragão[1], Érica Patrícia Lima Pereira[2]

[1]SENAI CIMATEC University; [2]SENAI CIMATEC University, Industrial Microbiology; Salvador, Bahia, Brazil

Studies on peanuts (*Arachis hypogaea* L.) have shown that this food is rich in beneficial substances such as phenolic compounds and flavonoids. Peanut skin, the reddish-pink layer that surrounds the seed, is considered a by-product of processing and has a rich nutritional composition, containing a variety of phenolic compounds, including resveratrol and flavonoids, especially proanthocyanidins and their derivatives, which are predominant. These compounds have high antioxidant capacity and are able to neutralize free radicals, reducing oxidative stress associated with several chronic diseases. Some phenolic compounds also exhibit antifungal activity by inhibiting cell wall synthesis or altering fungal membranes. This study aimed to evaluate the presence and activity of phenolic compounds in peanut skin, focusing on antioxidant and antifungal properties. Ethanol extracts were tested through spectrophotometric quantification of total phenolics, flavonoids, and tannins, antioxidant activity using the DPPH method, and antifungal activity via agar disk diffusion against *Fusarium* sp. The extract showed strong antioxidant activity and high levels of phenolic compounds but limited antifungal activity. These findings support the potential of peanut skin compounds in food and pharmaceutical applications.
Keywords: Peanut Skin. Phenolics. Antioxidant. *Fusarium* sp.

Peanut (*Arachis hypogaea* L.) is a legume native to South America, cultivated in tropical and subtropical countries. One of the by-products generated after its processing is the peanut skin.

The composition of peanuts varies according to climate and soil conditions, consisting mainly of 41% carbohydrates, 10 to 20% lipids, 19% proteins, and 18% fiber. Peanut skin, in turn, is composed of a variety of phenolic compounds, such as resveratrol and flavonoids, with high antioxidant capacity and the ability to inhibit enzymes that are precursors of disorders and diseases [1].

Research on new natural bioactive substances has increased significantly in recent years, and their various health benefits are being increasingly elucidated and disseminated. Among these substances, antioxidants stand out, compounds capable of combating oxidative damage caused by free radicals, with wide applications in the pharmaceutical, cosmetic and food industries [2].

Brazil's economy is strongly based on agribusiness, which generates a large volume of byproducts that can harm the environment. However, according to studies, peanut skin has potential for the development of new products in various fields. Therefore, the main objective of this study is to evaluate the bioactive compounds present in peanut skin and their antioxidant potential and antifungal activity against the fungus *Fusarium* sp.

Materials and Methods

The present study is a qualitative-quantitative exploratory study, employing procedures such as literature review and experimental research.

Preparation of Peanut Skin Extract (*Arachis hypogaea* L.)

The peanut skins (*Arachis hypogaea* L.) used in this study were provided by the cereal company NP Zanchetta, located in Borborema, São Paulo, Brazil.

Received on 18 February 2026; revised 23 April 2026.
Address for correspondence: Letícia de Lima Santos Ferreira. Av. Orlando Gomes, 1845 - Piatã, Salvador – BA – Brazil, Zipcode: 41650-010. E-mail: leticia.santos17@ba.estudante.senai.br.

J Bioeng. Tech. Health 2026;9(5):436-442

The extract was prepared by the maceration process, at a ratio of 1:3.5 (dry mass:solvent), using ethyl absolute alcohol for 48 hours [3]. The pure ethanolic extract (EE) was obtained through simple distillation.

The extraction percentage yield was calculated using the equation 1, proposed by Xiao and colleagues [4], where the yield (%) is obtained by dividing the mass of the pure extract (mo), in grams, by the mass of the dehydrated biomass (mf) of derived from the agro-industrial residue of peanut skin, and then multiplying the result by 100 to obtain the percentage:

$$Yield(\%) = mo/mf \; x \; 100 \quad (1)$$

Quantification of Total Phenolics

Total phenolic compounds (TPC) were evaluated using the spectrophotometric method with 6% Folin–Ciocalteu reagent [5], with modifications. A standard curve was established using different concentrations of gallic acid (20 to 100 mg/L).

Four different concentrations (100, 10, 1, and 0.1 mg/mL) of the ethanolic extract from peanut skin were tested.

To perform the analysis, 0.25 mL of each extract concentration was pipetted into test tubes, followed by 2.75 mL of Folin–Ciocalteu reagent. The mixture was homogenized, and after 5 minutes, 0.25 mL of 10% sodium carbonate was added.

After 1 hour of incubation protected from light, the absorbance was measured at 755 nm using a spectrophotometer. All assays were performed in triplicate.

Flavonoid Quantification

The determination of total flavonoids was carried out, with modifications, according to the method described by Silva and colleagues [6]. Aliquots of 500 µL from different concentrations (100, 10, 1, and 0.1 mg/mL) of the ethanolic extract were added to analytical-grade methanol and a 2% methanolic solution of aluminum chloride ($AlCl_3$). After 30 minutes, the absorbance was measured at 415 nm using a spectrophotometer. All assays were performed in duplicate.

Quantification of Tannins

The quantification of total tannin content was performed using the method described by Pansera and colleagues [7], with modifications, using tannic acid as the standard. Two different concentrations (0.008 and 0.08 mg/mL) of the ethanolic extract were used.

To each 1 mL aliquot of extract, 1 mL of Folin–Ciocalteu reagent was added. Then, 1 mL of 8% sodium carbonate solution was added to the mixture, which was shaken and left to rest for 2 hours, protected from light. After this period, the absorbance was measured at 725 nm using a spectrophotometer. All assays were performed in duplicate.

Antioxidant Activity

Antioxidant activity was determined using the 2,2-diphenyl-1-picrylhydrazyl (DPPH) free radical method, as described by Rufino and colleagues [8], with modifications. For this procedure, a previously prepared DPPH solution was used, along with the test substance at four different concentrations (100, 10, 1, and 0.1 mg/mL). In this assay, 50% methanol and 70% acetone were also used as reference substances.

Each determination consisted of 3.9 mL of DPPH solution and 100 µL of the test concentration. The control reaction (blank) was performed using 4 mL of methanol. Absorbance readings were taken at 515 nm after 45 minutes of incubation at room temperature, protected from light, using a spectrophotometer. All assays were performed in duplicate.

Antioxidant activity (AA) was expressed according to equation 2, where Abs_{DPPH} is the initial absorbance of the 60 mM DPPH solution,

and Abs_{sample} is the absorbance of the reaction mixture [5].

$$AAT(\%) = \frac{\{[Abs_{DPPH} - (Abs_{sample} - Abs_{blank})]x100\}}{Abs_{DPPH}} \quad (2)$$

Agar Disk Diffusion Test

To evaluate the antifungal capacity of the ethanolic extract, tests were conducted using the agar disk diffusion method. A subculture of the main strain was made on Petri dishes containing PDA medium (Potato Dextrose Agar), previously sterilized in an autoclave (121 °C, 1 atm).

On each plate with the *Fusarium* sp. subculture, three sterile filter paper discs were placed 3 cm apart from each other and 1 cm from the edge of the plate. Then, 10 µL of the extract concentration was applied to each disc. The ethanolic extract was tested at two concentrations: 10 and 100 mg/mL. A control test was also performed to evaluate the effect of ethanol on the fungus, applying 10 µL of ethanol per disc. In the negative control, the fungus was not exposed to any degrading agent.

The disc tests were performed in triplicate, and all assays were duplicated.

The plates were incubated in a bacteriological oven at 28 °C for 7 days. After fungal growth, results were collected by measuring the diameter of the mycelium. The percentage of mycelial growth inhibition was calculated according to França [9], where dc is the average diameter of the control and dt is the average diameter of the fungus treated with the ethanolic extract (Equation 3).

$$\%mycelial\ inhibition = (dc\text{-}dt / dc) \times 100 \quad (3)$$

Results and Discussion

The obtained data reveal that the yield of the ethanolic extract of peanut skin (EEPS) was 2.8% in relation to the total biomass. The process for obtaining this value is shown in Table 1.

Quantification of Total Phenolics

At the concentration of 0.1 mg/mL, a total phenolic content (TPC) of 2.26% was observed. The 1 mg/mL concentration showed a TPC of 6.06%. At 10 mg/mL, the TPC reached 7.16%, and the highest percentage was observed at 100 mg/mL, with a TPC of 36.86%, as shown in Table 2.

The data indicates that increasing the concentration of the extract is associated with a higher total phenolic content, as illustrated in Figure 1, which compares the TPC values at each concentration analyzed.

A study also evaluated the phenolic content in peanut skin extracts using 80% ethanol as the solvent [10]. The TPC of the 25 mg/mL extract concentration from the IAC Runner 886 and IAC-Tatu-ST peanut varieties was determined, with values of 0.5438 mg GAE/g and 0.6478 mg GAE/g, respectively. These values are lower than those obtained in the present study, which may be attributed to the extraction procedure, evaporation techniques, and the concentrations used.

These findings highlight the importance of experimental conditions and confirm the potential of analytical-grade ethanol (P.A.) as a solvent to enhance the extraction of target compounds.

Determination of Flavonoids

Flavonoid content was expressed as a percentage of quercetin equivalence (QE). At the

Table 1. Representation of the calculated results using Formula 1.

Ethanolic Extract	Extract Yield in Grams	Dehydrated Biomass in Grams	Extraction Percentage
EEPA	16.85g	600g	2.80%

Table 2. Representation of total phenolic content in concentrations.

[] mg/mL	[] AG/mL	% Phenolic Content
0.1	3,596	2,266
1	9,626	6,066
10	11,371	7,166
100	58,499	36,866

Figure 1. Percentage of phenolic content at concentrations of 0.1, 1, 10 and 100mg/mL.

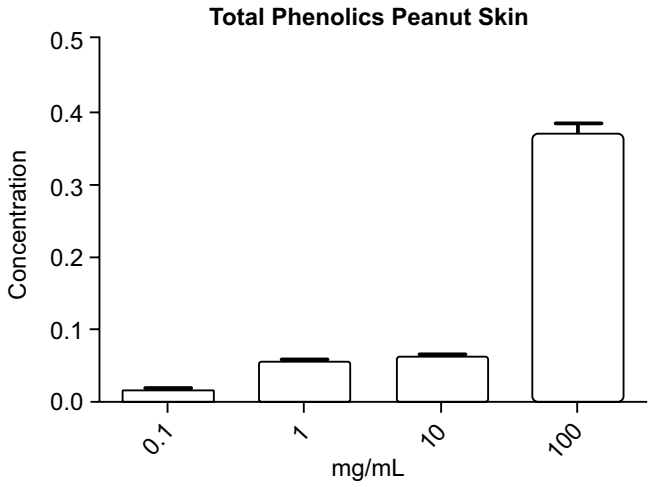

Table 3. Representation of flavonoids in concentrations.

[] mg/mL	QE %
0.1	7.70
1	8.70
10	9.20
100	177.70

Figure 2. Percentage of flavonoids at concentrations of 0.1, 1 and 10mg/mL.

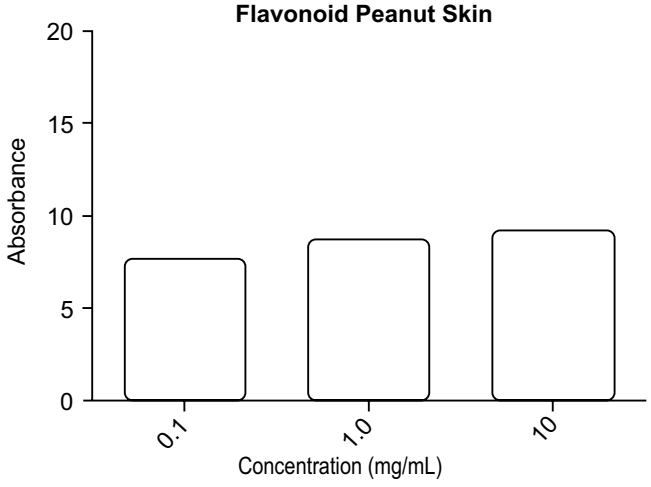

concentration of 0.1 mg/mL, the value obtained was 7.7% QE; at 1 mg/mL, it was 8.7% QE. For the 10 mg/mL concentration, the value was 9.2% QE. At 100 mg/mL, the value reached 177.7% QE, representing an exponential increase, as shown in Table 3 and illustrated in Figure 2, which compares the flavonoid content at each concentration.

The results obtained can be compared to those presented in another study [11], which employed a colorimetric method to evaluate the presence of flavonoids in eight legumes, reporting values ranging from 135 to 191 mg QE/g, which are higher than the data obtained in this study.

This difference may be related to several factors, such as the concentration analyzed, the solvent used for bioactive compound extraction, and the legume species.

Quantification of Total Tannins

At the concentration of 0.008 mg/mL, a total tannin content (TTC) of 0.017% was obtained, indicating a lower tannin level. At the concentration of 0.08 mg/mL, the TTC was 0.253%, demonstrating a considerable increase in tannin content at higher concentrations, as shown in Table 4 and Figure 3, which compares tannin levels at each concentration.

The results obtained can be compared with the values reported by Benevides and colleagues [12],

Table 4. Representation of tannins in concentrations.

[] mg/mL	TTP %
0.008	0.017
0.08	0.253

Figure 3. Percentage of tannins at concentrations of 0.008 and 0.08 mg/mL.

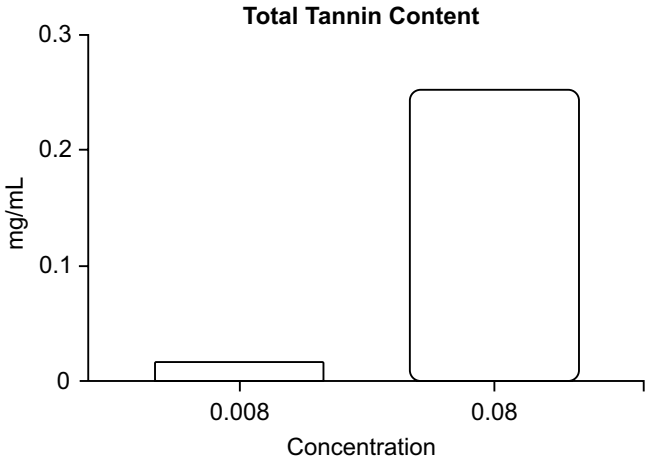

who evaluated the tannin content in legumes such as green beans and pigeon peas, finding values of 4.71 mg/100 g and 6.05 mg/100 g, respectively. These values are higher than those found in the present study, which may be attributed to differences in legume species and the method used for the quantification of this bioactive compound.

Antioxidant Activity of Peanut Skin Extract (*Arachis hypogaea* L.)

The results demonstrated that the peanut skin extract exhibits significant antioxidant activity at all tested concentrations (0.1, 1, 10, and 100 mg/mL). The 100 mg/mL EEPS concentration reached 95.7%, while the 10 mg/mL concentration achieved 91.8%, followed by 55.6% at 1 mg/mL, and 48% at 0.1 mg/mL. These values demonstrate an excellent antioxidant capacity of peanut skin, even at low concentrations, as illustrated in Figure 4.

When analyzing the data from this study alongside a research conducted by Diniyah and

Figure 4. Percentage of antioxidant activity at concentrations of 0.1, 1, 10 and 100 mg/mL.

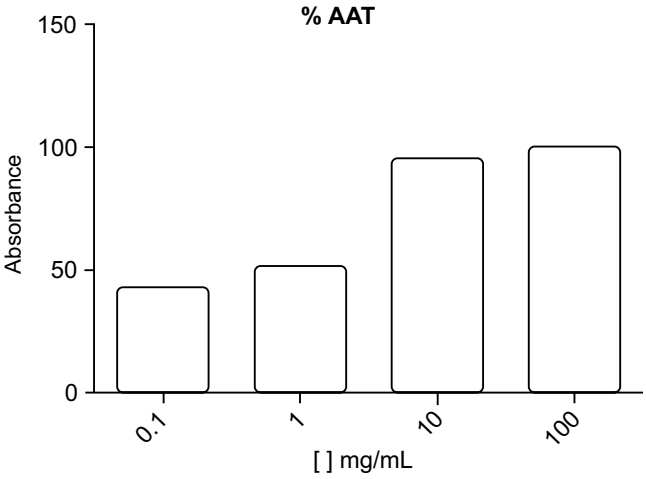

colleagues [13], which provides information on antioxidant activity in non-oilseed legumes, specifically *Phaseolus lunatus* and *Canavalia ensiformis*, it was shown that for the analyzed seeds, the amount required to reduce the initial DPPH concentration ranged from 1.83% to 19.42%.

These value variations may be related to several factors, such as the legume species, the extraction method of the target compound, and the solvent used.

Antifungal Activity of Extract on *Fusarium* sp.

After 7 days of incubation, mycelial growth was measured under treatment with the peanut skin extract. At the 10 mg/mL, an inhibition rate of 17.17%. However, at 100 mg/mL, the lowest inhibition percentage was recorded, at 13%, as shown in Table 5. Figure 5 displays images of mycelial measurements on the 7th day, along with the negative control and the solvent test, which is essential for evaluating the direct impact on fungal growth.

The average measurement of the negative control was conducted in duplicate, resulting in a value of 69 mm. The ethanol assays showed a moderate effect on fungal growth, exhibiting an inhibition rate of 14.13%.

Table 5. Representation of data from different concentrations of peanut skin extract under *Fusarium* sp. The mycelial mean value was calculated from a duplicate test.

Sample	Concentration	Mycelial Inhibition (%)
Peanut skin extract	10 mg/mL	17.17%
Peanut skin extract	100 mg/mL	13.0%
Ethanol Control	100%	14.13%
Negative Control	-	0 %

Figure 5. Mycelial growth measurement of *Fusarium* sp. isolate under treatment with ethanolic extract of peanut skin after 7 days of incubation. A) Peanut skin extract 10 mg/mL; B) Peanut skin extract 100 mg/mL; C) Ethanol control; D) Negative control.

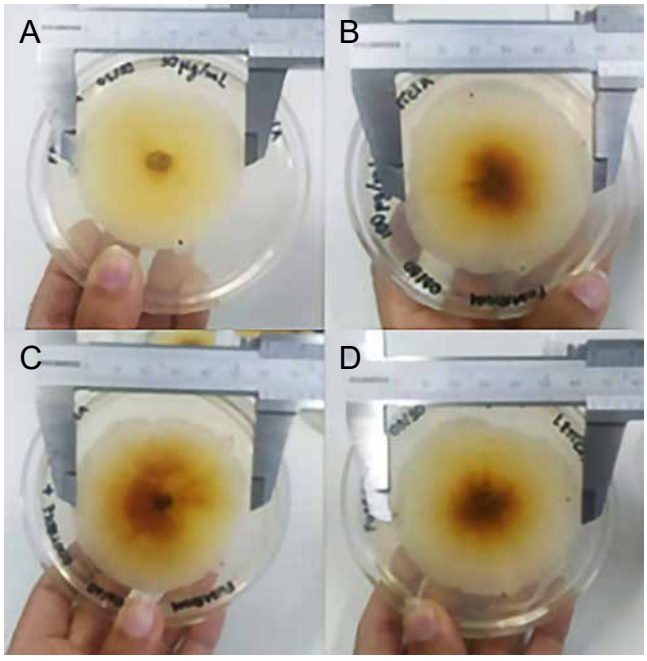

Although the extract demonstrated some inhibitory capacity, the mycelium was able to proliferate on the discs subjected to this treatment, which may be associated with several factors such as fungal resistance to the bioactive compounds.

In a study that investigated the antimicrobial effects of *Dioclea grandiflora* Mart. ex Benth, it was observed that the ethanolic extract of this plant did not exhibit inhibitory activity against *Fusarium* sp., whereas the hydroalcoholic extract showed a satisfactory response against dermatophytes [14].

This highlights the importance of evaluating different extraction methods and solvents to increase the amount of bioactive compounds and enhance antifungal activity.

Conclusion

This study showed that peanut skin (*Arachis hypogaea* L.) contains a significant amount of phenolic compounds, flavonoids, and tannins, attributing remarkable antioxidant properties to this by-product. It was observed that antioxidant activity is directly related to the concentration of the ethanolic extract, reaching values above 90% at higher concentrations. This highlights the extract's ability to neutralize free radicals.

Regarding antifungal activity, the results indicated limited inhibition against *Fusarium* sp. Future research may investigate solvent combinations or improvements in extraction techniques to increase the yield of compounds with antifungal properties and also explore their application in food and pharmaceutical systems, expanding their impact on health and sustainability.

References

1. Lorenzo JM, Munekata PES, Sant'Ana AS, Zhu Z, Barba FJ, Toldrá F, et al. Main characteristics of peanut skin and its role for the preservation of meat products. Trends Food Sci Technol. 2018;77:1-10. doi:10.1016/j.tifs.2018.04.007.

2. Camargo AC. Hurdles and potentials in value-added use of peanut and grape by-products as sources of phenolic compounds [thesis on the Internet]. Piracicaba: Universidade de São Paulo; 2016. Available from: http://www.teses.usp.br/teses/disponiveis/11/11141/tde-09112016-171820/
3. Braga GC, Melo PS, Bergamaschi KB, Tiveron AP, Massarioli AP, Alencar SM. Extraction yield, antioxidant activity and phenolics from grape, mango and peanut agro-industrial by-products. Cienc Rural. 2016;46(8):1498-504. doi:10.1590/0103-8478cr20150531.
4. Xiao J, Wang Y, Zhang Y, Liu X, Zhao Y, Li X, et al. Evaluation of yields and quality parameters of oils from *Cornus wilsoniana* fruit extracted by subcritical n-butane extraction and conventional methods. Grain Oil Sci Technol. 2022;5:204-12. doi:10.1016/j.gaost.2022.09.003.
5. Sousa CMM, Silva HR, Vieira-Júnior GM, Ayres MCC, Costa CLS, Araújo DS, et al. Fenóis totais e atividade antioxidante em cinco plantas medicinais. Quim Nova. 2007;30(2):351-5.
6. Silva JB, Rodrigues S, Feás X, Estevinho LM. Quantificação de fenóis, flavonoides totais e atividades farmacológicas de geoprópolis de *Plebeia aff. flavocincta* do Rio Grande do Norte. Pesq Vet Bras. 2016;36(9):874-80. doi:10.1590/S0100-736X2016000900014.
7. Pansera SR, Santos ACA, Paese K, Wasum R, Rossato M, Rota LD, et al. Análise de taninos totais em plantas aromáticas e medicinais cultivadas no Nordeste do Rio Grande do Sul. Rev Bras Farmacogn. 2003;13(1):17-22. doi:10.1590/S0102-695X2003000100002.
8. Rufino MSM, Alves RE, Brito ES, Morais SM, Sampaio CG, Pérez-Jiménez J, et al. Metodologia científica: determinação da atividade antioxidante total em frutas pela captura do radical livre DPPH [Internet]. Fortaleza: Embrapa Agroindústria Tropical; 2007. Available from: http://www.infoteca.cnptia.embrapa.br/infoteca/handle/doc/426953
9. França KRS. Potencial fungitóxico do óleo essencial de *Lippia gracilis* (Schauer) *in vitro* sobre fitopatógenos [monografia/dissertação]. Campina Grande: Universidade Federal de Campina Grande; 2019.
10. Carrilho KTA. Extratos de películas de amendoim (*Arachis hypogaea* L.) como antioxidantes naturais em óleo de soja [dissertation on the Internet]. São José do Rio Preto: Universidade Estadual Paulista; 2018 Available from: http://hdl.handle.net/11449/154041
11. Sharma K, Giri G. Quantification of phenolic and flavonoid content, antioxidant activity, and proximate composition of some legume seeds grown in Nepal. Int J Food Sci. 2022;2022:4629290. doi:10.1155/2022/4629290.
12. Benevides CMJ, Souza MVB, Lopes MV, Silva FO. Efeito do processamento sobre os teores de oxalato e tanino em maxixe (*Cucumis anguria* L.), jiló (*Solanum gilo*), feijão verde (*Vigna unguiculata* L. Walp) e feijão andu (*Cajanus cajan* L. Millsp.). Alim Nutr. 2013;24(3):321-7.
13. Diniyah N, Subagio A, Akhiriana A, Yuwana S, Puspitasari E, Kurniawati N, et al. Antioxidant potential of non-oil seed legumes of Indonesian ethnobotanical extracts. Arab J Chem. 2020;13(5):5208-17. doi:10.1016/j.arabjc.2020.02.019.
14. Silva LLS, Costa JGM, Matias EFF, Rodrigues FFG, Campos AR, Fernandes CN, et al. Avaliação da atividade antimicrobiana de extratos de *Dioclea grandiflora* Mart. ex Benth., Fabaceae. Rev Bras Farmacogn. 2010;20(2):208-14. doi:10.1590/S0102-695X2010000200012.

Assessment of the Nutraceutical Potential of the Biochemical Profile of *Dunaliella salina* Biomass

Sabrina dos Santos Rocha[1]*, Clara Dias da Silva Marins Brandão[2], Mariah Clara Oliveira Fernandes da Silva[2], Roseane Santos Oliveira[1], Tatiana Oliveira do Vale[1], Fernando Leal Barreiros Moutinho[2]

[1]SENAI CIMATEC University, Industrial Microbiology; [2]Social Service of Bahia Industry - SESI; Salvador, Bahia, Brazil

Microalgae are recognized as promising sources of bioactive compounds for human health; however, gaps remain in the characterization and functional application of their biomass in dietary supplements. *Dunaliella salina*, despite its high biotechnological value, still lacks integrated studies addressing its nutraceutical potential and applicability in food products. Therefore, this study evaluated *D. salina* biomass as a sustainable food ingredient. The cultivation exhibited a well-defined exponential growth phase ($\mu = 0.0113\ h^{-1}$), allowing the identification of an optimal harvesting window (~10 days), which supported the efficient production of nutritionally rich biomass containing high levels of proteins (25.7 ± 0.42%), lipids (18.5 ± 0.06%), carbohydrates (28.5 ± 0.71%), and ash content (26%), along with phenolic compounds (2.16 ± 0.21 mg GAE 100 g^{-1} DW) associated with antioxidant activity and oxidative stress reduction. These findings highlight the biotechnological potential of *D. salina* biomass as a sustainable nutraceutical supplement.

Keywords: Microalgae. *Dunaliella salina*. Biochemistry.

Microalgae are recognized as reliable sources of biochemically active compounds, with potential applications as raw material for various products, due to their high biodiversity and the wide variability in the chemical composition of their biomass, combined with their sustainable and renewable nature [1].

In this context, the use of microalgae extends across multiple industrial sectors, not limited to the pharmaceutical and cosmetic areas, but also encompassing the dietary supplementation industry [2]. This versatility results from their capacity to co-produce different biomolecules, such as pigments, proteins, polyunsaturated fatty acids, and antioxidant compounds, which has increased their interest as therapeutic agents as well as in the form of nutraceuticals [3].

Among biotechnologically relevant microalgae, *Dunaliella salina* is the focus of this study, being widely applied in the production of high-value compounds with industrial relevance, with research on the topic showing a growing trend [4].

Received on 26 February 2026; revised 18 April 2026.

Address for correspondence: Sabrina dos Santos Rocha. Av. Orlando Gomes, 1845 - Piatã, Salvador – BA – Brazil, Zipcode: 41650-010. E-mail: saabrinarocha07@gmail.com.

J Bioeng. Tech. Health 2025;9(5):443-448

The present study evaluates whether the biomass of *D. salina*, obtained under the established conditions, exhibits adequate quality regarding its macromolecular and bioactive compound profile for application as a nutraceutical.

Materials and Methods

The study evaluated proteins, lipids, ash and carbohydrates, as well as total phenolic content as an indicator of bioactive compounds. Experiments were conducted at the Didactic Biotechnology Laboratory of SENAI CIMATEC and at the Didactic Undergraduate Research Laboratory of Serviço Social da Indústria - SESI Djalma Pessoa.

Cultivation of the Microalga *D. salina*

The microalgal strain was obtained from the Iracema Nascimento Microalgae Bank, Institute of Biology, Federal University of Bahia, Salvador, Brazil. The inocula were cultivated following a methodology adapted from Fonseca and colleagues [5], under closed batch culture conditions, using artificial seawater (ASW) [6] composed of distilled water and salts (g L^{-1}) at the following concentrations: 30.07 NaCl, 4.08 Na_2SO_4, 0.72 KCl, 0.17 $NaHCO_3$, 1.16 $CaCl_2$, 5.20 $MgCl_2$, and 0.72 KNO_3. The culture medium was supplemented

with 1 mL of Conway medium containing macro- and micronutrients and 0.5 mL of vitamin solution [7]. Microalgal growth was maintained under continuous illumination using fluorescent lamps at a light intensity of 40.5 μE m^{-2} s^{-1}, with aeration provided by atmospheric air compressors with a nominal airflow rate of 795 L h^{-1} (210 GPH).

Cell Growth Kinetics

Microalgal growth was monitored for 13 days by optical density measurements [8]. 60 mL of microalgal culture were inoculated into 140 mL of artificial seawater (ASW) in 250 mL culture flasks, supplemented with 0.2 mL of Conway medium and 0.2 mL of vitamin solution. Optical density was measured at 740 nm using a UV–Vis spectrophotometer [8], and the values obtained were used to construct the growth curve.

The Δ parameter [9] was calculated as the absolute difference between the initial and final optical density values of each growth phase. Δ was used to quantify the magnitude of biomass accumulation during the exponential and stationary phases.

$$\Delta = X_2 - X_1 \quad (1)$$

X_1: corresponds to the optical density value at the initial time (t_1).

X_2: corresponds to the optical density value at the final time (t_2) of the analyzed interval.

The specific growth rate (μ) [9] was determined from the slope of the linear regression of the natural logarithm of optical density values (OD_{740}) as a function of time, considering only the exponential growth phase.

$$\mu = \frac{ln\, X_2 - ln\, X_1}{t_2 - t_1} \quad (2)$$

X_1 and X_2: correspond to the optical density values measured at 740 nm (OD_{740}) at times t_1 and t_2, respectively;

t_1 and t_2: represent the initial and final times of the selected interval within the exponential growth phase;

ln: denotes the natural logarithm.

The doubling time (td) was calculated to estimate the time required for the microalgal biomass to double during the exponential growth phase. The calculation was based on the specific growth rate (μ), assuming exponential growth, according to the following equation:

$$td = \frac{ln(2)}{\mu} \quad (3)$$

td: corresponds to the cellular doubling time;

μ: represents the specific growth rate;

ln(2): is the natural logarithm of 2.

Biomass Extraction by Flocculation

Biomass was extracted using NaOH as a coagulant at 2 g L^{-1} [5]. Wet biomass was dried in an oven at 70 °C for 4 h, then macerated, sieved, and weighed.

Total Lipid Determination

For total lipid analysis [10], 50 mg of dried biomass were weighed and 25 mL of a chloroform–methanol solution (2:1, v/v) was added. The mixture was heated at 60 °C for 15 min to extract the lipids. The resulting extract was filtered, and 10 mL were collected, followed by the addition of 2 mL of distilled water and centrifugation at 4,000 rpm for 10 min. The organic phase was transferred to pre-treated aluminum containers and heated until complete solvent evaporation to obtain the lipid content, which was calculated using equation:

$$\text{Lipid (\%)} = \frac{m1 - m2}{m3} \times 100 \quad (4)$$

m_1: mass of the container with lipids (g) after solvent evaporation;

m_2: mass of the empty container (g);

m_3: mass (g) of the biomass after dilution in chloroform–methanol solution.

Total Carbohydrates Determination

Total carbohydrates were quantified using the phenol–sulfuric acid method [11,12]. A 0.002 g

sample of dried biomass was weighed, followed by the addition of 1 mL of H_2SO_4 solution (1.0 mol/L) and 5 min of ultrasonic bath. Then, 4 mL of H_2SO_4 (1.0 mol/L) were added, and the mixture was heated in an oven at 100 °C for 1 h, followed by centrifugation at 4,000 rpm for 15 min and simple filtration. One milliliter of 5% phenol was added to the acid filtrate, and after 40 min, 5 mL of H_2SO_4 were added. Total carbohydrate content was calculated using equation:

$$\text{Carbohydrates (\% m/m)} = \frac{\left[\left(\frac{C}{Va}\right) x\, Ve\right]}{m} \text{ x } 100 \quad (5)$$

C: carbohydrate concentration (mg/mL);
V_a: sample volume (L) used;
V_e: volume (L) of the acid extract used in the treatment;
m: amount of dried biomass (g).

Total Protein Determination

Total proteins were quantified following the method described by Lowry and Colleagues and Fachet and colleagues [13,14]. Solutions were prepared as follows: A (1 mol/L NaOH), B (5% Na_2CO_3), C (0.5% $CuSO_4$ and 1% $KNaC_4H_4O_6 \cdot 4H_2O$), D (2 mL of solution C and 50 mL of solution B), and E (Folin–Ciocalteu reagent). Five milligrams of dried biomass were weighed and dissolved in 0.5 mL of distilled water and 0.5 mL of solution A. The mixture was heated at 60 °C for 10 min in an oven, followed by the addition of 2.5 mL of solution D and incubation for 10 min in the dark. Then, 0.5 mL of solution E was added, followed by 30 min incubation in the dark. Absorbance was measured at 580 nm using a UV–Vis spectrophotometer. Total protein content was calculated according to the following equation:

$$\text{Protein (\% m/m)} = \frac{C\, x\, 100}{m} \quad (6)$$

C: protein concentration (mg/mL);
m: weight of dried biomass (g).

Total Total Ash Determination

Total ash analysis was performed following Freitas and colleagues [15]. Crucibles were preheated at 100 °C for 1 h in an oven. One gram of dried biomass was weighed and subjected to muffle furnace calcination at 525–550 °C for approximately 5 h. The ash content (%) was calculated using the following equation:

$$\text{Ash (\%)} = \frac{(Pa - Pc)}{m} \text{ x } 100 \quad (7)$$

P_a: weight of the crucible with ash;
Pc: weight of the empty crucible;
m: weight of the sample.

Total Phenolic Determination

Total phenolic content was determined following Fonseca and colleagues, and Singleton and Rossi [5,16]. 5 mL of microalgal culture were mixed with 500 µL of 10% (v/v) Folin–Ciocalteu reagent, followed by the addition of 1,000 µL of 7.5% (w/v) sodium carbonate and 3.5 mL of distilled water. The mixture was incubated in the dark at room temperature for 2 h. Absorbance was measured at 580 nm using a UV–Vis spectrophotometer. Results were expressed as gallic acid equivalents per 100 g of dry weight (mg GAE 100 g^{-1} DW).

Results and Discussion

Study Related to Cell Growth

The evaluation of microalgae cell growth in the ratio 30:70 (chopped culture/culture medium) proved to be effective, where it was possible to observe (Figure 1) the exponential growth until reaching high cell density, defined as ideal for biomass harvesting.

The Δ value was used as a comparative growth descriptor to highlight differences in cellular behavior throughout the cultivation phases. The calculation considered two time intervals: from

Figure 1. Growth curve of *Dunaliella salina* during a 13-day cultivation period.

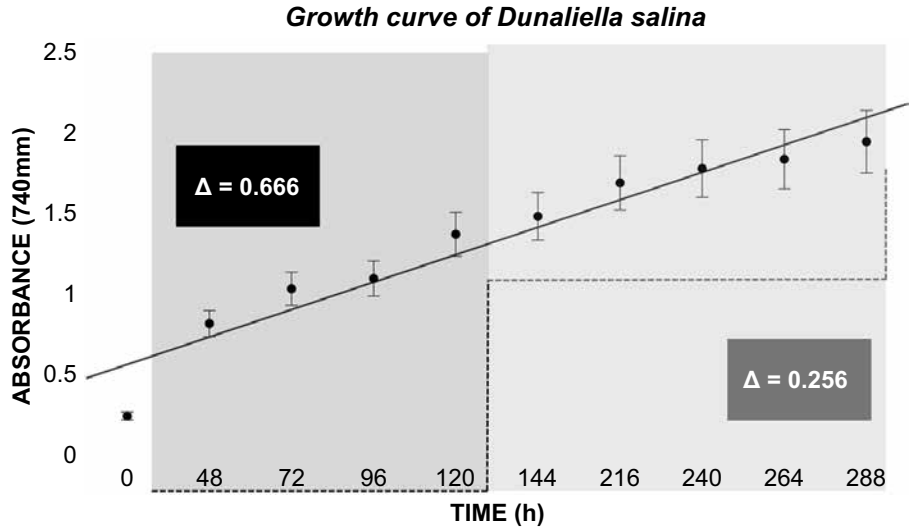

day 2 (~48h) to day 7 (~144h), with Δ = 0. 666 corresponding to the exponential growth phase, and from day 8 (~168h) to day 13 (~288h), with Δ = 0.256, corresponding to the stationary phase.

The higher Δ observed during the first interval indicates more intense cell growth, characteristic of the exponential phase, marked by rapid biomass accumulation and low cell mortality, which favors efficient metabolic activity. In contrast, the reduction in Δ during the second interval reflects the transition to the stationary phase, associated with decreased nutrient availability, metabolite accumulation, and physiological adjustments of the microalga [17].

Thus, the Δ values clearly demonstrate the occurrence of physiologically distinct growth phases during the cultivation of *Dunaliella salina*. The cultivation system combined with the adopted peaking regime proved effective for the rapid production of viable biomass, allowing the identification of an optimal harvesting window within 10 days (~216h) of cultivation and supporting the biotechnological optimization of the produced biomass.

The specific growth rate (μ) obtained during the exponential phase was 0.0113 h^{-1}, indicating a moderate and sustained growth pattern. This value is consistent with typical growth rates reported for *Dunaliella* species under non-limiting cultivation conditions [18]. The calculated doubling time (~61 h) further supports the occurrence of a well-defined exponential growth phase prior to growth stabilization.

Yield Obtained from the Extraction of Biomass by Flocculation with NaOH

The extraction of *Dunaliella salina* biomass using sodium hydroxide as a chemical coagulant showed promising results, obtaining an average yield of 3.100 g of dry biomass per 1L of culture. In the studies directed by Andrade [19], the yield is 1.194 g L^{-1}, in which he highlights the effectiveness of the approach adopted.

Determination of Lipids, Carbohydrates and Total Proteins

The results corresponding to the levels of proteins, lipids and total carbohydrates are presented in Table 1, in which the values were promising for a potential supplement.

When we analyze the results obtained with other studies with *D. salina*, such as carried out by Sui and Vlaeminck [20] in a constant photoperiod regime, a rate of 54% of proteins,

Table 1. Proximate biochemical composition of *Dunaliella salina* biomass (proteins, carbohydrates, and lipids).

Compounds	Content (%)
Proteins	25.7 ± 0.42
Carbohydrates	28.5 ± 0.71
Lipids	18.5 ± 0.06

however, the carbohydrate rates registered values below 20%. In another study carried out by Gharajeh et al. in a light and dark phase regime, 40% of proteins and 32% of carbohydrates were obtained, but values of less than 6% of lipids. As for the lipid content, in a study directed by Gharajeh and colleagues [21], the lipid content present in dry biomass.

Therefore, the cultivation regime used has shown potential in obtaining a rich biomass, evidenced by the concentrations of the three main biochemical compounds in a balanced manner, highlighting their efficacy and adaptability for the production of biomolecules of interest through microalgae.

Determination of Total Ashes

The ash value obtained from the dry biomass was 26%, which is higher than the value reported in the literature (approximately 11%) [17]. This value may be related to the precipitation of calcium carbonate ($CaCO_3$) in the culture medium, which can be influenced by the concentration of calcium ions (Ca^{2+}), dissolved inorganic carbon (DIC), elevated pH, and availability of nucleation sites. According to the literature, this process is known as biocementation and has been used in microalgae for the development of biocement [22]. In principle, the salts present can be interpreted as possible mineral salts available in the biomass composition; however, for this confirmation, it will be necessary to identify these salts as well as their respective concentrations.

Determination of Total Phenolic

The total phenolic content found in the biomass was 2.16 ± 0.21 gallic acid equivalents per 100 g of dry weight (mg GAE 100 g^{-1} DW), thus confirming the presence of antioxidant activity in the microalgal biomass content, in accordance with the literature [17]. It is important to emphasize that, despite the lower concentration observed, the microalga still demonstrates antioxidant potential, since phenolic compounds are associated with the neutralization of reactive oxygen species and the reduction of oxidative stress, processes related to the prevention of chronic diseases and the promotion of human health, reinforcing its potential application as a nutraceutical [23,24].

Conclusion

The results of this study demonstrate the potential of *Dunaliella salina* biomass for application in supplementation aimed at human health. Moreover, the analyses revealed an adequate biochemical composition and the presence of bioactive compounds, particularly phenolic compounds, which consequently contribute to its antioxidant activity and functional value. Therefore, these characteristics support the potential use of *D. salina* biomass in the development of nutraceuticals and functional ingredients for human consumption. Finally, future studies should focus on optimizing biomass yield, standardizing the production process, and validating its application through appropriate models for human use.

Acknowledgments

The authors gratefully acknowledge SENAI CIMATEC and Serviço Social da Indústria - SESI for the financial support, infrastructure, and institutional resources provided for the development of this research.

References

1. Severo IA, Nascimento TC, Fagundes MB, editors. Microalgas: potenciais aplicações e desafios. Canoas: Mérida Publishers; 2021.
2. Victora MM, Moutinho FLB, Riatto VB. Microalgas: uma estratégia sustentável na transformação e obtenção de compostos orgânicos. Quim Nova. 2024;47(2). doi:10.21577/0100-4042.20230107.
3. Bule MH, Ahmed I, Maqbool F, Bilal M, Iqbal HMN. Microalgae as a source of high-value bioactive compounds. Front Biosci (Schol Ed). 2018;10(2):197-216. doi:10.2741/s509.
4. Celente GS, Rizzetti TM, Sui Y, Schneider RCS. Uso potencial da microalga Dunaliella salina para bioprodutos com relevância industrial. Biomass Bioenergy. 2022;167:106647. doi:10.1016/j.biombioe.2022.106647.
5. Fonseca YBT, Almeida NM, Caldas JC, Morais GN, Silva IMJ, Riatto VB, et al. Effect of the seed coating with biomass of Dunaliella salina on early plant growth and in the secondary metabolites content of Coriandrum sativum. An Acad Bras Cienc. 2022;94(4). doi:10.1590/0001-3765202220201735.
6. Millero FJ. Chemical oceanography. 2nd ed. Boca Raton: CRC Press; 1996.
7. Walne PR. Culture of bivalve molluscs: 50 years' experience at Conwy. 2nd ed. Farnham: Fishing News Books; 1979.
8. Santos RS. Avaliação do crescimento e da produção de lipídios da microalga Chlorella vulgaris empregando meio de cultivo sintético e resíduo agroindustrial [dissertação]. São Cristóvão: Universidade Federal de Sergipe; 2021.
9. Trenkenshu RP. Raschet udel'noi skorosti rosta mikrovodoroslei (Calculation of the specific growth rate of microalgae). Mar Biol J. 2019;4(1):100-8. doi:10.21072/mbj.2019.04.1.09.
10. Freeman NFT, Lindgren YC, Nichols AV. Serum lipid analysis by chromatography and infrared spectrophotometry. J Biol Chem. 1957;227:449-64. doi:10.1016/S0021-9258(18)70828-4.
11. Dubois M, Gilles KA, Hamilton JK, Rebers PA, Smith F. Colorimetric method for determination of sugars and related substances. Anal Chem. 1956;28(3):350-6. doi:10.1021/AC60111A017.
12. Lehninger AL. Princípios de bioquímica. São Paulo: Sarvier; 2005.
13. Lowry OH, Rosebrough NJ, Farr AL, Randall RJ. Protein measurement with the Folin phenol reagent. J Biol Chem. 1951;193:265-75. doi:10.1016/S0021-9258(19)52451-6.
14. Fachet M. Systematic analysis of carotenogenesis in microalgae for model-based process design [thesis]. Magdeburg: Otto von Guericke University Magdeburg; 2017.
15. Freitas SC, Silva TS, Carvalho PGB, Tupinambá DD, Koakuzu SN, Carvalho AV, et al. Procedimento operacional padrão para determinação de fibras solúvel e insolúvel. 1st ed. Rio de Janeiro: EMBRAPA; 2008.
16. Singleton VL, Rossi JA. Colorimetry of total phenolics with phosphomolybdic-phosphotungstic acid reagent. Am J Enol Vitic. 1965;16(3):144-58.
17. Andrade DS, Filho AC. Microalgas continentais: potencialidades e desafios do cultivo. Londrina: IAPAR; 2014. (Coleção IPR de Microalgas; v. 2).
18. Xi Y, Zhang J, Kong F, Che J, Chi Z. Kinetic modeling and process analysis for photo-production of β-carotene in Dunaliella salina. Bioresour Bioprocess. 2022;9:40. doi:10.1186/s40643-022-00495-6.
19. Andrade BB. Produção de microalgas cultivadas em meio reutilizado e uso da eletrofloculação como método de separação de biomassa [dissertação]. Salvador: Universidade Federal da Bahia; 2021.
20. Sui Y, Vlaeminck SE. Dunaliella microalgae for nutritional protein: an undervalued asset. Trends Biotechnol. 2020;38(1):1-10. doi:10.1016/j.tibtech.2019.07.011.
21. Gharajeh NH, Valizadeh M, Dorani E, Hejazi MA. Biochemical profiling of three indigenous *Dunaliella* isolates with main focus on fatty acid composition towards potential applications. Biotechnol Rep (Amst). 2020;26.
22. Fré NC. Influência das condições de cultivo da microalga Dunaliella tertiolecta na produção de carotenoides e lipídios [dissertação]. Porto Alegre: Universidade Estadual do Rio Grande do Sul; 2016.
23. Hadiyanto H, Ariyanti D, Handayani NA. An overview of biocement production from microalgae. Int J Eng Sci. 2011;2(2):30-3. doi:10.12777/ijse.2.2.31-33.
24. Ampofo J, Abbey L. Microalgae: bioactive composition, health benefits, safety and prospects as potential high-value ingredients for the functional food industry. Foods. 2022;11(12):1744. doi:10.3390/foods11121744.

Comparative Performance Analysis of Public Lighting Luminaires According to NBR 5101:2018 and 2024 Standards

Rafael Argolo Ferreira[1]*, Wild Freitas da Silva Santos[1,2,3], Felipe Mendes de Vasconcellos[1]

[1]Federal University of Bahia, Polytechnic School, Electrical Engineering Department; Salvador, Bahia; [2]State University of Feira de Santana, Department of Technology; Feira de Santana, Bahia; [3]SENAI CIMATEC University, Department of Technology; Salvador, Bahia, Brazil

This study compares the performance of approximately 1,300 public lighting luminaires according to Brazilian standards NBR 5101:2018 and NBR 5101:2024. Using Dialux® software, over 37,500 simulations were conducted with IES photometric data from luminaires certified by INMETRO and listed by PROCEL. Five standard installation scenarios were modeled based on NBR 5101:2018 reference layouts. Results identify the most efficient luminaires for each case and outline the main changes in the 2024 standard, including correlated color temperature limits, stricter light pollution control, and reduced mounting angles. The findings indicate significant impacts on current projects and provide guidance for future public lighting implementations.

Keywords: Public Lighting. NBR 5101. Lighting Efficiency. Dialux Simulation.

Abbreviations: ABNT, Brazilian Association of Technical Standards. INMETRO, National Institute of Metrology. PROCEL, National Program for Electric Energy Conservation. IES, Illuminating Engineering Society. TCC, Correlated Color Temperature.

Public lighting is a key component of urban infrastructure, contributing to safety, quality of life, and the proper functioning of society, far beyond the basic function of illuminating streets [1]. Well-designed lighting systems reduce traffic accidents, discourage criminal activity, and encourage the use of public spaces during nighttime, fostering cultural and economic vitality in municipalities [2].

In Brazil, the Brazilian Association of Technical Standards (ABNT) defines technical requirements for public lighting through NBR 5101 – Public Lighting: Procedure [3]. This standard specifies the performance parameters for luminaires according to the classification of roads, including average luminance, global and longitudinal uniformity, threshold increment, and the luminance ratio of adjacent areas.

Other institutions also play important roles in public lighting regulation, like the National Institute of Metrology (INMETRO), through Ordinance No. 62 [4], certifies luminaires for public lighting to ensure compliance with efficiency and safety standards. Additionally, the National Program for Electric Energy Conservation (PROCEL) [5] promotes energy efficiency by encouraging the adoption of more efficient technologies and practices.

In addition to meeting efficiency and safety standards, the actual performance of luminaires in the field must be evaluated according to photometric criteria. IES (Illuminating Engineering Society) curves, which represent the spatial distribution of luminous intensity [6], are essential for determining light directionality and uniformity, enabling the selection of the most appropriate luminaires for each road type or application scenario [7].

Moreover, the recent update from NBR 5101:2018 to NBR 5101:2024 introduced significant changes, such as correlated color temperature limits, stricter light pollution control, and reduced installation angle allowances.

Understanding these changes and their implications for public lighting projects is essential for achieving efficiency, regulatory compliance, and sustainability in urban environments. This study addresses this gap by performing large-

Received on 10 February 2026; revised 22 April 2026.

Address for correspondence: Rafael Argolo Ferreira. Rua Raul Leite. Zipcode: 40270-010. Salvador, Bahia, Brazil. Salvador, Bahia, Brazil. E-mail: rafaelargoloferreira@gmail.com.

J Bioeng. Tech. Health 2026;9(5):449-455

scale simulations to evaluate the impact of these regulatory updates.

Theoretical Background

Photometric Parameters

The design of public lighting systems is governed by photometric principles established in ABNT NBR 5461 [1] and operationalized in ABNT NBR 5101 [2], which define the parameters required to ensure visual comfort, safety, and energy efficiency in urban environments.

The primary photometric parameters are:

- Luminous flux (Φ) – the total quantity of light emitted by a source, measured in lumens (lm). It indicates the overall light output of a luminaire.
- Luminous intensity (I) – the amount of light emitted in a specific direction, expressed in candela (cd). It defines the directional distribution of the emitted light.
- Illuminance (E) – the amount of luminous flux incident per unit area, measured in lux (lx). It quantifies how much light reaches a surface.
- Luminance (L) – the measure of the perceived brightness of a surface, expressed in candela per square meter (cd/m²), directly related to visual comfort and uniformity perception.
- Uniformity factors – overall uniformity (Uo), given by the ratio of minimum to average luminance or illuminance, and longitudinal uniformity (Ul), given by the ratio of minimum to maximum luminance along the driving axis. These factors ensure consistent light distribution and reduce visual fatigue.
- Threshold increment (TI) – a percentage value that quantifies the loss of visual performance due to disability glare, affecting the ability to detect objects on the road. Lower TI values indicate better glare control.
- Correlated color temperature (CCT) – expressed in kelvin (K), it describes the color appearance of the emitted light, influencing visual comfort, object recognition, and environmental perception.

Photometric data for luminaires is typically provided in IES files standardized by ANSI/IES LM-63 [3], which encode the spatial distribution of luminous intensity in polar coordinates. These files also contain essential technical specifications such as rated power, luminous efficacy, optical classification, and light distribution pattern.

Luminaire Mounting Data

The mounting configuration of luminaires plays a decisive role in the photometric performance of public lighting systems. For this study, the installation parameters were defined according to the standard road and pedestrian classes described in ABNT NBR 5101:2018, ensuring comparability across all scenarios.

For each class, the following variables were fixed:

- Mounting height (Hm) – vertical distance from the luminaire to the road surface, determined by road class.
- Overhang (O) – horizontal displacement between the pole and the road edge.
- Spacing (S) – center-to-center distance between poles along the road.
- Number of lanes (NL) – total traffic lanes considered in the design, influencing the required mounting height and luminaire distribution.
- Road width (R) – total pavement width, measured between curb edges, directly impacting pole spacing and light distribution requirements.
- Arrangement type – single-sided, opposite, or staggered configuration, depending on the road class.
- Mounting angle (Tilt) – angle between the luminaire optical axis and the horizontal plane, limited by standard requirements.

Road Classification

In NBR 5101:2018, road lighting classes are divided into V1–V5 for motorized traffic and

P1–P4 for pedestrian areas, each with specific photometric requirements [2]. The 2024 revision replaces these with Class C (conflict areas, C0–C5) and Class P (pedestrian areas, P1–P6), using parameters such as vehicle speed, traffic volume, and ambient luminance for classification [4].

Main Updates in NBR 5101:2024

The 2024 revision of NBR 5101 introduced significant changes in classification criteria, photometric performance thresholds, and environmental considerations, aiming to improve safety, efficiency, and sustainability in public lighting systems. While average luminance values remain unchanged, the new version establishes stricter requirements for global (Uo) and longitudinal uniformity (Ul), as well as lower permissible threshold increment (TI), enhancing visual comfort and glare control. A key modification is the adoption of a much warmer correlated color temperature (CCT) range of 1800–2200 K, replacing the typical LED values of 4000–5000 K used in the 2018 standard. This change is intended to reduce blue light emission and its associated impacts on human health, wildlife, and the night sky.

The 2024 update also strengthens light pollution control, introducing mandatory uplight emission limits in the 90–180° zone. Installation constraints have been tightened, with the maximum mounting tilt reduced from 15° to 5°, directly contributing to glare reduction and minimizing light trespass.

Overall, these updates reflect a shift towards more rigorous technical and environmental performance standards, requiring municipalities, designers, and manufacturers to adapt luminaire selection and installation practices to meet both regulatory compliance and sustainable urban lighting objectives.

Materials and Methods

This study followed a structured sequence of steps to evaluate the performance of public lighting luminaires under the criteria of both NBR 5101:2018 and NBR 5101:2024. The methodology comprised the following stages:

1. Acquisition of all IES photometric files available on the PROCEL website for luminaires certified by the National Institute of Metrology (INMETRO);
2. Organization and completion of photometric curve data provided by manufacturers;
3. Simulation of five standardized installation scenarios defined in NBR 5101:2018, due to the absence of reference scenarios in NBR 5101:2024, using all available luminaires and processed data in Dialux® software;
4. Analysis of the simulated performance results in compliance with NBR 5101:2024 requirements;
5. Comparison of luminous source performance with NBR 5101:2018 parameters to assess the impact of the latest standard update.
6. Identification and ranking of the best-performing suppliers based on their presence among the top 10 luminaires in each scenario, providing insights into portfolio versatility and market competitiveness.

Acquisition of Photometric Curves

INMETRO Ordinance No. 62 (INMETRO, 2023) defines the technical and safety requirements for road public lighting luminaires in Brazil, as established in the Technical Quality Regulation. One of the mandatory tests is the luminous distribution measurement, carried out by accredited laboratories. These laboratories generate the luminaire's photometric curve, which is converted into an IES file following ANSI/IES LM-63 standards and published both by manufacturers and PROCEL.

For this study, photometric curves were obtained from PROCEL Publication No. 22, which compiles LED luminaires for public lighting that meet INMETRO certification requirements. Approximately 1,300 IES files were collected for analysis.

The downloaded IES files contained inconsistent or incomplete information, such as missing luminaire model names, rated power, or correlated color temperature (CCT). To ensure compatibility with Dialux® simulation requirements, all IES files were manually reviewed and edited, standardizing metadata fields to enable automated processing and scenario generation.

Simulation Scenarios

Five installation scenarios were defined based on the standard mounting patterns in NBR 5101:2018 (Table 1). The 2018 configurations were adopted for both standards due to the absence of standardized mounting layouts in NBR 5101:2024. Each scenario corresponds to a specific roadway class for motorized traffic, paired with a pedestrian lighting class. The unilateral arrangement was used in all cases, with a maintenance factor of 0.8 to account for photometric performance degradation over time.

Table 1. Mounting configurations adopted in simulations.

Mounting Configurations Adopted in Simulations					
Class	**S (m)**	**Hm (m)**	**NLs**	**R (m)**	**O (m)**
V5	35.0	7.0	3	8.10	1.5
V4	35.0	8.0	3	9.0	1.5
V3	35.0	8.0	3	9.0	1.5
V2	35.0	9.0	4	10.8	2.5
V1	40.0	12.0	4	12.0	3.0

The simulations covered five combined scenarios of roadway and pedestrian lighting classes (Table 2). Pedestrian classes (P1–P4) were assigned according to NBR 5101:2018 requirements, without specific mounting standards, ensuring consistency between the two standards in the comparative analysis.

Table 2. Simulated scenarios.

Simulated Scenarios		
Scenario	**Roadway Class**	**Pedestrian Class**
1	V1/C1	P1
2	V2/C2	P2
3	V3/C3	P3
4	V4/C4	P4
5	V5/C5	P4

For NBR 5101:2024, the corresponding Conflict Area Classes (C1–C5) and Pedestrian Classes (P1–P5) were adopted for direct comparison, maintaining the same physical layouts from the 2018 scenarios.

Selection of Optimal Luminaires

For each scenario, the most efficient luminaire was selected from the set of models that fully met the requirements of both NBR 5101:2018 and NBR 5101:2024. Only the best-performing luminaire from each manufacturer was considered, ensuring that the analysis reflected optimal energy use.

Results

This section presents the outcomes of the simulations performed for the five scenarios defined by NBR 5101, applied to all luminaires certified by INMETRO. In total, approximately 37,500 simulations were conducted, allowing for a comprehensive evaluation of luminotechnical parameters under both the 2018 and 2024 versions of the standard.

The 2024 revision introduced stricter requirements, including a maximum tilt angle of 5° for luminaire mounting (compared to 15° in 2018) and more demanding pedestrian walkway lighting criteria, particularly the introduction of minimum horizontal illuminance instead of only uniformity factors. These changes significantly impacted

approval rates, reducing the number of compliant luminaires in some scenarios but resulting in more realistic power ratings and energy consumption values.

Scenario Comparison

The Table 3 presents the number of approved luminaires for each scenario under both standards, along with the percentage relative to the total number tested in that scenario, and the power rating of the most energy-efficient approved luminaire.

The analysis reveals clear trends in how the 2024 update reshaped luminaire approval rates:

- Scenarios 1 to 3 (higher traffic and more demanding lighting classes) saw a substantial increase in approved luminaires, indicating that the revised criteria allowed more models to comply while still ensuring realistic power ratings. For example, in Scenario 2, approvals increased from 7 to 70 models, with a power reduction from 121 W to 100 W.
- Scenarios 4 and 5 (lower traffic or predominantly pedestrian areas) experienced a sharp drop in approved luminaires, from 800 to 90 in Scenario 4 and from 4,000 to 260 in Scenario 5. This is mainly due to the introduction of the minimum illuminance requirement for pedestrian walkways, which proved harder to meet than the previous uniformity-only criteria.
- In terms of power optimization, the 2024 standard maintained or reduced wattage in high-demand scenarios. However, in Scenario 4, the best- compliant luminaire under the new standard had a slightly higher wattage (48 W) than the most efficient 2018 model (33 W).
- The percentage of approved luminaires shows how the 2018 standard was more permissive in low- demand classes, potentially allowing oversized luminaires, whereas the 2024 revision imposes stricter alignment with actual operational needs.

Overall, the transition to NBR 5101:2024 resulted in more consistent and technically sound compliance, particularly for urban areas with complex lighting demands. However, the stricter pedestrian area criteria reduced the variety of compliant products, which could impact market options for low-intensity lighting applications.

Best Suppliers by Scenario Coverage

Beyond individual scenario results, the study consolidated performance to identify the suppliers with the broadest presence across scenarios, considering only their most energy- efficient approved luminaire per case.

Table 3. Approved luminaires and power comparison (NBR 2018 *vs*. NBR 2024).

Approved Luminaires and Power Comparison (NBR 5101:2018 *vs*. NBR 5101:2024)				
Scenario	**Quantity Approved Luminaires**		**Average Power (W)**	
	NBR 2018	**NBR 2024**	**NBR 2018**	**NBR 2024**
1	5 (0.05%)	40 (0.42%)	196	179
2	7 (0.08%)	70 (0.75%)	121	100
3	9 (0.09%)	90 (0.94%)	195	195
4	800 (8.60%)	90 (0.97%)	33	48
5	4,000 (43.0%)	260 (2.8%)	20	24

The Table 4 ranks suppliers by the number of different scenarios in which they appeared among the top 10 performers for that scenario, providing an indicator of portfolio versatility under the diverse requirements of NBR 5101.

Table 4. Top Suppliers by scenario.

Top Suppliers by Scenario		
Rank	**Manufacturer**	**Scenarios**
1	Philips	1, 3, 4, 5
2	Unilumen	3, 4, 5
3	Esb	2, 3, 4
4	Zagonel	1, 2
5	Sxlight	4, 5
6	Demape	4, 5
7	Tecnowatt	2, 4
8	Soneres	4, 5
9	Tradetek	1, 5
10	Lumer	3, 4

The supplier ranking analysis highlights notable differences in market presence and adaptability among manufacturers. Philips stands out as the most versatile supplier, achieving approvals in four different scenarios and demonstrating strong adaptability to varied urban lighting requirements. Unilumen and Esb follow, with approvals in three scenarios each, indicating a balanced ability to combine efficiency and compliance under both the 2018 and 2024 standards.

Manufacturers such as Zagonel, Sxlight, and Demape show solid competitiveness in specific applications, particularly in moderate-traffic and pedestrian-oriented lighting contexts, where technical performance requirements differ from those of high-traffic scenarios. Even suppliers that appear in only two scenarios, such as Tecnowatt and Soneres, present high- performance solutions within their targeted niches, suggesting specialization in certain roadway or pedestrian classes.

Overall, this supplier-based perspective complements the scenario-specific performance results by providing an additional layer of analysis for market evaluation. It also offers valuable insights for strategic procurement decisions in public lighting projects, enabling municipalities and designers to align supplier selection with regulatory compliance, energy efficiency, and application-specific performance goals.

Conclusion

This study evaluated INMETRO-certified luminaires under NBR 5101:2018 and 5101:2024 through 37,500 simulations in five roadway and pedestrian scenarios. The 2024 revision introduced stricter mounting tilt limits, higher uniformity, and minimum illuminance requirements for pedestrian areas, affecting both approval rates and optimal power ratings.

Approval counts increased in high-demand scenarios (1–3) but dropped sharply in low-demand/pedestrian scenarios (4–5). The power comparison revealed reductions in Scenario 1 (196 W to 179 W) and Scenario 2 (121 W to 100 W), stability in Scenario 3 (195 W to 195 W), and increases in Scenario 4 (33 W to 48 W) and Scenario 5 (20 W to 24 W). These changes show efficiency gains in demanding contexts, while stricter criteria for pedestrian lighting can raise power needs.

Supplier analysis identified Philips as the most versatile (approved in four scenarios), followed by Unilumen and Esb in three scenarios each.

The results indicate that NBR 5101:2024 promotes safer, more efficient, and environmentally responsible public lighting, but also narrows options for pedestrian-focused applications. Municipalities and designers must adapt luminaire selection to balance compliance, performance, and energy efficiency.

References

1. Assis JF, Lima AO. Iluminação pública: aspectos técnicos e socioeconômicos. Rev Bras Energ. 2019;25(2):45-57.
2. Santos VLS, Costa MR. Sustainable public lighting: challenges and perspectives. J Urban Technol. 2022;29(3):55-70.
3. Associação Brasileira de Normas Técnicas. NBR 5101:2024: iluminação pública – procedimento. Rio de Janeiro: ABNT; 2024.
4. Instituto Nacional de Metrologia, Qualidade e Tecnologia. Portaria nº 62: regulamento técnico da qualidade para luminárias para iluminação pública viária. Brasília: INMETRO; 2023.
5. Programa Nacional de Conservação de Energia Elétrica. Publicação nº 22: luminárias LED para iluminação pública. Rio de Janeiro: Eletrobras/PROCEL; 2023.
6. Illuminating Engineering Society. ANSI/IES LM-63-19: approved method – file format for the electronic transfer of photometric data. New York: Illuminating Engineering Society; 2019.
7. Fragoso R, Silva WF, Almeida JP. Photometric analysis of public lighting for urban safety. Light Eng J. 2020;28(4):33-42.
8. Ribeiro L, Coelho P, Caires J. Efeitos da temperatura de cor na iluminação urbana. Rev Ilum Arq. 2012;19(1):12-19.
9. Lee K, Moreno T, Sun C. Evaluation of mounting angle effects in LED street lighting. Light Res Technol. 2013;45(5):601-15.

Quali-Quantitative Evaluation of *Ficus benjamina* L. in Street Tree Planting of Áureo Filho Housing Complex – Feira de Santana, BA, Brazil

Yasmin Santana da Silva[1]*, Gleidson Martins da Costa[1], Marcos de Souza Rodrigues[2], Jorge Lepikson Neto[2]
[1]State University of Feira de Santana, Department of Technology (DTEC); Feira de Santana, Bahia
[2]SENAI CIMATEC University, Integrated Manufacturing and Technology Campus; Salvador, BA, Brazil

Urban tree planting plays an essential role in the environmental quality of cities, offering ecological, aesthetic and social benefits. Among the species commonly used in Brazilian urban landscaping, *Ficus benjamina* L. stands out, although there is a scarcity of studies addressing its behavior and adaptability in the urban environment. Considering this, the present work aims to evaluate qualitatively and quantitatively the individuals of the species present in the street tree planting of the Áureo Filho Housing Complex, in Feira de Santana (BA). For this purpose, an in loco inventory was carried out, considering variables such as total height and bifurcation height, in addition to aspects such as the phytosanitary condition and the need for management. The results showed that the species represents a high percentage of the local tree planting, with heights that vary between 2 and 17 meters (average of 9.7 m). The presence of recurrent damage caused by drastic and inadequate pruning was also found. The general analysis indicated that 48.7% of the trees had phytosanitary issues, and that 53.8% need corrective actions. Therefore, the high frequency of planting the species, associated with the proximity between individuals, may be favoring the dissemination of pests and diseases. The data indicate the low suitability of Ficus benjamina L. to local conditions, thus reinforcing the need for careful planning in the selection of species for urban tree planting.

Keywords: Urban Tree Planting. *Ficus benjamina*. Urban Infrastructure. Exotic Species.

Urban tree planting plays a fundamental role in promoting the quality of life in cities [1], as it offers ecological, aesthetic, economic and social benefits. According to the Companhia Paraense de Energia Elétrica (Copel), it helps in regulating the microclimate, reducing pollution, and protecting the soil and fauna, in addition to valuing urban spaces and properties, as well as contributing to energy savings, making neighborhoods attractive and touristic [2].

However, urban tree planting faces challenges in hostile areas, such as pollution, contaminated soil, lack of space, and mechanical damage caused by people and vehicles. In addition, interferences with paving and conflicts with underground and overhead electrical networks compromise the survival of trees, which, many times, do not reach maturity and remain in the juvenile stage [3]. These problems are, for the most part, a consequence of the absence of planning based on technical-scientific criteria, which generates various disturbances in urban areas [4].

One of the main criteria for the success of urban tree planting is the appropriate choice of species. According to Gonçalves and colleagues (2004) [5], the appropriate choice is essential for the success of an urban plan, as it avoids excessive maintenance costs, as well as problems resulting from planting in inadequate locations and without planning. In addition, exotic species, when introduced into environments without natural enemies, can adapt quickly, compete with native species, and alter ecological processes, becoming dominant in a short time [6].

The species *Ficus benjamina* L. is currently one of the most cultivated exotic trees in southeastern Brazil [7], with the presence of this species also being notorious in the street tree planting of other regions of the country. It originated in southern and southeastern Asia, where it is considered the official tree of Bangkok, in Thailand.

Received on 19 February 2026; revised 24 April 2026.
Address for correspondence: Yasmin Santana da Silva. Av. Transnordestina - Novo Horizonte. Feira de Santana, Bahia, Brazil. Zipcode: 44036-900. E-mail: minsantana03@gmail.com.

J Bioeng. Tech. Health 2026;9(5):456-461

It is widely used in urban tree planting, in gardens and parks, due to its high ornamental value. It can reach more than 30 meters in height and up to 40 centimeters in diameter. The rapid development of its roots, in search of nutrients, can cause damage to urban infrastructure, which is why its planting is prohibited in some cities [8]. In this context, the present article aimed to evaluate the use of *Ficus benjamina* L. in the tree planting of the Áureo Filho Housing Complex in Feira de Santana, Bahia (BA).

Materials and Methods

The present work focuses on the study of the species *Ficus benjamina* L. and is part of a research project that is characterized as a descriptive and exploratory field study. This study aims to analyze the street tree planting of the Áureo Filho Housing Complex, located in the Campo Limpo neighborhood of the city previously mentioned.

Delimitation of the Study Area

The mentioned housing complex is located in the city of Feira de Santana, in the state of Bahia, in the northeast region of Brazil. The city has a reference point at the following geographical coordinates: latitude 12°16'S, longitude 38°58'W, and 234 m altitude. In addition, according to Instituto Brasileiro de Geografia e Estatística (IBGE), it has a territorial extension of 1,338 km² and a population of 616,272 inhabitants [9].

Feira de Santana stands out as one of the most relevant municipalities in the state of Bahia, with a spatial and socioeconomic dynamic strongly influenced by the commercial sector, the main local economic activity [10]. In this scenario, the evaluation of the species Ficus benjamina L. was carried out in the Feira VI Housing Complex, also known as Áureo Filho, which was designed by Habitação e Urbanização da Bahia (Urbis), in the 1980s, to serve the military of the 1st Battalion, as well as their families.

Over time, the complex underwent a process of irregular occupation, driven mainly by the arrival of students from Universidade Estadual de Feira de Santana (UEFS), in search of housing near the institution [11]. This disordered expansion led to the informal construction of residences and businesses, whose effects still impact the urban organization and social relations of the locality (Figure 1).

Data Collection and Analysis

Data collection was carried out through the application of a tree inventory, conducted from the delimitation of the study area and the on-site survey of the tree individuals, from February to March 2025. To record the information, a manual collection sheet was used, adapted from Silva Filho and colleagues (2002), structured into five sections: (i) location and identification, containing data such as street, individual number, and species; (ii) dimensions, such as the measurement of total height and the height of the first branching; (iii) biology, covering the general state and phytosanitary changes and (iv) definition of actions, where the interventions performed and management recommendations are recorded.

The survey allowed for a quali-quantitative analysis of the *Ficus benjamina* L. individuals, considering both morphological aspects and the environmental and urban conditions of the surroundings. To ensure greater accuracy and efficiency in data collection, different instruments and technological tools were used. Among the resources used, the following stand out: QGIS software, used for spatial analysis and delimitation of the study area; Tree Height Measurement Tool (Tress), used to estimate the height of individuals; and the PlantNet application, used to identify tree species.

In addition to the digital resources, a manual tape measure was used to measure the distance between the tree and the observer, which is necessary information for Tress to function.

Figure 1. Location map of the Campo Limpo neighborhood.

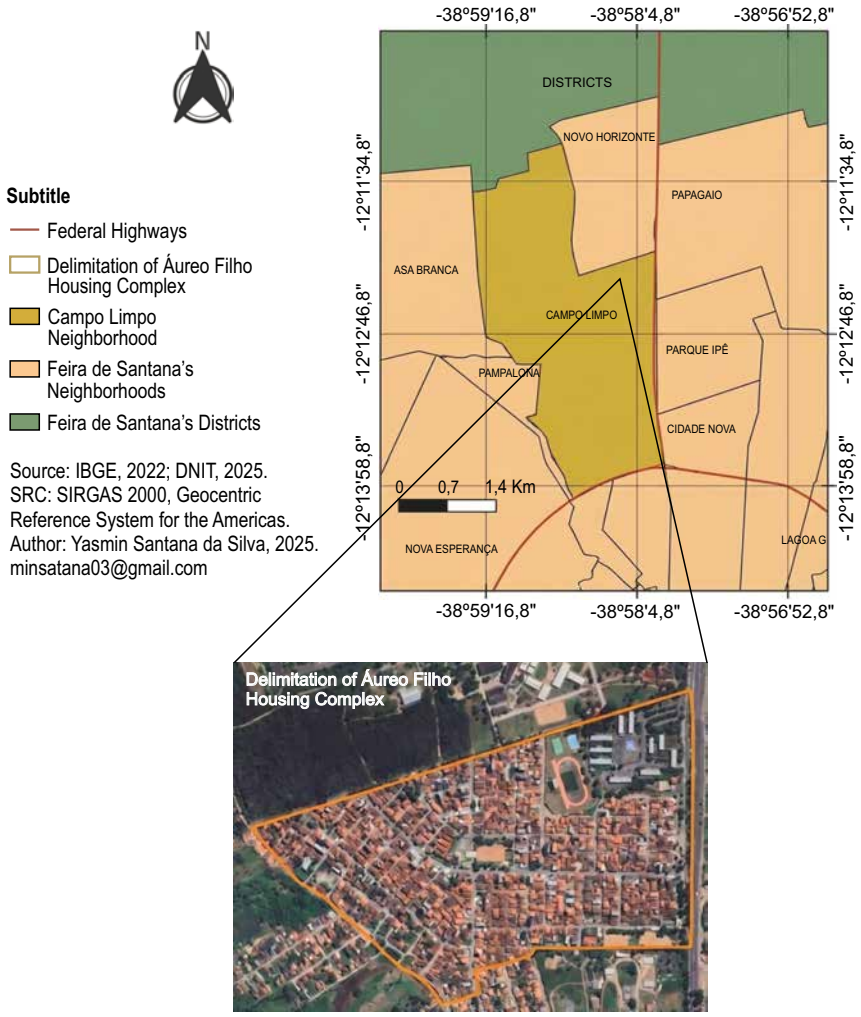

Finally, all collected data were organized and processed in Microsoft Office Excel® software, aiming at the systematization and analysis of the results obtained.

Results and Discussion

A total of tree individuals were counted in the street tree planting of the Áureo Filho Housing Complex. Among these, 39 belong to the *Ficus benjamina* L. species, which represents 15.9% of the total sampled. This frequency exceeds the recommendation of Santamour Junior (2002)[13], according to which no species should represent more than 10% of the total trees planted in urban areas, since the high frequency of a single species in urban tree planting can favor the emergence of pests and diseases, due to low plant diversity.

In addition to the high frequency of individuals of the same species, the proximity between them also represents a risk factor, as it facilitates the dissemination of pests and diseases, due to the sharing of pathogenic agents. That said, the analysis of the tree arrangement revealed that 84.6% of the specimens were grouped with two or more individuals of the same species, while only 15.4% were isolated, which reinforces the phytosanitary vulnerability resulting from plant homogeneity.

Furthermore, the widespread use of this species, for the urban tree planting of the housing complex, can be justified by its suitability to local conditions.

As a species with high morphological plasticity, that is, with a great capacity for adaptation in terms of shape, *Ficus benjamina* can develop as an ornamental tree, shrub, bonsai, hedge, or in other configurations [8].

According to Oliveira, Inácio, and Pantoja (2017) [8], individuals of the genus Ficus have accelerated growth in urban areas and can reach more than 30 meters in height. However, the evaluated specimens presented an average height of 9.7 meters, with values between 2 and 17 meters. This limitation is attributed to the constant practice of pruning, which, although necessary, when performed inadequately, compromises the natural development of the tree.

In addition, the average bifurcation height (the point of insertion of the first branch on the trunk) was only 1 m, a value lower than the recommended minimum of 1.8 m, in order to avoid obstacles to pedestrian traffic, especially those with reduced mobility [14]. Therefore, this low bifurcation requires frequent pruning, motivated mainly by the need to prevent conflicts with the overhead electrical network and nearby buildings.

It is worth noting that pruning plays a fundamental role for the proper management of urban trees, as it contributes to safety, healthy development, and the balance of vegetation. However, when performed with excessive frequency and without technical basis, they can become harmful, compromising the phytosanitary conditions of the tree individuals.

Moreover, poorly executed pruning favors the entry of pathogens, reduces the vigor of the trees, and causes deformities in the crown, resulting in the need for new interventions [15]. In this context, the types and quality of the pruning performed on the *Ficus benjamina* specimens in the Áureo Filho Housing Complex were evaluated.

Thus, it was found that 46.2% of the trees underwent drastic pruning, while 30.8% were subjected to maintenance pruning, as illustrated in Figure 2.

Regarding the quality of these interventions, it was observed that 7.7% were considered excellent,

Figure 2. Actions performed on the trees inventoried in the Áureo Filho Housing Complex.

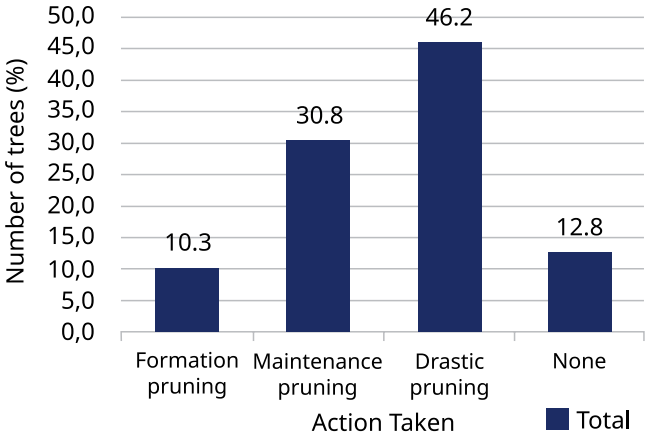

2.6% good, 23.1% regular, 56.4% very poor, and 10.3% of the individuals had no previous pruning. Corroborating these data, it was noted that 41% of the specimens were classified with regular quality (1), 10.3% in a very poor state and 7.7% dead. In good or excellent conditions were only, respectively, 25.5% and 15.4% of the *Ficus benjamina* L. tree individuals. Thus, the results on the state are in Figure 3.

Regarding the phytosanitary changes, 48.7% presented them, such as pests and mechanical damage, which are understood as a result, mainly, of incorrect pruning. In Figure 4, it is observed

Figure 3. General state of the trees inventoried in the Áureo Filho Housing Complex.

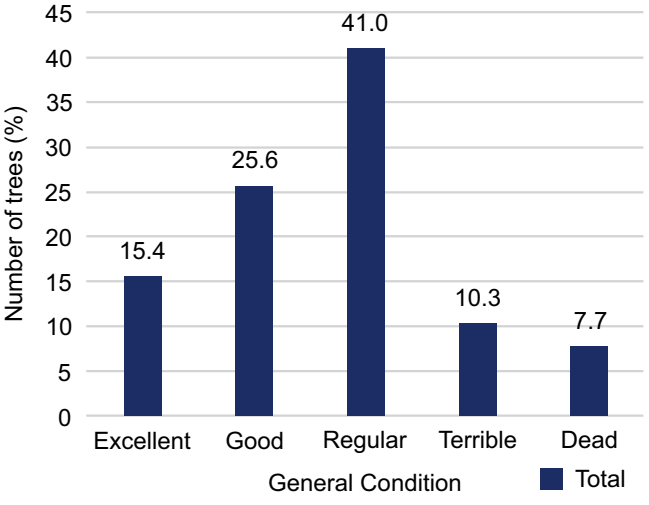

that a little more than half of the tree individuals did not present any phytosanitary problems.

A high number of individuals of the species *Ficus benjamina* L. had the presence of pests and diseases, as can be observed in Figure 4. Such a fact reinforces the inadequacy of planting a large number of trees of the same species, with a certain proximity, as it facilitates the proliferation of pests. In addition, regarding mechanical damage, according to Gilman (2012) [16], such practices favor the emergence of epicormic sprouts, fragile branches that further compromise the tree's structure (Figure 5).

Figure 4. Data on the phytosanitary alteration of the trees - (a) Graph (b) Tree individual from the locality.

(a)

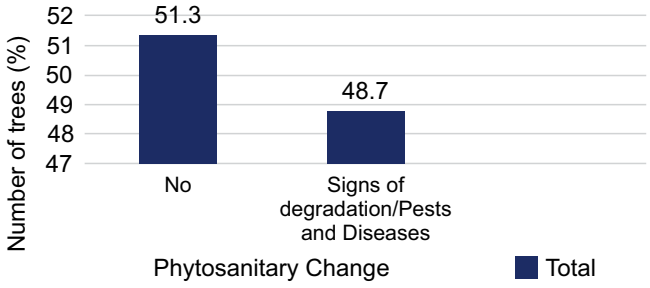

(b)

Figura 5. Epicormic sprouts.

Additionally, the results evidenced different types of interferences related to the presence of *Ficus benjamina* L. in the urban environment. Thus, it was verified that 53.8% of the evaluated individuals need repairs (Figure 6), due to structural and phytosanitary damage already installed.

Conclusion

Based on the interferences observed in the individuals of *Ficus benjamina* L., evaluated in the Áureo Filho Housing Complex, it was possible to identify that some problems faced by the species in the study site are related to the absence of technical management and the inadequacy of the urban environment. It was found that 53.8% of the trees need repairs, whether due to structural damage, phytosanitary issues, or deformities caused by previous interventions. In addition, 28.2% of the specimens presented direct conflicts with elements of the urban infrastructure, such as sidewalks,

Figura 6. Recommended actions for the trees inventoried in the Áureo Filho Housing Complex.

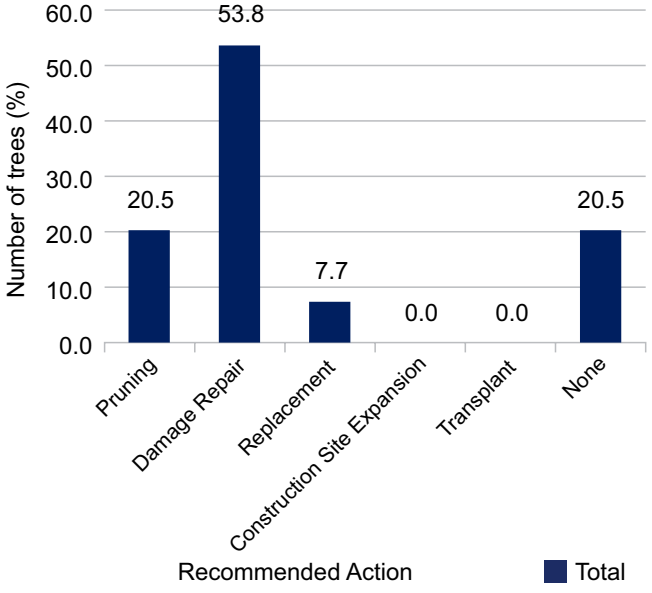

walls, and service networks, highlighting the lack of planning in the planting of this species.

Furthermore, other relevant factor was the occurrence of root surfacing in 69.2% of the individuals analyzed, which represents a risk to the stability of the pavement and other constructed structures. Therefore, these data reinforce the vulnerability of the species in dense urban environments, especially when there is no adequate technical monitoring. Thus, the importance of training the professionals responsible for tree planting is highlighted, as well as the re-evaluation of the use of Ficus benjamina in tree planting plans in Brazil, in order to consider the impacts caused and the frequency of the species above what is recommended by the literature.

References

1. Falcão RS, Gomes R, Péres MZ, Oliveira JT, Callegaro RM. Análise quali-quantitativa da arborização de cinco praças em Jerônimo Monteiro, Espírito Santo. Rev Soc Bras Arboriz Urbana. 2020;15(2):90-103.
2. Companhia Paranaense de Energia (COPEL). Arborização de vias públicas: guia para os municípios. Curitiba: COPEL; 2009.
3. Teixeira IF, Silva RM, Tatsch GL. Compatibilidade da arborização de ruas da Avenida Celestino Cavalheiro, São Gabriel-RS. Floresta Ambient. 2011;18(4):438-50.
4. Lacerda RMA, Lira Filho JA, Santos RV. Indicação de espécies de porte arbóreo para a arborização urbana no semiárido paraibano. Rev Soc Bras Arboriz Urbana. 2011;6(1):51-68.
5. Gonçalves W, Paiva HN. Árvores para o ambiente urbano. Viçosa: Aprenda Fácil; 2004.
6. Biondi D, Muller E. Espécies arbóreas invasoras no paisagismo dos parques urbanos de Curitiba, PR. Floresta. 2013;43(1):69-82.
7. Alves LP, Costa JAS, Costa CBN. Arborização urbana dominada por espécies exóticas em um país megadiverso: falta de planejamento ou desconhecimento? Rev Bras Geogr Fís. 2023;16(3):1304-75.
8. Oliveira ACS, Inácio LS, Pantoja SCS. Estudo da presença de cristais na folha de Ficus benjamina L. (Moraceae) em Realengo, RJ. Rev EA. 2017;(60).
9. Instituto Brasileiro de Geografia e Estatística (IBGE). Feira de Santana: panorama [Internet]. Rio de Janeiro: IBGE; 2022. Available from: https://cidades.ibge.gov.br
10. Teles AO. O comércio informal em Feira de Santana: a realidade da Rua Sales Barbosa. Sitientibus. 2017;(56):9-18.
11. Silva MS, Santos J. Trajetória da implantação do campus da UEFS no contexto regional de Feira de Santana. Rev Latino-Am Hist Geogr Histórica. 2021;1(1):132-52.
12. Silva Filho DF, Pizetta PUC, Almeida JBSA, Pivetta KFL, Ferraudo AS. Banco de dados relacional para cadastro, avaliação e manejo da arborização em vias públicas. Rev Árvore. 2002;26(5):629-42.
13. Santamour FS Jr. Trees for urban planting: diversity, uniformity, and common sense. Washington (DC): U.S. National Arboretum; 2002.
14. Lima Neto EM, Bardelli-da-Silva MY, Silva AR, Biondi D. Arborização de ruas e acessibilidade no bairro Centro de Curitiba-PR. Rev Soc Bras Arboriz Urbana. 2010;5(4):40-56.
15. Martins LFV, Andrade HHB, De Angelis BLD. Relação entre podas e aspectos fitossanitários em árvores urbanas na cidade de Luiziana, Paraná. Rev Soc Bras Arboriz Urbana. 2010;5(4):141-55.
16. Gilman EF. An illustrated guide to pruning. New York: Delmar; 2012.

Numerical and Experimental Analysis of a Pre-Stressed Aluminum 6061-T6 Chassis for Offshore Structural Applications

Juan Carlos Romero Albino[1]*, Roberto Guilherme Lopes[2], Jhonderson Oliveira Brazil[3], Frederico Garcia de Oliveira[4], Lucas Lincoln Fonseca Soares[5], Toni Antunes Ferraz[6]

[1]SENAI CIMATEC University, Industrial Product Development; Salvador, Bahia, Brazil

This paper presents an integrated experimental and numerical investigation of the tensile and modal behaviors of a pre-stressed aluminum chassis (Al 6061-T6) designed for offshore structural applications. The chassis, composed of four metallic parts assembled with a 0.15 mm interference fit, was subjected to a tensile test in which the base was fixed using bolted plates and the upper part was pulled via a gripping device. The experimental force–displacement curve revealed a maximum force of 486.6 N at 1.25 mm displacement. To complement the experimental results, a finite element analysis (FEA) was performed in ANSYS Workbench, employing a nonlinear contact model with friction. Simulations were conducted with friction coefficients of 0.15 and 0.3, and the best agreement with the experimental data was achieved for μ = 0.15, yielding a maximum force of 474.9 N at the same displacement. Modal analyses were carried out for two assembly conditions: bonded contact (no interference) and interference fit with μ = 0.15. The bonded model exhibited natural frequencies of 29.015 Hz, 117.47 Hz, 137.76 Hz, 142.81 Hz, 168.04 Hz, and 344.21 Hz, while the pre-stressed model showed significantly higher values: 72.543 Hz, 73.861 Hz, 83.645 Hz, 217.59 Hz, 264.61 Hz, and 267.74 Hz. These results demonstrate that pre-stressing through interference fit not only enhances the static load-bearing capacity but also increases the dynamic stiffness, shifting natural frequencies to higher values. The findings provide valuable insights for the design and reliability assessment of pre-stressed metallic components in offshore environments. This integrated approach, combining experimental validation and advanced numerical modeling, supports the development of safer and more efficient offshore structural systems, ensuring improved performance under demanding operational conditions.

Keywords: Aluminum Chassis. Interference Fit. Finite Element Analysis. Modal Analysis. Offshore Structures.

Offshore structures are constantly exposed to complex loading and environmental conditions, which demand robust design and evaluation methodologies to ensure their structural integrity and longevity. The dynamic and static behavior of structural components, especially those involving pre-stressed assemblies, is of paramount importance in offshore engineering, given its direct influence on safety, reliability, and service life [1,2]. Pre-stressing, achieved through interference fits or other methods, can significantly alter both the load-bearing capacity and the vibrational characteristics of metallic structures, impacting their response to operational and extreme events [1-3].

Received on 20 February 2026; revised 18 April 2026.

Address for correspondence: Juan Carlos Romero Albino. Avenida Orlando Gomes, 1865 – Piatã. Salvador, Bahia, Brazil. Zipcode: 41650-010. E-mail: juan.albino@fieb.org.br.

J Bioeng. Tech. Health 2026;9(5):462-467

However, assembly methods, including interference fits and bolted connections, introduce additional complexities into the mechanical behavior of these components. The interaction between contact surfaces, friction, and pre-stress levels can modify stress distribution, stiffness, and modal properties, all crucial aspects for static and fatigue performance [4,5].

Aluminum alloys, such as 6061-T6, have been increasingly employed in offshore applications due to their favorable strength-to-weight ratio, corrosion resistance, and manufacturability. Experimental investigations, such as tensile testing, provide direct insights into the force-displacement behavior and failure mechanisms of assembled structures. These tests are essential for validating numerical models and for understanding the influence of assembly parameters, such as interference fit and friction, on the overall mechanical response [3,6]. In parallel, finite element analysis (FEA) has become an indispensable tool for simulating

complex contact interactions, nonlinear material behavior, and dynamic responses under various loading scenarios [6,7]. The integration of experimental and numerical approaches allows for a more accurate and comprehensive assessment of structural performance, facilitating the optimization of design and maintenance strategies for offshore components.

Modal analysis, both experimental and numerical, is widely used to characterize the dynamic properties of offshore structures, including natural frequencies and mode shapes. These properties are sensitive to changes in boundary conditions, pre-stress levels, and assembly methods, making modal analysis a powerful technique for damage detection, structural health monitoring, and reliability assessment [4,7,8]. Recent advances in operational modal analysis and structural health monitoring have further enhanced the ability to detect and localize damage, evaluate fatigue life, and inform maintenance decisions in offshore environments [7,8].

This study focuses on the experimental and numerical analysis of an aluminum chassis assembled with a 0.15 mm interference fit. The objectives are: (1) to characterize the tensile behavior through experimental testing, (2) to calibrate a finite element model to replicate the observed force-displacement response, and (3) to investigate the impact of pre-stressing on the modal properties of the assembly. By systematically comparing bonded and interference-fit conditions, the study elucidates the role of assembly-induced pre-stress and friction in governing both static and dynamic behaviors. The results contribute to a broader understanding of pre-stressed metallic structures in offshore applications, supporting the development of more reliable and efficient design methodologies [1,2,4,7].

Materials and Methods

The investigation began with the fabrication of an aluminum chassis composed of four Al 6061-T6 parts, assembled using a 0.15 mm interference fit. The assembly process ensured uniform contact and pre-stress across all interfaces. The chassis was prepared for tensile testing by securing its base with two bolted plates, while the upper section was connected to a gripping device designed to apply axial loads in a controlled manner (Figure 1).

The experimental tensile test was conducted using a universal testing machine. The load was applied at a constant displacement rate,

Figure 1. Experimental tensile test setup and finite element model.

and both force and displacement were recorded continuously. The test proceeded until a maximum displacement of 1.25 mm was reached, at which point the maximum force was documented. The resulting force-displacement curve provided a direct measure of the assembly's stiffness and load-bearing capacity.

To complement the experimental work, a detailed finite element model of the chassis was developed in ANSYS Workbench. The model incorporated the precise geometry of the assembly, including the interference fit. Nonlinear contact elements were employed to simulate the interaction between mating surfaces, with friction modeled using a Coulomb friction law. Two friction coefficients, $\mu = 0.15$ and $\mu = 0.3$, were considered to assess their influence on the simulated response.

The FEA simulations replicated the experimental boundary conditions, with the base fixed and a prescribed displacement of 1.25 mm applied to the upper section. The resulting force-displacement curves were extracted for both friction coefficients and compared to the experimental data (Figure 2). The friction coefficient yielding the closest agreement with the experimental maximum force was identified as the most representative of the actual assembly conditions.

Modal analyses were performed on the finite element model to evaluate the dynamic properties of the chassis under different assembly scenarios. Two cases were considered: (1) bonded contact, representing an idealized assembly without interference or friction, and (2) interference fit with $\mu = 0.15$, reflecting the pre-stressed condition observed experimentally. The analyses computed the first six natural frequencies and corresponding mode shapes for each scenario. The results were visualized to illustrate the impact of pre-stressing on vibrational behavior (Figures 3, 4).

A comparative assessment of the natural frequencies obtained from both models was conducted and summarized in Table 1. This comparison provided quantitative insights into the effect of assembly-induced pre-stress and friction on the dynamic characteristics of the structure.

Throughout the study, the integration of experimental and numerical methods enabled a robust evaluation of the chassis's mechanical and dynamic performance. The approach facilitated the calibration of model parameters, the validation of simulation results, and the interpretation of the influence of assembly conditions on both static and modal behaviors. The methodology

Figure 2. Experimental and numerical ($\mu = 0.15$ and $\mu = 0.3$) force–displacement curves.

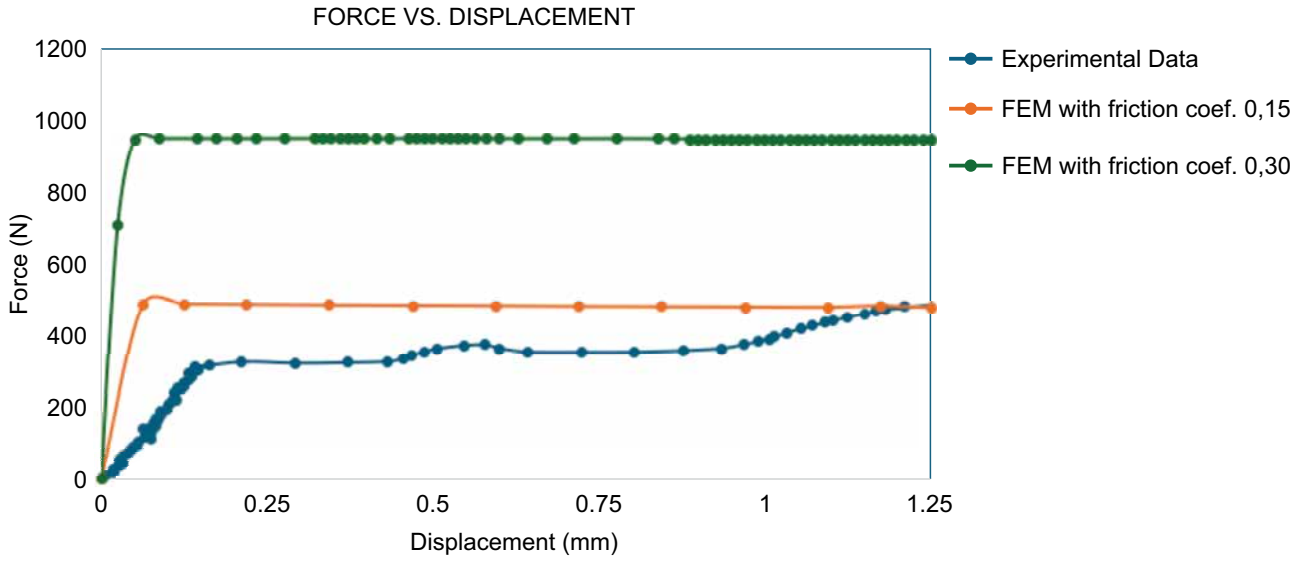

Figure 3. Vibration modes of the numerical model with bonded contact.

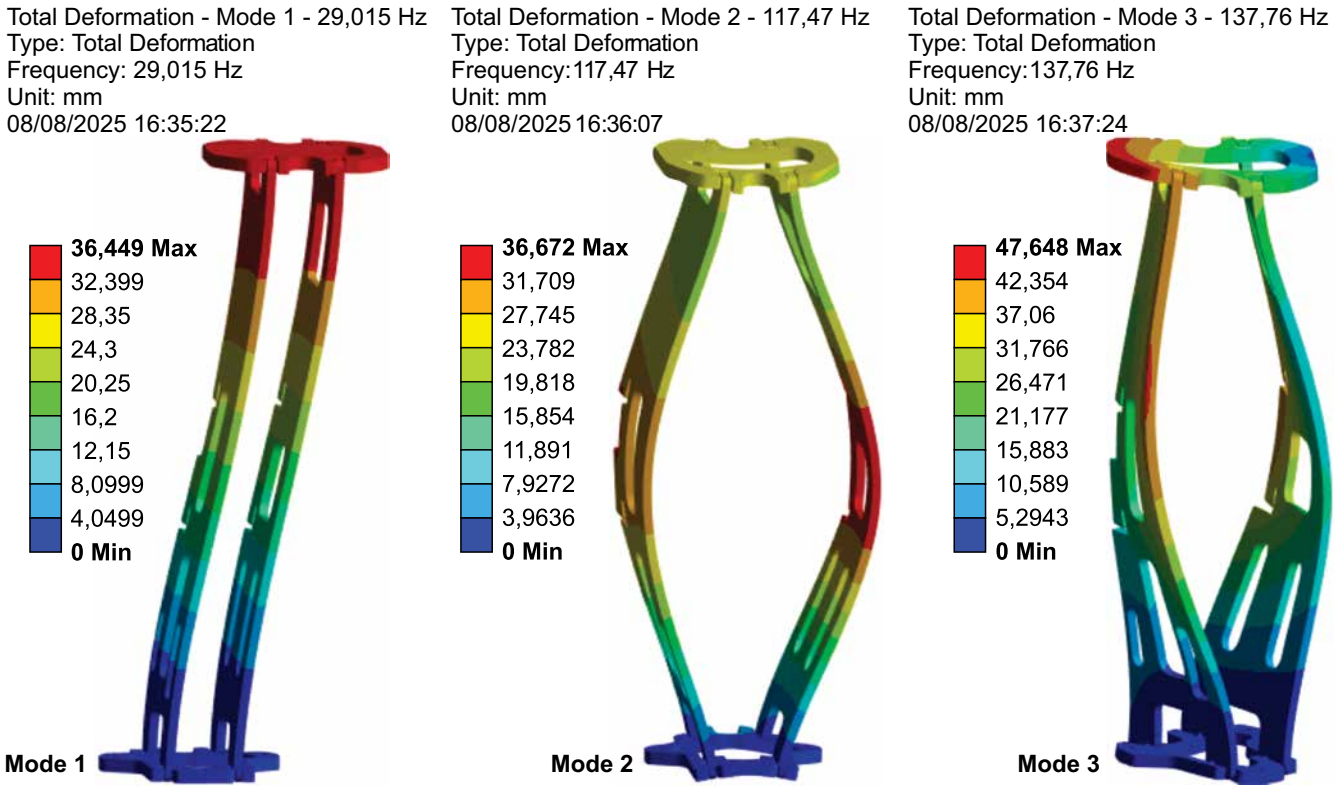

Figure 4. Vibration modes of the numerical model with 0.15 mm interference and $\mu = 0.15$.

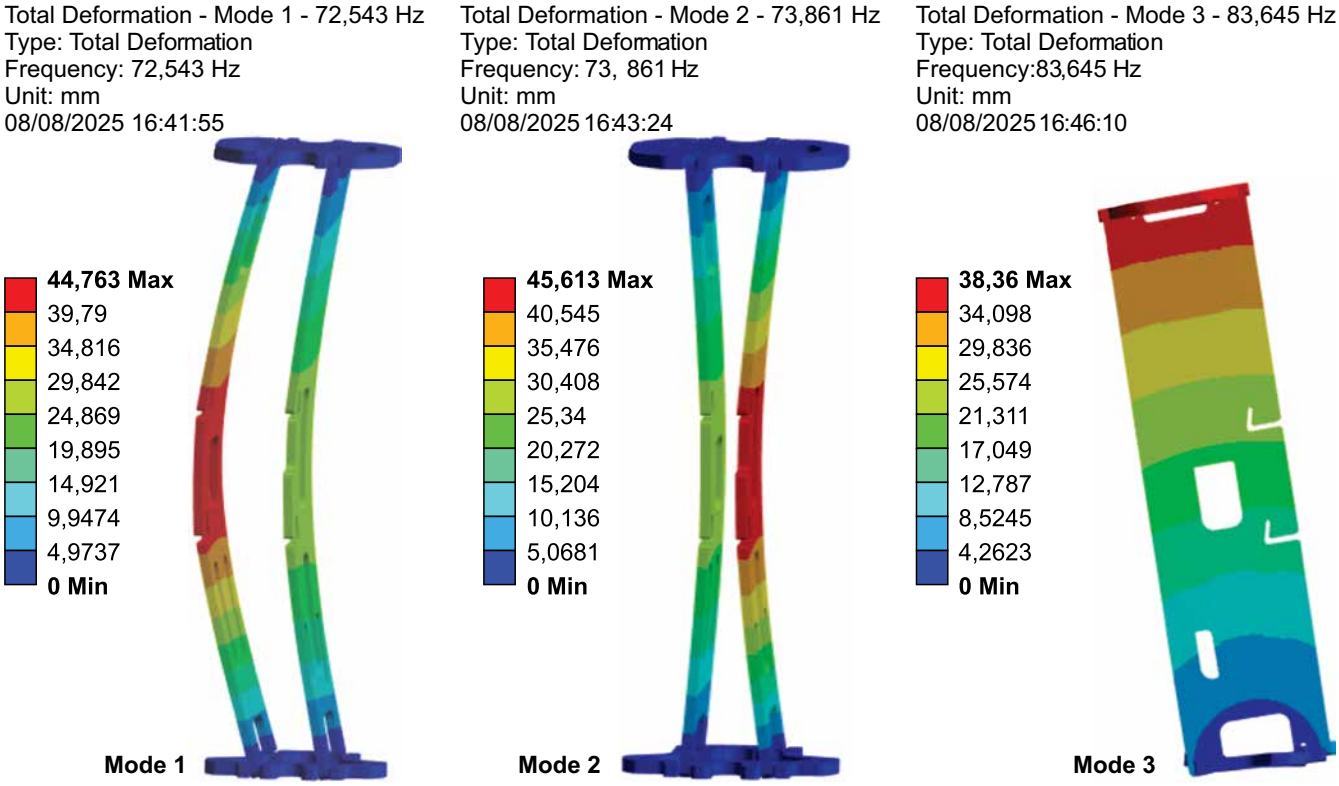

Table 1. Comparison of natural frequencies between bonded contact and interference (μ = 0.15) models.

Mode	Bonded Contact (Hz)	Interference Fit (Hz)
1	29.015	72.543
2	117.47	73.861
3	137.76	83.645
4	142.81	217.59
5	168.04	264.61
6	344.21	267.74

aligns with established practices in offshore structural analysis, where combined experimental and computational techniques are employed to address the complexities of pre-stressed metallic assemblies [1,2,4,7].

Results and Discussion

The experimental tensile test generated a force-displacement curve characterized by an initial linear region, followed by a plateau as the maximum force was approached. The maximum recorded force was 486.6 N at a displacement of 1.25 mm. This result served as a benchmark for evaluating the accuracy of the numerical simulations.

Finite element simulations with friction coefficients of μ = 0.15 and μ = 0.3 yielded distinct force-displacement responses. The model with μ = 0.15 produced a maximum force of 474.9 N at 1.25 mm displacement, closely matching the experimental result. In contrast, the μ = 0.3 model overestimated the force, indicating that a lower friction coefficient more accurately represented the actual assembly conditions. The comparison of experimental and numerical curves is presented in Figure 2.

Modal analysis of the bonded contact model revealed natural frequencies of 29.015 Hz, 117.47 Hz, 137.76 Hz, 142.81 Hz, 168.04 Hz, and 344.21 Hz. These values served as a baseline for assessing the impact of pre-stressing. When the interference fit (0.15 mm) and μ = 0.15 friction were introduced, the natural frequencies increased significantly to 72.543 Hz, 73.861 Hz, 83.645 Hz, 217.59 Hz, 264.61 Hz, and 267.74 Hz. The mode shapes for both scenarios are illustrated in Figures 3 and 4.

Table 1 summarizes the comparison of natural frequencies between the bonded and interference-fit models. The results demonstrate that pre-stressing through interference fit and friction not only enhances the stiffness of the assembly but also elevates its dynamic response, as evidenced by the higher natural frequencies. This behavior is consistent with findings in the literature, where pre-loading and assembly conditions are shown to influence both static and dynamic properties of offshore structural components [1,4,7].

Conclusion

This study offers a detailed experimental and numerical evaluation of the tensile and modal behaviors of a pre-stressed aluminum chassis for offshore structural applications. The integration of interference fit and friction in the assembly process demonstrated a significant influence on both the static load-bearing capacity and the dynamic characteristics of the structure.

The experimental tensile test established a maximum force of 486.6 N at 1.25 mm displacement, serving as a crucial reference for model calibration. Finite element analysis, incorporating nonlinear contact and friction, demonstrated that a friction coefficient of μ = 0.15 resulted in the best agreement with experimental data, highlighting the importance of accurate parameter selection in numerical simulations.

We observed a significant increase in the chassis's natural frequencies due to pre-stressing from the interference fit, indicating improved dynamic stiffness. This finding strongly supports

established trends in pre-stressed metallic structures [1,4,7]. Our results align with Zeinoddini and colleagues [1], who demonstrated that axial pre-loading can profoundly alter the dynamic characteristics of structural members, affecting their load-carrying capacity and energy absorption. Furthermore, consistent with the core principles of modal analysis for structural assessment [4,7], our results highlight how pre-stressing effectively modifies stiffness distribution, leading to measurable shifts in vibrational properties. By providing detailed experimental and numerical data for an Al 6061-T6 chassis with a 0.15 mm interference fit, our study presents a specific case that reinforces these broader insights, particularly relevant for offshore applications. This consistency underscores the importance of incorporating pre-stressing into design to optimize dynamic response and enhance the reliability of components in demanding environments.

The combined experimental and numerical approach adopted in this study offers a robust framework for evaluating the mechanical and dynamic behaviors of pre-stressed assemblies. The insights gained contribute to the optimization of design methodologies and the advancement of structural health monitoring and damage detection techniques in offshore engineering. Future work may extend these findings by exploring the effects of varying interference levels, material properties, and environmental conditions on the performance of offshore structural components.

Acknowledgement

We thank Senai Cimatec University for the support and resources allocated to the development of this work.

References

1. Zeinoddini M, Harding J, Parke G. Dynamic behaviour of axially pre-loaded tubular steel members of offshore structures subjected to impact damage. Ocean Eng. 1999;26(10):1045-63.
2. Lian J, Ding H, Zhang P, Yu R. Design of large-scale prestressing bucket foundation for offshore wind turbines. Trans Tianjin Univ. 2012;18(2):89-97.
3. Han S, Zhou A, Ou J. Relationships between interfacial behavior and flexural performance of hybrid steel-FRP composite bars reinforced seawater sea-sand concrete beams. Compos Struct. 2021;273:114287.
4. Liu G, Yuanzhuang Z, Leng D, Tian X, Weilei M. Research on structural damage detection of offshore platforms based on grouping modal strain energy. Ocean Eng. 2017;142:571-82.
5. Adumene S, Khan F, Adedigba S, Zendehboudi S, Shiri H. Offshore pipeline integrity assessment considering material and parametric uncertainty. J Pipeline Sci Eng. 2021;1(3):265-76.
6. Berkia A, Rebai B, Mansouri K, Chitour M, Khadraoui F. Using finite element modeling to predict stress concentration factors in tubular T, Y and K joints. Eng Solid Mech. 2023;11(4):307-16.
7. Khosravan A, Asgarian B, Shokrgozar HR. Improved modal strain energy decomposition method for damage detection of offshore platforms using data of sensors above the water level. Ocean Eng. 2020;218:108198.
8. Nabuco B, Tarpø M, Tygesen UT, Brincker R. Fatigue stress estimation of an offshore jacket structure based on operational modal analysis. Shock Vib. 2020;2020:1-13.

Unraveling Improvements in Underwater Leak Detection Using Color Channel Operations

Diego Perpétuo Andrade de Oliveira[1]*, Eric Oliveira Santos[1], João Paulo Barros Silva[1], Taniel Silva Franklin[1]
[1]SENAI CIMATEC University, Department of Software; Salvador, Bahia, Brazil

This paper presents a computer vision approach for detecting underwater liquid leaks in the oil and gas industry, focusing on scenarios with limited datasets. We propose the use of color indices—originally developed for vegetation studies, such as ExGR and CIVE—as preprocessing to enhance visual contrast and improve deep learning performance. A custom dataset of 240 simulated leak images, captured in an aquarium under blue lighting, was processed using ExGR, CIVE, and a modified CIVE index developed in this study. The YOLO12n model was trained and evaluated across these configurations. Results show that the modified CIVE index achieved the highest accuracy, surpassing RGB and other indices, with notable gains in mAP. These findings demonstrate that combining tailored color indices with lightweight object detection models can enhance leak identification under adverse conditions, offering a cost-effective and efficient solution for environmental monitoring and operational safety.
Keywords: Leak Detection. Computer Vision. Color Indices. Oil and Gas Industry.

The offshore oil and gas industry is one of the most profitable industries in the world. However, due to the nature of its deep subsea operations these industries could face some issues such as safety concerns and environmental impact. Such issues can directly impact enterprise profit and generate life risks. Machinery fluid leakages are examples of issues that can affect the external environment and normal operation conditions.

Subsea leak detection has traditionally been carried out using sensor-based methods, such as acoustic systems [1,2], fluorometers and sonars [3], thermal cameras, lasers [4], pressure sensors, and vibration sensors. However, their effectiveness is affected by environmental noise, inadequate sensor positioning, and difficulties in detecting small leaks [5]. Fluorometers, for example, are capable of detecting specific substances dissolved or suspended in water, but they have limited performance in environments with high background fluorescence and may suffer from sensitivity degradation over time [3].

Received on 20 February 2026; revised 18 April 2026.
Address for correspondence: Diego Perpétuo Andrade de Oliveira. Avenida Luís Viana Filho, 8812 – Paralela. Salvador, Bahia, Brazil. Zipcode: 41741-590. E-mail: diego.oliveira@fbter.org.br.

J Bioeng. Tech. Health 2026;9(5):468-473

In recent years, camera-based methods have gained prominence [6] due to their relatively low cost, high spatial and temporal resolution, and ability to capture rich visual information. With the advancement of computer vision, deep learning techniques have been applied to detect leaks from underwater images [7]. However, these techniques face a key limitation: the scarcity of suitable datasets. Collecting real-world subsea leak imagery is costly and logistically complex, resulting in small, highly variable datasets that hinder the training of robust neural networks [8]. This constraint affects the training of deep neural networks, which require a large volume and diversity of samples to generalize well in real-world scenarios.

One strategy to optimize learning and reduce this dependency is image preprocessing using color indices. These indices, based on the RGB color space, transform the input image into a single-channel representation where green vegetation is enhanced, simplifying the identification task for the neural network and improving detection performance in many cases. Most of them target using Image enhancement, color correction, image dehazing [9] to obtain the data that then is post processed by deep learning models to extract patterns indicating presence of leakages.

This work proposes the application of color indices widely documented in the literature as a

strategy for underwater leak detection, aiming to mitigate the constraints arising from the limited availability of data. For the validation of the proposed approach, images of simulated leaks in a controlled environment (aquarium) were used, which were processed and analyzed using the YOLO12n[10] detection model.

Related Works

Several color indices have been proposed in the literature to enhance the segmentation of regions of interest, especially for distinguishing vegetation from soil in agricultural images. The Excess Green Index (ExG) [11], for example, amplifies the green component in the image, producing high-contrast representations that facilitate segmentation. Other indices, such as the Color Index of Vegetation Extraction (CIVE) [12], were derived through statistical optimization to maximize the separation between vegetation and background. To improve robustness, variations such as ExGR [13] have emerged, which reduce false positives by suppressing yellowish debris, as well as MExG [14] and VEG [15], which are designed to be more consistent under varying lighting conditions — a common challenge in open-field environments.

Using a color indice as input to a CNN instead of the traditional RGB image represents an approach that provides a strategic advantage to the detection model, especially in cases of limited datasets. This technique converts the image into a single channel where vegetation is already highlighted, allowing the network to focus on learning more complex morphological features such as leaf shape and texture, rather than expending resources to separate the plant from the background. For instance, Milioto and colleagues [16] fed a lightweight encoder-decoder network with only the ExG index to perform real-time crop and weed segmentation. Similarly, Silva and colleagues [17] used ExGR as the sole input to a CNN for maize plant detection. In both cases, simplifying the input resulted in lighter and faster models, optimized for practical applications that require high computational efficiency.

Beyond the complete replacement of RGB, color indices can also be used to enrich the input data or to increase model robustness in field conditions. Kerim and colleagues [18], for example, demonstrated that adding CIVE as an extra channel to an input image (along with RGB and other indices) improved the performance of a U-Net network in rice field segmentation, compared to using only RGB. These approaches show that, whether by simplifying or enriching input data, color indices are versatile and promising tools for optimizing neural network performance in detection tasks.

Materials and Methods

A series of experiments was conducted to evaluate how different input configurations influence object detection performance using the YOLO12n model.

To improve the efficiency of the training and inference processes, we adopted YOLO Nano[10] (YOLO12n model), a lightweight version of the YOLO architecture specifically designed for real-time applications and deployment in environments with limited computational resources. Despite its compact size and reduced number of parameters, YOLO Nano maintained competitive detection performance, demonstrating its suitability for the task of leak identification. Its architecture is optimized to balance accuracy and speed, making it a practical choice for scenarios where latency and hardware constraints are critical.

The experiments were conducted under four main configurations: (i) training with RGB images (baseline); (ii) training using the ExGR color indice; (iii) training with the CIVE color indice; and (iv) training with a modified version of the CIVE indice, developed in this work to enhance the visibility of leaks in the samples. The Table 1 shows the color indices formulas with the coefficients used for experimentation.

An experimental setup was created to simulate an aquatic environment, as shown in Figure 1. Using a water-filled aquarium, a camera is positioned

Table 1. Color ratio index.

Index	Formula
CIVE	0.441R − 0.811G + 0.385B + 18.78745
CIVE (ours)	0.141R − 0.111G + 0.185B + 1.78745
ExGR	(2G − R − B) − (1.3R − G)

Figure 1. Laboratory setup for tests.

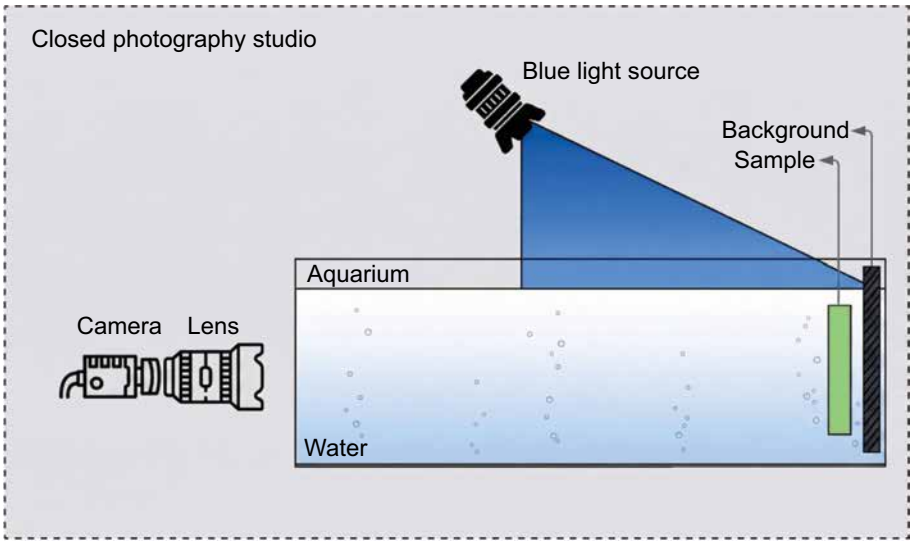

toward the aquarium, which has a background to aid visualization. Additionally, a light source is positioned to illuminate the environment with a selected color—in this case, blue.

The use of blue light was chosen because it enhances the identification of the color green, as green objects exhibit high reflectance in this spectral range, resulting in greater contrast compared to other surfaces. In an underwater environment, this choice is even more relevant since water quickly absorbs longer wavelengths, better preserving blue light and, consequently, the visual distinction of green targets [19].

Dataset

The dataset used in the experiments consists of 240 annotated images, each containing bounding boxes that delineate the objects of interest. The images were randomly split into three subsets: 144 samples for training, 36 for validation, and 60 for testing. Prior to training, all images were resized to 640 × 640 pixels, maintaining their original aspect ratio to ensure consistency across inputs. Figure 2 (a) shows an example of an aquarium environment using white light for illumination. The use of blue light offers several advantages in the context of visual analysis and computer vision. Blue light enhances the contrast of certain surface textures and materials, particularly in cases where defects, edges, or fluid residues may be subtle under standard white light. This characteristic helps to accentuate features that are otherwise difficult to detect, improving the signal-to-noise ratio in the image and highlighting relevant regions for object detection. It is possible to see in Figure 2 (b), where the experimental environment is illuminated with blue light.

Figure 2. Comparison of samples under different lighting conditions.

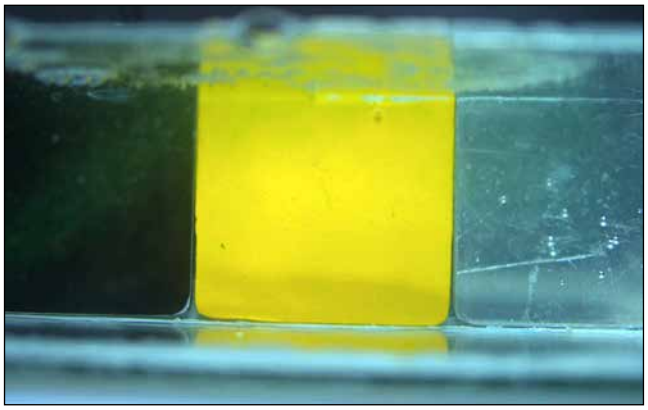

(a) Sample with white light.

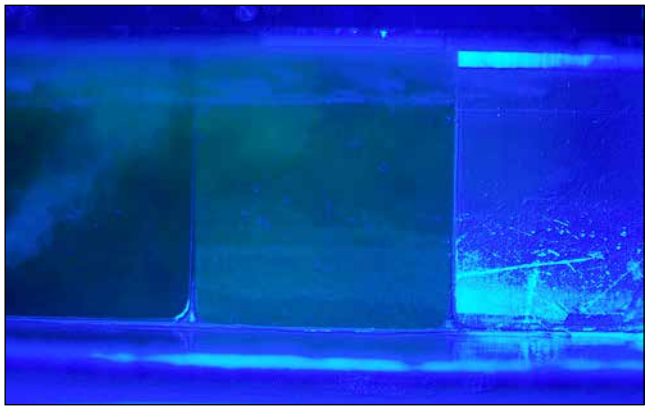

(a) Sample with blue light.

Images generated through index calculation and channel stacking offer alternative representations that can emphasize specific visual properties not always evident in standard RGB formats. In the case of index-based images, a mathematical formula is applied to the original RGB channels to produce a single-channel grayscale image that highlights particular features. These single-channel images were then resized and normalized to be compatible with the YOLO12n model's input requirements, enabling the network to learn from a condensed yet feature-rich representation of the scene.

For the channel-stacked configuration, a hybrid image was created by replacing the red (R) channel with the index map while retaining the original green (G) and blue (B) channels. This approach aimed to preserve the spatial and chromatic context of the original image while injecting the enhanced discriminatory power of the color indice. This type of input is particularly useful in applications where certain features are more salient in transformed domains than in raw RGB space.

To select the most suitable indices for visually enhancing leak detection, different color indices documented in the literature were evaluated based on their ability to highlight leak regions against the background. Among the tested indices, CIVE and ExGR exhibited the most pronounced visual contrast, making them the main candidates for experimentation. The ExGR and CIVE indices were selected for demonstrating a high capability to isolate leak areas from the surrounding structures.

Training

The training process is carried out using the YOLO12n model, initialized with COCO-pretrained weights [20]. Each variant is trained for 100 epochs, with an image size of 640 × 640 pixels and a batch size of 16 samples. The experiments are performed on a workstation equipped with an NVIDIA RTX 3060 GPU, 16 GB of RAM, and an 11th-generation Intel Core i7 processor.

Results

The results confirm that our model can generalize well on the dataset, even when trained on index-transformed images rather than standard RGB inputs. By adjusting the channel coefficients of the best-performing index, CIVE, it is possible to maximize the visual contrast of the leak relative to the background, making it easier for the object detection model to detect. As shown in Table 2, the modified CIVE index achieved the highest performance, surpassing RGB, ExGR, and the original CIVE formulation. The results confirm that the adjusted coefficients in the modified index were able to maximize the visual contrast between the leaks and the background, facilitating the learning process of the YOLO12n.

In contrast, the original CIVE index showed limited performance (0.157 mAP@50), indicating that its default coefficients were not optimal for the optical properties of the underwater environment with blue lighting.

The use of the modified CIVE index enabled the detection model to generalize better on the test set, reducing false negatives and improving the localization of leaks even in visually challenging scenarios. These results confirm the initial hypothesis that adjusting the index coefficients to the specific optical characteristics of the experimental setup would increase leak–background contrast and, consequently, detection accuracy, enabling accurate and computationally efficient detection in contexts where large-scale datasets are unavailable. Furthermore, the approach proved to be compatible with lightweight architectures such as YOLO12n, demonstrating that high-performance results can be achieved without the need for complex or resource-intensive models, which is a key requirement for real-time applications in off-shore operations.

Conclusion

In this study, we propose an approach for detecting underwater liquid leaks using image-based techniques, vegetation indices, and deep learning. To address the limitation of available data, we employed color indices calculated from RGB channels. The YOLO12n model was trained on a custom dataset of fluid leaks captured under external blue lighting, applying post-processing techniques to the CIVE vegetation index to maximize the contrast between the leak and the background. This strategy resulted in a model that outper-formed the use of raw RGB images without post-processing, as well as other evaluated indices.

This research highlights the potential of deep learning for leak detection through image processing techniques applied to solving environmental problems.

Table 2. YOLO12n performance using index + G + B channel combinations as input (RGB as baseline).

Input Configuration	mAP@50	mAP@50:95	Image Sample
CIVE (modified, proposed)	0.555	0.278	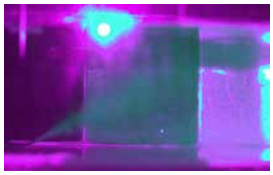
RGB (original image)	0.225	0.079	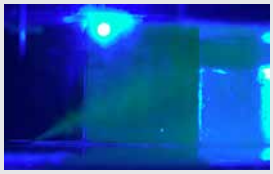
CIVE (original)	0.157	0.058	
ExGR	0.087	0.017	

For future work, we intend to improve the models and expand the dataset. We will also investigate new coefficients to optimize vegetation indices, aiming to maximize leak contrast. This optimization seeks to enhance algorithm learning and improve evaluation metrics. In addition, we plan to employ quantitative metrics for coefficient determination, replacing the exclusively visual criterion currently used.

Acknowledgment

This research was executed in partnership between SENAI CIMATEC and Shell Brasil. The authors would like to acknowledge Shell Brasil Petroleo LTDA, the Brazilian Company for Industrial Research and Innovation (EMBRAPII), and the Brazilian National Agency for Petroleum, Natural Gas and Biofuels (ANP) for the support and investments in RD&I.

References

1. Feng C, Zhao J, Ran Q, Qu M, Guo Z. Acoustic-based approach for micro-leakage detection and localization in water supply pipelines. Environ Sci Water Res Technol. 2024.
2. Tu Q, Wu K, Cheng E, Yuan F. Dual-feature-based bubble sound detection method and its application in passive acoustical detection of underwater gas leakage. IEEE J Ocean Eng. 2024;49(4):1657-74.
3. Wang Y, Thanyamanta W, Bulger C, Bose N, Brown R. An experimental study of the cooperation between sonar and a fluorometer for detecting underwater oil from an underwater vehicle. In: OCEANS 2022 - Chennai. Chennai: IEEE; 2022. p. 1-4.
4. Fedotov YV, Belov M, Kravtsov D, Titarenko K, Gorodnichev V. Selecting laser fluorosensor detection band to monitor oil pipeline leaks. In: IOP Conference Series: Materials Science and Engineering. Vol. 1155. Bristol: IOP Publishing; 2021. p. 012074.
5. Yong G. Research on AI-based oil and gas pipeline leak detection and localization technology. In: 2023 International Conference on Intelligent Computing, Communication Convergence (ICI3C). Piscataway (NJ): IEEE; 2023. p. 418-23.
6. Zhao X, Wang X, Du Z. Research on detection method for the leakage of underwater pipeline by YOLOv3. In: 2020 IEEE International Conference on Mechatronics and Automation (ICMA). Piscataway (NJ): IEEE; 2020. p. 637-42.
7. Jiang X, Dai Y, Zhang P, Wang Y, Du T, Zou Y, et al. Study of a machine vision approach to leak monitoring of a marine system. J Mar Sci Eng. 2023;11(7):1275.
8. Duarte AC, Zaffari GB, Rosa RTS, Longaray LM, Drews P, Botelho SS. Towards comparison of underwater SLAM methods: an open dataset collection. In: OCEANS 2016 MTS/IEEE Monterey. Piscataway (NJ): IEEE; 2016. p. 1-5.
9. Mohammad KM. Real-time underwater image enhancement: a systematic review. J Real Time Image Process. 2021.
10. Jocher G, Chaurasia A, Qiu J. Ultralytics YOLO [Internet]. 2023. Available from: https://github.com/ultralytics/ultralytics
11. Woebbecke DM, Meyer GE, Von Bargen K, Mortensen DA. Color indices for weed identification under various soil, residue, and lighting conditions. Trans ASAE. 1995;38(1):259-69.
12. Kataoka T, Kaneko T, Okamoto H, Hata S. Crop growth estimation system using machine vision. In: Proceedings of the IEEE/ASME International Conference on Advanced Intelligent Mechatronics. Vol. 2. 2003. p. 1079-83.
13. Neto JC. A combined statistical-soft computing approach for classification and mapping weed species in minimum-tillage systems [dissertation].
14. Lincoln (NE): University of Nebraska-Lincoln; 2004. Meyer GE, Hindman TW, Laksmi K. Machine vision detection parameters for plant species identification. In: Precision Agriculture and Biological Quality. Vol. 3543. Bellingham (WA): SPIE; 1999. p. 327-35.
15. Hague T, Tillett ND, Wheeler H. Automated crop and weed discrimination in color field images. In: Proceedings of the 5th International Conference on Precision Agriculture. Bloomington (MN); 2000.
16. Milioto A, Lottes P, Stachniss C. Real-time semantic segmentation of crop and weed for precision agriculture robots leveraging background knowledge in CNNs. In: IEEE International Conference on Robotics and Automation (ICRA). Piscataway (NJ): IEEE; 2018. p. 2229-35.
17. Silva MAT, Sousa JM, Souza AM. Maize plant detection using convolutional neural networks with ExGR index. Comput Electron Agric. 2019;167:105064.
18. Kerim Z, Kaya A, Tuncer M. Rice field segmentation using U-Net with color indices as additional input channels. Comput Electron Agric. 2021;184:106127.
19. Roesler C. Absorption by oceanic constituents [Internet]. Ocean Optics Web Book; 2021. Available from: https://oceanopticsbook.info
20. Lin TY, Maire M, Belongie S, Hays J, Perona P, Ramanan D, et al. Microsoft COCO: common objects in context. In: Proceedings of the European Conference on Computer Vision (ECCV). Cham: Springer; 2014. p. 740-55.

Advances in Continuous Glucose Monitoring Systems: A Systematic Review of Sensor Technologies and Mobile Health Integration

Sara Lorena Martins Silva das Virgens[1]*, Herman Augusto Lepikson[1,2]
[1]Federal University of Bahia, Institute of Computing, Graduate Program in Mechatronics; [2]SENAI CIMATEC University; Salvador, Bahia, Brazil

Several studies have focused on the evolution of Continuous Glucose Monitoring Systems (CGMS), particularly regarding their integration with mobile devices and the application of predictive strategies. Considering the increasing relevance of this technology in the healthcare sector, this systematic literature review aims to explore recent scientific advances, highlighting the main types of sensors, algorithms, and connectivity solutions described in the selected studies. The included articles presented innovative approaches involving microwave and electrochemical sensors, as well as techniques for glycemic trend prediction and mobile communication. The findings indicate significant progress in the development of CGMS, especially in real-time monitoring capabilities and the integration of artificial intelligence models for data analysis. However, challenges remain, such as improving sensor sensitivity and specificity, achieving clinical validation in real-life scenarios, and ensuring interoperability between different platforms and devices. The literature also emphasizes the importance of advancing user-centered design, data privacy, and regulatory compliance to facilitate the adoption of these systems in both clinical and personal health monitoring contexts. It is concluded that expanding the technological maturity and accessibility of CGMS is essential to support personalized diabetes management and to improve the quality of life for patients worldwide.

Keywords: Continuous Glucose Monitoring. Sensor Technologies. Mobile Health Integration. Predictive Algorithms.

Abbreviations: CGMS, Continuous Glucose Monitoring Systems; SLR, Systematic Literature Review.

Continuous Glucose Monitoring Systems (CGMS) represent a significant technological advancement in the management of diabetes mellitus, offering a dynamic and real-time method for tracking fluctuations in blood glucose levels throughout the day and night [1]. Unlike traditional methods such as finger-prick capillary blood glucose testing, which provides only isolated snapshots of glycemic status, CGMS enable the continuous collection of interstitial glucose data, allowing for the identification of patterns, trends, and critical fluctuations that may otherwise go undetected. This continuous feedback facilitates timely clinical decision-making, enhances individualized treatment plans, and plays a crucial role in preventing acute complications such as hypoglycemia and hyperglycemia [2].

As the global prevalence of diabetes continues to rise—fueled by aging populations, urban lifestyles, and dietary changes—there is a growing demand for monitoring strategies that are not only clinically effective but also accessible, user friendly, and economically sustainable, especially in resource-constrained settings [3]. Traditional CGMS technologies, although clinically validated, are often limited by their high cost, limited availability in public health systems, and the need for frequent sensor replacement, which restricts their widespread adoption [4].

In response to these challenges, the development of next-generation CGMS has increasingly focused on creating low-cost, minimally invasive or non-invasive solutions [5] that can be seamlessly integrated with mobile devices such as smartphones and smartwatches. These innovations aim to expand the reach of glucose monitoring technologies beyond hospital settings, enabling remote patient monitoring, real-time alerts, and

Received on 20 February 2026; revised 18 April 2026.
Address for correspondence: Sara Lorena Martins Silva das Virgens. Federal University of Bahia; R. Prof. Aristides Novis, 2 - Federação. Salvador, Bahia, Brazil. Zipcode: 40210-630. E-mail: saravirgens@ufba.br.

data-driven interventions. The integration with mobile platforms also opens possibilities for incorporating additional functionalities, including cloud-based analytics, artificial intelligence (AI) for glycemic pattern prediction, and improved user engagement through mobile health (mHealth) applications [6].

Although commercial CGMS devices have demonstrated proven effectiveness, their high cost remains a barrier to large-scale adoption, particularly within public healthcare systems [7]. Furthermore, there are still limitations regarding full integration with mobile platforms and a lack of robust clinical validation in real-world settings [8].

The incorporation of mobile devices into the CGMS ecosystem has proven to be a critical factor in improving treatment adherence and user engagement, especially through wearable technologies that promote autonomy and personalized monitoring [9].

The present systematic literature review aims to answer the following research question: What are the advances, challenges, and trends in the development of low-cost Continuous Glucose Monitoring Systems with mobile integration and predictive potential?

The general objective of this study is to identify, analyze, and synthesize emerging technological solutions for sensors applied to CGMS, with an emphasis on low-cost approaches, mobile integration, and predictive strategies. Specifically, the study aims to: (i) characterize the types of sensors used; (ii) describe the transmission technologies and integration platforms involved; (iii) identify the predictive analysis strategies adopted; and (iv) highlight research gaps and future directions.

Materials and Methods

The methodology adopted in this study was based on the model proposed by Kitchenham and Charters [10] in a systematic literature review applied to software engineering. Accordingly, the concept of SLR (Systematic Literature Review) was adapted to the proposed topic. The methodological process involved four main stages: definition of the research question, development of the search strategy, application of eligibility criteria, and data extraction and analysis.

Search Sources and Research Strategies

The bibliographic search covered the following scientific databases: IEEE Xplore, PubMed, Scopus, ScienceDirect, Web of Science, and Google Scholar — the latter used as a complementary source to expand coverage and identify academic works not indexed in traditional databases.

The search strategy was structured around five main thematic axes: (i) continuous glucose monitoring; (ii) sensors and biosensors; (iii) low-cost technologies; (iv) integration with mobile devices and digital health; and (v) predictive approaches to glycemic events. To this end, descriptors were used, combined with Boolean operators. The main search terms included: “continuous glucose monitoring”, “low cost”, “affordable”, “biosensor”, “sensor technology”, “mobile health”, “Bluetooth”, “smartphone”, “data analytics”, “prediction”, and “hypoglycemia”.

Search terms were adapted according to the structure and features of each database. Initially, only a temporal filter (2015 to 2025) was applied to ensure the relevance and timeliness of the studies. The types of documents considered included scientific articles, theses, dissertations, reviews, and book chapters.

Inclusion and Exclusion Criteria

In addition to the temporal delimitation, this review considered studies published in Portuguese, English, or Spanish that investigated technologies applied to continuous glucose monitoring. Eligible studies addressed the development of economically viable sensor devices, connectivity with mobile technologies and digital health solutions, the use of analytical models for predicting glycemic

events, as well as technical advancements and clinical outcomes related to the implementation of such systems.

Studies with overlapping content, conference abstracts without full-text articles, duplicated records across different databases, and research focused exclusively on theoretical discussions related to diabetes pathophysiology, metabolic processes, or clinical perspectives unlinked to the development, evaluation, or application of technological solutions were excluded.

Data Extraction

After conducting the searches in the selected databases, the results were imported into Zotero, a reference management software that also offers functionalities for organizing and screening studies in systematic reviews. Through Zotero, it was possible to identify and remove duplicate records, assign tags based on predefined inclusion and exclusion criteria, and perform title and abstract screening, ensuring greater transparency, consistency, and traceability in the selection process.

The studies considered potentially eligible were then assessed in full text to verify their alignment with the objectives of this review. Bibliographic data and relevant study information were extracted and organized within Zotero. In parallel, the extracted variables were systematized in structured Microsoft Excel spreadsheets, using standardized fields such as authorship, year of publication, type of sensor, predictive approach, transmission technology, integration with mobile platforms, estimated cost, reported impacts, and key methodological notes.

In addition to these objective elements, representative textual excerpts were also extracted from the full texts, specifically related to the following categories: main findings, reported limitations, and identified gaps and recommendations. This qualitative layer of analysis guided the interpretative selection of content directly from the articles, contributing to a deeper understanding of the evidence and informing the discussion of the review's findings. The triangulation between technical variables and textual excerpts enabled the identification of recurring patterns, contradictions, emerging technological trends, and methodological gaps, thereby enhancing the analytical depth and explanatory power of the review.

Results and Discussion

The Table 1 shows the search results, a total of 464 references were initially retrieved from the selected databases. The study selection process was conducted sequentially through progressive filtering steps.

Table 1. Search results in scientific databases.

Scientific Databases	Number of Items
Google Scholar	20
IEEE Xplore	88
CAPES	30
PUBMed	130
Scopus	114
Web of Science	18
ScienceDirect	64

In the first stage, 97 potential duplicates were identified. After evaluating titles and DOIs—considering that some studies appeared in more than two databases—51 records were excluded. This step resulted in 413 unique references.

Next, keyword filtering was applied to exclude studies involving animal models, using terms such as *in vitro*, rat, rats, animal, and animals. This step excluded 26 studies, reducing the dataset to 387 references.

In the following step, additional terms such as insulin and sensitivity were used to exclude studies focused on insulin-related mechanisms. A total of 33 records were removed, resulting in 354 references.

Subsequently, a temporal filter was applied, excluding studies published before 2015, in accordance with the eligibility criteria. This step removed 94 studies, leaving 260.

Finally, a thematic scope analysis was performed to exclude studies with a purely clinical, metabolic, or pathophysiological focus unrelated to technological applications in glucose monitoring. This step led to the exclusion of 183 studies, with 77 references selected for full-text reading and in-depth analysis and 10 were selected for reading. The Figure 1 summarizes this flow.

The data extraction phase included ten selected studies that proposed sensor technologies. The devices analyzed exhibit diversity in technological principles, transmission mechanisms, analytical strategies, and modes of integration with mobile platforms.

Sensor types vary across microwave-based systems (including antennas and dual-band structures), optical biosensors (featuring technologies such as nanopillar SPR), and electrochemical sensors (including three-electrode amperometric systems and flexible sensors). Near-infrared spectroscopy (NIR)-based solutions were also identified.

Regarding data transmission, most studies employed wireless technologies such as Bluetooth, Bluetooth Low Energy, NFC, microwave networks, integrated circuits with microcontrollers, and ISM-band radar modules. These transmission systems are generally designed to communicate with mobile applications or wearable devices.

In terms of analytical approaches, the predictive strategies reported include regression algorithms, real-time signal detection with defined detection limits, signal correlation for calibration, and Sparameter analysis—some of which are associated with machine learning techniques.

Integration with mobile platforms is mentioned in nearly all studies, either through smartphone applications, wearable system connectivity, or references to interoperability with electronic health records. Only a few articles do not explicitly detail this aspect, although they imply it as part of the proposed architecture.

When reported, cost estimates reflect a focus on affordability, with explicit mention of low-cost prototypes or economical design strategies. However, in many cases, cost data are not precisely quantified.

The studies included in this systematic review reflect a growing effort in the literature to develop non-invasive and affordable technologies for CGMS. Despite the diversity of sensors and

Figure 1. Study selection flow – Systematic Review.

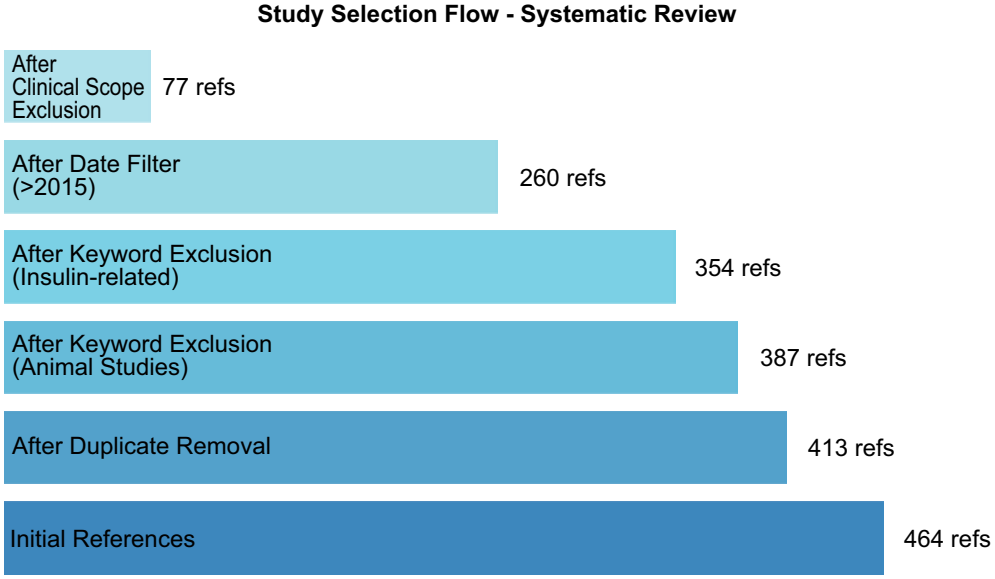

technical approaches, there is a common trend toward portability and integration with mobile devices, which supports their use in both clinical and home-based settings.

Connectivity with digital platforms—such as mobile applications and wearable systems—is a recurring feature, with potential to enhance remote monitoring and promote greater autonomy in diabetes management. Additionally, analytical strategies like statistical regression and machine learning algorithms are being incorporated into systems for glycemic event prediction, although often applied in simulated conditions.

From a methodological standpoint, important limitations were observed, including the lack of robust clinical validation, small sample sizes, and a lack of standardization in data presentation. Technical terms such as "low cost" or "high accuracy" are frequently used without reference to clear metrics, which hinders comparisons between studies and the generalization of results.

Conclusion

This systematic review highlighted significant advancements in the field of CGMS, with particular emphasis on innovations in alternative sensor technologies, increased integration with mobile platforms, and the adoption of predictive strategies based on computational intelligence. The analysis of ten studies — five of which were examined in depth — revealed a promising technological landscape, albeit marked by ongoing challenges related to methodological standardization, clinical validation, and large-scale feasibility.

The main contribution of this review lies in identifying the convergence of low cost, connectivity, and analytical capabilities as key pillars for the development of more accessible and effective diabetes management solutions. Despite notable progress, critical gaps remain, particularly regarding practical validation, user experience, and integration with public healthcare systems.

Future research should prioritize empirical assessments of CGMS devices, focusing on usability, scalability, and social impact. Additionally, the use of more rigorous and reproducible data extraction protocols — such as the one employed in this review — is essential to strengthen the evidence base and improve comparability across studies.

Acknowledgments

The main author thanks Professors Herman Lepkison and Raimundo Maêdo for their guidance and support; and Thamiles Melo for her encouragement, and to my family and friends for their unwavering support, especially during challenging moments.

References

1. Oliveira BC, Leme MBP. Monitoramento contínuo da glicemia e educação em diabetes. Cad UniFOA. 2024;19(54):1-8.
2. Hossain GMM, Jalal A, Pala N, Alam F. Advancements in glucose monitoring: a thin film ZnO-nanoflakes based highly sensitive wearable biosensor for noninvasive sweat-based point-of-care monitoring for diabetes. ECS Meet Abstr. 2024;MA2024-01:2736-2736.
3. Mohammadi P, Mohammadi A, Kara A. Dual-frequency microwave resonator for noninvasive detection of aqueous glucose. IEEE Sens J. 2023;PP:1-1.
4. Aldhaheri R, Babu J, Nella A, Sobahi N. A novel compact highly sensitive non-invasive microwave antenna sensor for blood glucose monitoring. Open Phys. 2023;21.
5. Aragão ICS, Aragão FMS, Reis FP, Aragão JA. Inovações no tratamento da diabetes tipo 2: terapias de alta precisão e monitoramento contínuo de glicose. IOSR J Nurs Health Sci. 2024;13(6):1-9.
6. Jesus PC, Moura PHM, Silva DMRR, Silva EED, Albuquerque RCC, Xavier LHM, et al. Análise do uso da monitorização contínua de glicose em pacientes com DM sem suporte multidisciplinar prévio: uma perspectiva observacional. J Assist Farm Farm. 2023;8(Suppl 2).
7. Silva SMJ, Negri JVA, Barreto TC, Correa SCS, Leão AQ, Silvestre MA. Eficácia do monitoramento contínuo da glicose no manejo do diabetes mellitus tipo 2 em adultos. Acervo Méd. 2024;24:e18451.
8. Tahmid A, Rahman T, Emam SMA, Reza SM, Hosen MI, Inum R, et al. Low-cost and easy-to-fabricate microwave sensor for sensitive glucose monitoring: a

step towards continuous glucose monitoring. IEEE J Electromagn RF Microw Med Biol. 2025;9(2):221-8.
9. Verma K, Preity P, Ranjan R. An insight into wearable devices for smart healthcare technologies. In: 2023 13th International Conference on Cloud Computing, Data Science & Engineering (Confluence). Piscataway (NJ): IEEE; 2023.
10. Kitchenham B, Charters S. Guidelines for performing systematic literature reviews in software engineering. Keele (UK): Keele University; 2007.

Literature Review on the Feasibility of Recycling Electrical and Electronic Waste (WEEE)

Alice Bispo dos Santos[1]*, Morgana Sousa Fernandes[2], Henrique Cesar Santos de Jesus[3], Juliana Ricardo de Souza[4], Nilmar de Souza[5]

[1]Federal University of Recôncavo da Bahia, Department of Assistive Technology and Accessibility Engineering; [2]Federal University of Recôncavo da Bahia, Department of Materials Engineering; [3]Federal University of Recôncavo da Bahia, Department of Materials Engineering; Feira de Santana, Bahia; [4]Federal Rural University of the Semi-Arid; Caraúbas, Bahia; [5]Federal University of Recôncavo da Bahia; Feira de Santana, Bahia, Brazil

The growing amount of waste electrical and electronic equipment (WEEE) is a global problem, with generation increasing five times faster than documented recycling. In 2022, 62 million tons of e-waste were produced, but less than 22.3% was collected and recycled properly. The aim of the work was to analyze the main polymers in WEEE, discuss the challenges of recycling and characterizing them, and explore the feasibility of applying them in the production of filaments for 3D printing. The methodology consisted of a qualitative analysis of 8 scientific articles selected from the Scopus and Web of Science databases. The research was limited to publications in English between 2003 and 2025. The results highlight the importance of characterization for recycling. Techniques such as FTIR, TGA and DSC are essential for understanding the chemical, thermal and mechanical properties of polymers. FTIR identifies compounds such as hydrocarbons and aromatic rings and is useful for unknown polymers. TGA measures the loss or gain of mass with temperature, indicating thermal degradation. DSC identifies changes in physical state, such as melting temperature (Tm), glass transition temperature (Tg) and crystallization temperature (Tc). Two recycling techniques are promising: chemical and mechanical. Chemical recycling, via pyrolysis, can convert plastics into useful monomers or fractions. However, plastics with brominated flame retardants (BFRs) can generate toxic substances. Pre-treatment methods, such as the CreaSolv® process, have proven effective in removing BFRs. Mechanical recycling faces challenges such as property degradation and material heterogeneity. Additive manufacturing (AM), especially FDM/FFF technology, is an alternative for reusing WEEE plastics and adding value. However, the variability of equipment shapes and sizes makes process automation complex.

Keywords: Recycling. WEEE. Polymers. Characterizations.

Abbreviations: (WEEE), Waste electrical and electronic equipment. (PS), Polystyrene. (ABS), Acrylonitrile Butadiene Styrene. (PC/ABS), Polycarbonate/Acrylonitrile Butadiene Styrene. (HIPS), High Impact Polystyrene. (PP), Polypropylene. (PLA), Polylactic acid. (FTIR), Fourier Transform Infrared Spectroscopy. Thermogravimetric Analysis, (TGA).(NIR), Near Infrared Spectroscopy. (DSC), Differential Scanning Calorimetry. Additive Manufacturing, (AM). (FDM), Fused Filament Deposition.(FFF), Fused Filament Fabrication. (PABS), (Poly (Acrylonitrile Butadiene Styrene)). (LDPE), Low Density Polyethylene. (TBBPA), Tetrabromobisphenol A. (TBPE), Decabromodiphenyl ethane (DecaBDE), Decabromodiphenyl ether. (PBDEs), Polybrominated diphenyl ethers. (BRFs), Flame retardants.

The amount of plastic waste grows every year. Since 1950, 8.3 billion metric tons have been produced, with only 9% recycled [1]. In waste electrical and electronic equipment (WEEE), plastic accounts for 21% by weight [2]. The management of this waste is necessary to mitigate improper disposal and promote the circular economy. According to the Global E-waste Monitor 2024 [3], global e-waste generation is growing five times faster than its documented recycling. In 2022, 62 million tons of electronic waste were produced, an increase of 82% since 2010, but only 22.3% was collected and recycled properly, highlighting the urgency of effective management.

WEEE recycling faces the challenge of plastic diversity, with more than 15 types of engineering polymers [4]. It is essential to characterize these materials to define the best ways to recycle and

Received on 22 February 2026; revised 17 April 2026.

Address for correspondence: Juan Carlos Romero Albino. Federal University of Recôncavo da Bahia; Av. Centenário, 697 Sim, Feira de Santana, Bahia, Brazil. Zipcode: 44042-280. E-mail: alicebispotmi@gmail.com.

J Bioeng. Tech. Health 2026;9(5):480-486

reuse them. Ma and colleagues (2016) [5] indicate that Polystyrene (PS), Acrylonitrile Butadiene Styrene (ABS), PC/ABS, High Impact Polystyrene (HIPS), and Polypropylene (PP) represent 55% of plastics in WEEE. Among the recycling techniques, mechanical and chemical recycling stand out. Chemical recycling, especially pyrolysis, breaks down polymers into monomers or useful fractions, and is promising for mixed or degraded plastics [6]. Mechanical recycling involves shredding, washing, and reprocessing, but it is sensitive to contaminants and degradation.

As an alternative for recovery and circular economy, Additive Manufacturing (AM), especially Fused Filament Fabrication (FDM/FFF), emerges as a viable way to reuse waste, expanding recycling with cleaner and more efficient processes [7].

To optimize reuse and recycling, material characterization is essential, with Fourier Transform Infrared Spectroscopy (FTIR), Thermogravimetric Analysis (TGA), and Differential Scanning Calorimetry (DSC) standing out [4].

Thus, it is essential to understand the characteristics of plastics in WEEE and assess the potential of chemical, mechanical, and additive manufacturing recycling. This work analyzes the main polymers in WEEE, the challenges of recycling and characterization, and explores their application in the production of recycled filaments for 3D printing.

Materials and Methods

This study adopts a qualitative approach, combining an analysis based on scientific articles in databases with a careful analysis of the works produced, with the aim of deepening knowledge on the subject and understanding the various methodologies and applications of the materials in question.

For data collection, the Scopus and Web of Science databases were selected due to their wide reach and reliability in the academic community and their rigorous indexing of scientific journals.

The search strings were constructed with the terms “waste electric and electronic equipment,” “recycling,” and “polymer,” applied in the title, abstract, and keyword fields (Scopus) and in “Topics” (Web of Science). The search was limited to English-language publications of the “article” type, covering the period from 2003 to 2025.

After the search, the data were exported in Bibtex format and RStudios was used to exclude possible duplicate works, where a single RIS file was generated and imported by a software extension, Bibliometrix, so that a spreadsheet could be created. The file resulted in 32 articles. These were submitted to a two-step selection process: first, the titles were read to exclude works that did not align with the scope of the research. Next, the abstracts of the remaining articles were analyzed, with the criterion of selecting those most relevant to the objectives of this study. This refinement process resulted in a final portfolio of eight articles, which formed the basis for the subsequent analysis.

Results and Discussion

As the last resort for waste that cannot be reduced or reused, recycling consists of transforming the material from a discarded product into raw material for the manufacture of new items, a fundamental process for sustainability, in which the importance lies in the ability to address problems in an integrated manner and generate profits from environmental benefits, such as the conservation of natural resources and reduction in pollution, to economic benefits in the form of job creation and reduced production costs, as well as social benefits in the development of environmental awareness and improved quality of life.

How to Characterize Samples

To this end, it is crucial to separate and characterize materials that have been discarded, especially given the enormous complexity and

variety of polymers, where they are the basis that guarantees the success, viability, and purpose of recycling. Without efficient separation and characterization, plastic recycling becomes impractical, generating low-quality products and, in many cases, rendering the entire cycle unfeasible.

Among the characterization techniques, Fourier Transform Infrared Spectroscopy (FTIR) stands out as one of the most widely used for the identification of polymeric materials from WEEE. Through this analysis, a beam of infrared light interacts with the sample, allowing the identification of characteristic functional groups, such as aromatic rings and double or triple bonds. This capability is of great importance for the evaluation of unknown polymers, since each material has a unique infrared absorption spectrum, which acts as a molecular "fingerprint." Thus, FTIR has established itself as a simple, fast, and accurate identification method [8].

According to research by Achilias and colleagues (2009) [4] on the development of polymer recycling techniques from WEEE, using FTIR made it possible to identify polymers such as PABS (Poly (Acrylonitrile Butadiene Styrene)), where, according to the study, some characteristic functional groups were observed, such as absorption bands from 3000 to 3100, 700, and 755 cm^{-1}, referring to styrene structural units, stretching vibrations of the aromatic ring at 1494 and 1452 cm^{-1}, the band at 1602 cm^{-1} caused by the double bond of aromatic carbon and C=C stretching vibration, as well as the nitrile group (-C≡N) by the acrylonitrile units in ABS at 2238 cm^{-1} and the bands at 911 and 966 cm−1 corresponding to the unsaturated groups of the butadiene phase in ABS.

On the other hand, Charitopoulou and colleagues (2023) [6] used various polymers from WEEE (remote controls, calculators, computers, printers, and televisions) to identify, debrominate, and recycle them through pyrolysis, in order to reduce the volume of this waste through an environmentally friendly approach. By using FTIR on samples from each piece of equipment, the author was able to identify obvious bands in the 2840-2950 cm^{-1} range, which are due to the C–H bond, but also a band of lower intensity at approximately 1550–1600 cm^{-1} due to the C=C double bond. This combination indicates the presence of styrenic polymers, characterized by the presence of benzene rings in their polymer chain, such as ABS and HIPS, polymers commonly used in the manufacture of these products. However, when observing two samples of different products, a band was noted around 1750 cm^{-1}, a vibration value characteristic of polyesters, such as PC, due to the C=O bond, i.e., it indicates that it includes a mixture of PC with HIPS or ABS.

Thermal analysis is another fundamental method for identifying polymeric materials, as their thermal properties are directly linked to their molecular structure. For example, linear and branched polymers generally have higher thermal expansion coefficients due to weak secondary bonds between chains. As the number of cross-links increases, the structure becomes more restricted, resulting in a lower expansion coefficient.

Following this same structural logic, each polymer exhibits a unique thermal profile, with distinct points of degradation, melting (Tm), glass transition (Tg), and crystallization (Tc). Tm is the temperature at which the crystalline structure of the material breaks down and it changes from a solid to a liquid state. Tg, in turn, is a transition characteristic of amorphous polymers, where the material changes from a rigid and brittle state to a flexible or "rubbery" state due to the increased mobility of the chains. After this transition, the amorphous material can release heat and reorganize itself into a crystalline structure, an event that defines its crystallization temperature, Tc.

Differential Scanning Calorimetry (DSC) is a technique used to identify changes in the physical state of a material. It works by measuring the energy that the sample absorbs or releases when subjected to a constant heat flow compared to an

inert reference. Based on the energy difference between the two, DSC accurately identifies the temperatures of key events, such as melting and glass transition, which are unique to each polymer. Such reference values are well documented in works such as Textbook of Polymer Science [9] and Introduction to Physical Polymer Science [10].

Other common thermal characterization is Thermogravimetric Analysis (TGA). This technique measures the mass change of a sample as a function of temperature or time while it is subjected to a controlled heating program. Additionally, TGA results can be expressed as the first derivative of the mass loss curve, which allows for clearer identification of the temperatures at which the main stages of material degradation occur.

In a study that sought to examine the thermal behavior and products obtained after the pyrolysis of polymer blends, it was shown that, after the TGA test, ABS and HIPS have very similar thermal degradation, since their degradation begins and ends at very similar temperatures. Specifically, ABS completes its degradation at 515 °C and HIPS at 509 °C, but they had different residual mass percentages, 2.3% and 1.1%, respectively. This can be explained by the presence of aromatic rings in their structure, which makes it difficult to break bonds at low temperatures. On the other hand, the same study observed that the degradation and decomposition of PC occur at high temperatures, 664 °C, and has a residual mass of 23%, showing that it is more heat resistant than the other polymers evaluated. Its high residual mass can be attributed to carbon, which is formed from the aromatic parts [11]. The use of polymers with high flame retardancy in Electrical and Electronic Equipment (EEE) is a safety requirement due to contact with components capable of generating heat or sparks. In contrast, common polymers such as Low Density Polyethylene (LDPE), composed solely of carbon and hydrogen, are highly flammable; when heated, they melt, drip, and burn similarly to candle wax. To meet this safety requirement, the electronics industry uses additives, notably brominated flame retardants. Among them, tetrabromobisphenol A (TBBPA) is the most widely used in plastics for this sector [11-13].

Although it is possible to “get to know” the polymer using a single technique, the complete characterization of an unknown material requires a set of tests to create its “performance profile.” By combining the results, it becomes possible to compare them with data from known materials and thus arrive at an accurate classification. In this context, mechanical tests are fundamental methodologies for drawing up this profile.

Polymers are, in many ways, different from metals and ceramics, as they exhibit three different types of stress-strain behavior. Some, such as thermosets, exhibit rigid and brittle behavior, fracturing with little deformation. Others, such as elastomers (rubbers), exhibit fully elastic deformation, with large elongations under low stresses. Thermoplastics, in turn, are the most widely used in the EEE industry and exhibit behavior similar to that of metals: their initial deformation is elastic and reversible, followed by a creep that initiates plastic deformation, which is permanent [14]. From these behaviors, it is possible to obtain important information about the mechanical performance of each polymer, since, like thermal characteristics, each material has a performance “signature.”

The tensile test, for example, evaluates the performance of a material when subjected to a tensile force. Among the various data obtained, the Modulus of Elasticity (or Young's Modulus) is fundamental, as it determines the stiffness of the material. Defined as the ratio between stress and strain in the elastic region, a high modulus value indicates that the material is stiff. In contrast, a low value characterizes a flexible material [15].

The impact resistance test evaluates the toughness of a material, that is, its ability to resist deformation at high speed. This analysis was used by Pelto and colleagues (2023) [16] in a study on the mechanical properties of PC and ABS polymer

blends. In the test, the samples were subjected to the Charpy notch test under standard conditions (23 °C and 50% humidity). It was observed that the blend composed only of recycled polymers, without additives, had very low impact resistance, confirming it as a fragile material. However, when a compatibilizer was added to the recycled mixture to overcome this problem, the improvement in performance was dramatic. The toughness of the material increased significantly, reaching levels comparable to or even higher than those of a similar blend made with virgin polymers.

Even though it was not an application to determine information about an unknown polymer, the test served to verify whether, after some type of change in the structure of the material, it would retain, lose, or increase its properties.

Recycling Techniques

Some of the main polymers commonly found in EEE are HIPS, PC, PP, and ABS, as well as PC/ABS blends, representing about 20-30% of the total weight [4-6]. The recycling of these materials is of great importance due to the amount of waste currently produced. Thus, there are several recycling methods that can be used, including:

Pyrolysis

Pyrolysis is a thermochemical method that allows the recovery of monomers and the formation of valuable secondary materials. The process occurs in an inert atmosphere, at medium to high temperatures (300 °C–900 °C), with or without the presence of catalysts. During pyrolysis, plastic waste is converted into liquids, gases, and solid waste. This method enables the recovery of material and energy from waste polymers. The quality and distribution of pyrolysis products are influenced by several parameters, such as temperature, residence time, and heating rate, in addition to the presence of catalysts. These materials can be used as fuels or raw materials for the production of new products [6-12].

Despite this, the pyrolysis of plastics containing brominated flame retardants can generate toxic substances, which compromises the reuse of the products obtained. This obstacle can be overcome by applying catalytic pyrolysis, in which the selectivity of the derived products is increased due to the presence of catalysts and the formation of undesirable substances can be inhibited [17]. To circumvent this problem, many pretreatment methods have been investigated. The study by Charitopoulou and colleagues (2023) [6] demonstrated that the CreaSolv® process was able to remove BFRs, such as TBBPA, Decabromodiphenyl ethane(TBPE), and Decabromodiphenyl ether (DecaBDE), reducing the bromine concentration to less than 500 ppm. Solvent extraction, such as the CreaSolv® process, has proven to be effective in decontaminating WEEE plastics by removing halogens and flame retardants. Another pretreatment technique, Soxhlet extraction with solvents such as butanol and isopropanol, has also been shown to be efficient in reducing the bromine content in WEEE plastics while maintaining the polymer structure for subsequent pyrolysis [16].

Mechanical Recycling

Mechanical recycling can also be a viable route, but the degradation of properties, especially notched impact strength, is a challenge. In addition, heterogeneity is another challenge posed by WEEE recycling. The study by Chancerel and Rotter (2009) [18] suggests that proper classification of equipment according to type would reduce the heterogeneity of the plastic fraction resulting from a treatment process. The thorough characterization of WEEE plastics, using techniques such as FTIR, XRF, and DSC, is essential to identify the composition and guide recycling strategies, ensuring that the final products meet the desired quality standards.

Thus, depending on the materials identified and their mechanical and chemical characteristics,

such as styrene-based polymers, ABS, and high-impact polystyrene (HIPS), which represent more than 50% by weight of WEEE plastics, can be used as filaments for additive manufacturing (AM) through fused deposition modeling technology. In fact, ABS with polylactic acid (PLA) is the most widely used material, in general, as polymers that can be melted at a suitable temperature without degradation and are generally useful candidates for material extrusion systems [19].

Possible Challenges

The recycling of WEEE poses a major challenge, mainly due to the complex nature of this equipment. Approximately 20% of the total weight of EEE is composed of polymeric material, covering up to 15 different types of engineering polymers. Improper disposal causes environmental impacts and health risks. Efficient management faces relevant issues, among which high cost stands out [4].

Among the challenges of treating WEEE are: the diversity of polymers, which makes sorting and recycling difficult; the presence of brominated aromatic compounds (BRFs); and the fact that the thermal treatment of these substances can generate halogenated dibenzodioxins and dibenzofurans, which are toxic compounds [4]. Perrin and colleagues (2016) [20] point to plastic waste as a significant source of pollution and argue that, considering the desired properties of recycled plastics, it would be possible to reduce waste. However, the number of studies is limited. There is potential for recycled plastics to meet more stringent specifications, but classification—especially by Near Infrared Spectroscopy (NIR)—still presents technical difficulties or practical unfeasibility.

Regarding BRFs, Altarawneh and colleagues (2019) [6] highlight environmental and health concerns, emphasizing the global discontinuation of mixtures such as polybrominated diphenyl ethers (PBDEs). Studies indicate that prolonged exposure to certain chemicals causes adverse effects on the endocrine, reproductive, and nervous systems [21].

Cafieiro and colleagues (2021) [18] point out that the variability in shapes and sizes of EEE—from refrigerators to smartphones—affects the efficiency of the recycling process, making the automation of the stages complex and compromising its viability.

Conclusion

Given the scenario in which the volume of electronic waste (WEEE) grows every year and there is a low rate of document management, it is urgent to create strategies to mitigate impacts and reuse polymeric materials. This study showed that plastics represent a significant portion of WEEE, composed of a variety of engineering polymers, whose identification and characterization are essential for efficient and sustainable recycling.

Characterization techniques—FTIR, TGA, and DSC—proved indispensable for understanding the chemical, thermal, and mechanical properties of polymers, enabling their identification, performance evaluation, and reuse potential. Chemical recycling, especially by pyrolysis, and mechanical recycling have proven to be promising avenues, especially when combined with pretreatments that minimize toxic contaminants.

Additive manufacturing emerges as an innovative and sustainable alternative, capable of adding value to recycled materials and expanding applications. However, technical, economic, and environmental challenges require investment in research, more accurate sorting technologies, and public policies that encourage the circular economy.

This work reinforces the importance of integrating characterization, recycling techniques, and emerging technologies, such as 3D printing, for more efficient management of WEEE. Advancing in this field is not only an environmental necessity but also an opportunity for economic and social transformation.

References

1. Lee A, Liew MS. Tertiary recycling of plastics waste: an analysis of feedstock, chemical and biological degradation methods. J Mater Cycles Waste Manag. 2021;23:32-43.
2. Ongondo FO, Williams ID, Cherrett TJ. How are WEEE doing? A global review of the management of electrical and electronic wastes. Waste Manag. 2011;31(4):714-30.
3. United Nations Institute for Training and Research (UNITAR). The Global E-waste Monitor 2024: electronic waste rising five times faster than documented e-waste recycling [Internet]. 2024. Available from: https://ewastemonitor.info
4. Achilias DS, Antonakou EV, Koutsokosta E, Lappas AA. Chemical recycling of polymers from waste electric and electronic equipment. J Appl Polym Sci. 2009;114(1):212-21.
5. Ma C, Yu J, Wang B, Song Z, Xiang J, Hu S, et al. Chemical recycling of brominated flame-retarded plastics from e-waste for clean fuels production: a review. Renew Sustain Energy Rev. 2016;61:433-50.
6. Charitopoulou MA, Lappas AA, Achilias DS. Thermo-chemical recycling of plastics retrieved from waste electric and electronic equipment (WEEE) by pyrolysis: identification of the polymer type, removal of bromine compounds from plastics based on an environmentally-friendly process and characterization of the pyrolysates. Sustain Chem Pharm. 2023;35:101210.
7. Fico D, et al. Fabricação sustentável de compósitos poliméricos por meio de tecnologias de impressão 3D usando polímeros e cargas recicladas. Polymers (Basel). 2022;14(18):3756.
8. Grigorescu RM, Grigore ME, Iancu L, Ghioca P, Ion RM. Waste electrical and electronic equipment: a review on the identification methods for polymeric materials. Recycling. 2019;4(3):32.
9. Billmeyer FW Jr. Textbook of polymer science. 3rd ed. New York: John Wiley & Sons; 1984.
10. Sperling LH. Introduction to physical polymer science. 4th ed. Hoboken (NJ): John Wiley & Sons; 2006.
11. Charitopoulou MA, Papadopoulou L, Achilias DS. Effect of brominated flame retardant on the pyrolysis products of polymers originating in WEEE. Environ Sci Pollut Res Int. 2022;29(20):29570-82.
12. Charitopoulou MA, Stefanidis SD, Lappas AA, Achilias DS. Catalytic pyrolysis of polymers with brominated flame-retardants originating in waste electric and electronic equipment (WEEE) using various catalysts. Sustain Chem Pharm. 2022;26:100612.
13. Charitopoulou MA, Papadopoulou L, Achilias DS. Removal of bromine from polymer blends with a composition simulating that found in waste electric and electronic equipment through a facile and environmentally friendly method. Polymers (Basel). 2023;15(3):709.
14. Callister WD Jr, Rethwisch DG. Ciência e engenharia de materiais: uma introdução. 8. ed. Rio de Janeiro: LTC; 2012.
15. Mano EB. Polímeros como materiais de engenharia. São Paulo: Edgard Blücher; 1991.
16. Pelto J, Barreto C, Anwar H, Strobl L, Schlummer M. Compatibilized PC/ABS blends from solvent recycled PC and ABS polymers from electronic equipment waste. Polym Test. 2023;120:107969.
17. Aguado J, Serrano DP, Escola JM. Catalytic upgrading of plastic wastes. In: Scheirs J, Kaminsky W, editors. Feedstock recycling and pyrolysis of waste plastics. Chichester: John Wiley & Sons; 2006. p. 73-110.
18. Chancerel P, Rotter S. Recycling-oriented characterization of small waste electrical and electronic equipment. Waste Manag. 2009;29(8):2336-52.
19. Cafiero L, De Angelis D, Di Dio M, Di Lorenzo P, Pietrantonio M, Pucciarmati S, et al. Characterization of WEEE plastics and their potential valorisation through the production of 3D printing filaments. J Environ Chem Eng. 2021;9(4):105532.
20. Perrin D, Mantaux O, Ienny P, Léger R, Dumon M, Lopez-Cuesta JM. Influence of impurities on the performances of HIPS recycled from waste electric and electronic equipment (WEEE). Waste Manag. 2016;56:438-45.
21. Ilankoon IMSK, Ghorbani Y, Chong MN, Herath G, Moyo T, Petersen J. E-waste in the international context: a review of trade flows, regulations, hazards, waste management strategies and technologies for value recovery. Waste Manag. 2018;82:258-75.

Energy Justice and Microgrids in Vulnerable Urban Areas: A Sustainable Approach

Celso Barreto da Silva[1,3]*, Filipe Cardoso Brito[1,3], Toni Alex Reis Borges[3,4], Hugo Saba[1,2,3], Aloísio Santos Nascimento Filho[1,3]

[1]SENAI CIMATEC University, Stricto Sensu Department; [2]University of the State of Bahia– UNEB, Department of Exact and Earth Sciences; [3]Applied Research and Innovation Nucleus —NPAI; Salvador, Bahia; [4]Federal Institute of Bahia (IFBA); Feira de Santana, Bahia, Brazil

This article explores the critical intersection between energy justice and the transformative role of microgrids in socially vulnerable urban areas. The research addresses inequalities in energy access that affect these communities, highlighting how the implementation of microgrids can promote equity, resilience, and sustainable development. The social, economic, and environmental benefits of integrating microgrids were analyzed, including benefits to communities, fostering the local economy, and reducing carbon emissions. The results achieved demonstrate that microgrids not only ensure a more reliable and accessible energy supply but also empower communities, allowing them greater control over their energy resources. The analysis of global success cases illustrates the viability and positive impact of these solutions, despite technical, financial, and regulatory challenges. We conclude that microgrids are an ally in building a more just and equitable energy future, with significant implications for public policies and future research aimed at overcoming energy poverty and promoting urban sustainability.

Keywords: Energy Justice. Microgrids. Social Vulnerability. Renewable Energy. Sustainable Development.

Equitable access to energy remains one of the main challenges in vulnerable urban areas, where structural inequalities persist that directly impact the quality of life and socioeconomic development [1].

These populations face not only precarious energy supply, but also high costs, deficient infrastructure, and environmental risks that amplify social and economic exclusion [2,3]. In this context, energy justice presents itself as a field of study that seeks to understand and mitigate disparities in access, promoting sustainable, safe, and socially just solutions.

Among the emerging alternatives, microgrids stand out, decentralized systems for energy generation, storage, and distribution that operate either integrated with or isolated from the main grid [4].

By allowing greater energy autonomy, integration of renewable sources, and strengthening of local infrastructure, microgrids emerge as a viable alternative to face the challenges posed by energy poverty, especially in communities with low socio-environmental resilience [5].

Such systems also enable new community arrangements and sustainable business models, aligning with a more inclusive energy transition. Considering these premises, this study seeks to critically analyze the potential of microgrids in promoting energy justice in vulnerable urban contexts.

The investigation focuses on identifying critical dimensions of energy injustice, evaluating the effectiveness of microgrids in terms of access, reliability, and sustainability, and formulating applicable guidelines for their implementation, with a view to maximizing community benefits and overcoming technical and institutional challenges.

Energy Justice in Vulnerable Areas

Energy justice seeks to ensure that the benefits and burdens related to energy production, distribution, and consumption are shared equitably among all individuals, regardless of their location, socioeconomic status, or origin [1]. In vulnerable

Received on 17 February 2026; revised 12 April 2026.
Address for correspondence: Celso Barreto da Silva. Av. Orlando Gomes, 1845 - Piatã, Salvador – BA – Brazil, Zipcode: 41650-010. E-mail: profcelsobarreto@hotmail.com.

J Bioeng. Tech. Health 2026;9(5):487-493

urban areas, poverty and precarious infrastructure frequently limit access to adequate energy services, reflecting in high costs, insecurity, and exclusion [2]. These challenges can manifest in the form of energy poverty, environmental risks, and vulnerability to disasters.

The understanding of social vulnerability and its relationship with energy access varies according to the context. In Chile, for example, the condition of immigrants can represent an additional barrier to accessing energy services [4]. In Spain, low-income communities are frequently the most exposed to the effects of pollution associated with energy generation and use [5]. In the United Kingdom, energy poverty remains a relevant factor that affects the health and well-being of millions of families [6]. In the United States, the lack of access to reliable energy intensifies the impacts of extreme climatic events on socially vulnerable populations [3].

In India, the absence of basic electricity infrastructure directly compromises areas such as education, health, and income generation, perpetuating cycles of exclusion [2]. In South Africa, issues such as food insecurity and inequality are strongly linked to restricted access to energy, affecting essential daily practices (16). In Australia, demographic and economic factors contribute to the vulnerability of remote communities, which face difficulties in accessing modern energy solutions [7].

These international experiences suggest that contexts of social vulnerability are multifaceted and require specific approaches to promote energy justice. The formulation of public policies and technical strategies must consider these variables so that the adopted solutions are effective, sustainable, and adapted to local realities.

Microgrids as a Solution: Functioning and Benefits

Microgrids are configured as decentralized energy systems that integrate generation, storage, and distribution of energy, capable of operating interconnected to the main electrical grid or autonomously. This characteristic provides them with flexibility and resilience in the face of conventional supply failures [8]. By incorporating renewable sources, such as solar and wind, and storage technologies, these systems enable the diversification of the local energy matrix and contribute to reducing dependence on fossil fuels.

In urban vulnerability contexts, microgrids represent a promising alternative to mitigate the impacts of energy poverty. Their implementation can expand energy access, improve supply reliability, and enable more sustainable practices in energy consumption and resource management [5]. Decentralization also allows for greater community autonomy, favoring the adaptation of solutions to local realities and strengthening technical and organizational capacities [6,9].

From an environmental perspective, the use of renewable sources associated with microgrids can contribute to the mitigation of greenhouse gas emissions and atmospheric pollutants, aligning with global sustainability goals and climate change combat [10]. Additionally, the reduction of technical losses in distribution and the possibility of managing local demand make microgrids more efficient systems [10,11].

In socioeconomic terms, studies demonstrate that the installation of microgrids can generate job opportunities, foster local businesses, and stimulate more participatory energy governance models [6,9,12]. Distributed generation can be converted into a source of income for communities, through the commercialization of energy surpluses, or in the reduction of household electricity expenses. These initiatives contribute to strengthening the local economy and community empowerment, especially when articulated with public policies and technical training programs.

Despite the identified benefits, the adoption of microgrids still faces barriers related to the initial implementation cost, technological complexity, and the need for regulatory adjustments. These limitations demand coordinated actions among

governments, the private sector, and civil society to enable their widespread diffusion.

Integration of Renewable Energies

The integration of renewable sources is one of the main components of microgrids, especially in vulnerable urban contexts [11]. Sources such as solar photovoltaic, wind, and biomass can be adapted in a decentralized way, meeting local needs. This approach contributes to the diversification of the energy matrix and to the strengthening of energy supply security.

Renewable generation associated with storage technologies, such as batteries, allows for the continuity of supply even in adverse conditions, such as conventional grid interruptions or climatic variations [10]. This aspect is particularly relevant in regions with fragile infrastructure, where the intermittency of energy compromises the functioning of schools, health posts, and small businesses.

In addition to reliability, the adoption of renewable sources can reduce operational costs and pollutant gas emissions, aligning with climate change mitigation goals. The decentralization of the system also enables the creation of cooperative generation arrangements, in which residents or community associations assume a leading role in the management and rational use of energy.

However, the effective integration of these technologies requires adequate technical planning, initial investment, and training of the communities involved.

Hybrid models that combine different sources and adapt to local characteristics have proven more efficient in overcoming the limitations imposed by environmental, regulatory, and economic factors.

Success Stories and Case Studies

Case studies documented in the literature demonstrate that the implementation of microgrids in vulnerable urban areas can generate positive results, provided they are adapted to local conditions.

In communities with limited infrastructure, microgrids have been employed as an alternative to ensure a more dependable, accessible, and sustainable energy supply [6]. Such experiences have contributed to broadening the debate on energy justice and social innovation.

In Brazil, initiatives such as those developed in isolated communities in the Amazon show that the adoption of hybrid solar microgrids can favor energy supply in hard-to-reach regions, reducing dependence on diesel generators and operational costs [4].

These projects involved community arrangements, institutional partnerships, and continuous technical support, factors that enabled their execution and maintenance.

In South Africa, experiences conducted in urban settlements demonstrate that the combination of solar energy with small-scale storage systems has the potential to meet basic residential demands, while fostering social participation and the development of local micro-enterprises [13].

The direct involvement of residents in planning and management was a differential for the acceptance of technology.

In Bangladesh, programs financed by international organizations enabled the installation of solar microgrids in rural and peri-urban areas, promoting significant improvements in health, education, and local productivity.

The replication of these models requires technological and institutional adaptation, according to the specificities of each territory [8].

These cases illustrate that, although promising, microgrids demand implementation strategies sensitive to the socioeconomic, environmental, and political context.

The success of projects is often related to the articulation between communities, local governments, the private sector, and financing agents.

Thus, the analyzed case studies reinforce the need for integrated approaches, with active community participation and continuous technical support, as a path to consolidate energy justice in vulnerable populations.

Materials and Methods

This study adopts an exploratory and descriptive approach, based on a literature review and analysis of case studies. The research was conducted using high-impact scientific databases, such as Scopus and Web of Science, employing key terms such as "energy justice," "microgrids," "urban vulnerability," and "renewable energy."

The selection of articles followed the principles of the PRISMA protocol (Preferred Reporting Items for Systematic Reviews and Meta-Analyses), as shown in Figure 1.

The methodological process included:

(i) Identification of studies through systematic search;
(ii) Screening of titles and abstracts;
(iii) Selection of full-text articles based on inclusion criteria; and
(iv) Analysis of the extracted data.

Priority was given to articles published in the last five years, focusing on empirical studies, systematic reviews, and theoretical works related to the intersection between energy justice and microgrids. Duplicate articles or those not directly aligned with the research objectives were excluded.

The qualitative analysis of the full texts followed the thematic content analysis technique, as proposed by Babalola and colleagues (6), based on the categorization of extracted data into themes such as: social impacts, technical and economic feasibility, community participation, and public policies.

This approach allowed the identification of patterns, gaps, and recurring contributions in the reviewed studies, enabling a critical discussion aligned with the research objectives.

Figure 1. Flowchart of the study selection process.

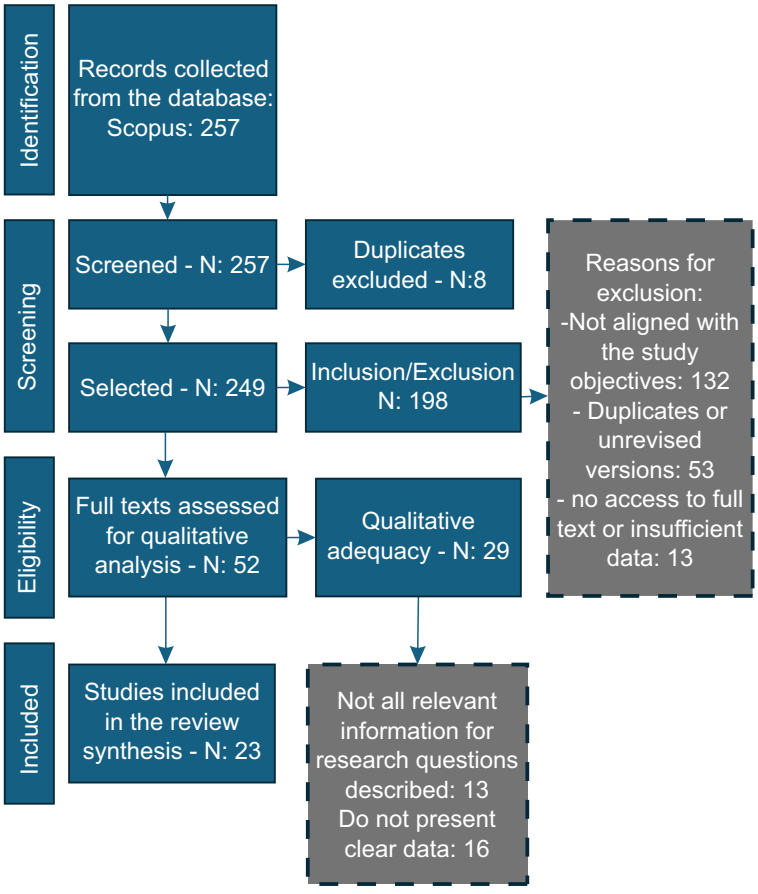

The integration of systematic review with qualitative analysis aimed to ensure that the study's findings were applicable to real-world contexts, sensitive to sociocultural specificities, and capable of supporting the formulation of public policies and innovative practices.

Results and Discussion

The analysis of the literature and case studies selected through the PRISMA methodology revealed that microgrids represent a promising alternative to address the challenges of energy access in vulnerable urban areas.

Although the results are qualitative, the data collected indicate significant impacts across social, economic, and environmental dimensions.

Table 1 presents a summary of the main impacts identified in the literature, organized by dimension and accompanied by the respective references.

The inclusion of quantitative indicators strengthens the findings. As shown in Table 1, microgrid projects have demonstrated tangible results: in Brazil, up to 300 households benefited from hybrid solar systems [4]; in India, energy supply increased from 8 to 24 hours daily [14]; and in South Africa, schools and health posts gained reliable electricity [13]. Economically, families reduced their bills by 20–40% (6), projects created 10–20 local jobs [5], and surplus energy generated revenues of up to US$ 15,000 annually in Bangladesh [8]. Environmentally, hybrid systems avoided up to 120 tons of CO_2 per year in the Amazon [10], while increasing the share of renewables to 70% in some communities [4,13] and reducing technical losses by 15% [10]. These figures reinforce the qualitative evidence, providing more robust support for the conclusions.

Based on these impacts, it is possible to deepen the discussion of qualitative evidence related to each dimension, as presented in the following paragraphs.

In the social dimension, several studies indicate that the implementation of microgrids contributes to strengthening community autonomy, access to basic services, and improving quality of life [1,5].

In projects carried out in Latin America, for example, communities began to have stable energy supply for schools, health posts, and public lighting, which enabled significant improvements in local daily life.

However, social benefits do not materialize uniformly. The literature highlights that the success of such initiatives strongly depends on community engagement, the existence of local leadership, and the capacity to maintain the systems in the long term [8].

In some contexts, the lack of technical training and adequate governance models compromised the continuity of operations.

From the economic perspective, the cases analyzed suggest that microgrids can reduce electricity costs for families and local enterprises, especially when power is generated from

Table 1. Impacts of microgrid implementation in vulnerable urban areas.

Dimension	Main Impacts	Indicators	References
Social	Quality of life, energy poverty reduction, community resilience	300 households served (Brazil); supply increased 8h→24h (India); schools and health posts benefited (South Africa)	[1,4,8]
Economic	Cost reduction, jobs, entrepreneurship	−20–40% energy cost; 10–20 jobs/project; annual revenue up to US$ 15,000 (Bangladesh)	[2,5,14]
Environmental	GHG reduction, efficiency, renewables	−120 tCO_2/year (Amazon); renewables up to 70% of matrix; −15% technical losses	[4,10,13]

renewable sources and storage technologies are used [5].

Additionally, job creation in the implementation, operation, and maintenance stages has the potential to boost the local economy. However, high initial costs and the lack of accessible financing lines remain significant barriers [5].

In the environmental dimension, the replacement of fossil sources with solar or wind energy contributes to the reduction of greenhouse gas emissions and improves air quality [10,13].

The decentralization of generation and the use of storage reduce transmission losses and increase energy efficiency. Despite these advances, studies warn that improper battery and waste management may represent new environmental challenges [10].

It is important to emphasize that, although the benefits are recurrent in the experiences analyzed, microgrids do not constitute a universal solution. Their effectiveness is conditioned by the political, institutional, and cultural context of each community.

Some authors point out that without public incentive policies, proper regulation, and continuous technical support, projects tend to lose momentum over time [14].

The convergence between the results obtained and the specialized literature reinforces the need for integrated and participatory approaches involving governments, the private sector, universities, and the community itself.

In this context, it is essential to develop methodological strategies that promote dialogue between technical-scientific knowledge and local knowledge, ensuring the adequacy of energy solutions to socio-territorial realities and strengthening the sustainability of interventions.

Conclusion

This study demonstrated that microgrids are an essential tool for mitigating inequalities in access to energy in vulnerable urban areas. Based on a systematic literature review and analysis of case studies, it was identified that the adoption of these systems can generate significant social, economic, and environmental benefits.

From a social perspective, microgrids not only improve the quality of life and strengthen community resilience but also deliver measurable results, such as providing reliable electricity to up to 300 households in Brazilian communities, expanding daily supply from 8 to 24 hours in Indian villages, and ensuring stable energy access to schools and health posts in South Africa.

In the economic dimension, projects have led to reductions of 20–40% in household electricity costs, the creation of 10 to 20 local jobs per initiative, and additional revenue of up to US$ 15,000 annually through the sale of surplus energy, as observed in Bangladesh. These figures highlight the potential of microgrids not only to reduce poverty but also to stimulate local entrepreneurship and strengthen community autonomy.

From an environmental standpoint, hybrid renewable systems have proven effective in avoiding up to 120 tons of CO_2 emissions annually, increasing the share of renewables in the local energy mix to nearly 70% in some communities, and reducing technical losses by approximately 15%. These quantitative indicators reinforce the role of microgrids in advancing climate goals and promoting sustainable urban development.

Despite these advances, the realization of benefits still requires overcoming significant barriers related to high initial costs, technological complexity, and regulatory challenges. The success of microgrid projects depends on active community participation, the presence of public incentive policies, and the provision of continuous technical support.

The integration of qualitative insights with quantitative evidence in this study strengthens the validity of the findings and provides a more solid foundation for policymaking. Future research is recommended to further expand the quantitative analysis of microgrid impacts and to develop replicable models adaptable to diverse urban contexts. By combining technical feasibility with social and environmental justice, microgrids

emerge as a viable pathway toward a fairer, more resilient, and sustainable energy future.

References

1. Carvalho PMS, et al. Vulnerabilidade social e pobreza energética no Brasil. Soc Sci Med. 2021;270:113733.
2. Babalola SO, Daramola MO, Iwarere SA. Socio-economic impacts of energy access through off-grid systems in rural communities: a case study of southwest Nigeria.
3. Philos Trans R Soc A. 2022;380(2221):20210140. Eklund M, et al. Barriers to community microgrids in fragmented communities: insights from a case study. Sustainability. 2023;15(1):123.
4. Norris SA, et al. Social vulnerability, food insecurity, and inequality in South Africa. Food Res Int. 2022;155:111117.
5. Muttaqee M, et al. Community response to microgrid development: case studies from the US. Energy Policy. 2023;175:113456.
6. Lewin K. Action research and minority problems. J Soc Issues. 1946;2(4):34-46.
7. Ramírez-Santana M, et al. Social vulnerability and immigrant conditions in Chile. Int J Infect Dis. 2019;80:123-9.
8. Karácsonyi D, et al. Social vulnerability and demographic and economic risks in Australia. Int J Disaster Risk Reduct. 2021;60:102523
9. ResearchGate. DC microgrids for remote community electrification [Internet]. 2024. Available from: https://www.researchgate.net/publication/DC_Microgrids_for_Remote_Community_Electrification
10. Hirsch A, et al. Microgrids: a review of technologies, key drivers, and outstanding issues. Renew Sustain Energy Rev. 2018;90:402-15.
11. Global Electricity Review. Community resilience and decentralized energy [Internet]. 2025 [cited 2025 Aug 8]. Available from: https://global-electricity-review.org
12. Bardin L. Análise de conteúdo. São Paulo: Edições 70; 2016.
13. Navarro CL, et al. Social vulnerability and environmental risks in Spain. Habitat Int. 2020;102:102280.
14. Das S, et al. Social vulnerability and basic infrastructure in India. Int J Disaster Risk Reduct. 2021;62:102465.

Instructions for Authors

The Authors must indicate in a cover letter the address, telephone number and e-mail of the corresponding author. The corresponding author will be asked to make a statement confirming that the content of the manuscript represents the views of the co-authors, that neither the corresponding author nor the co-authors have submitted duplicate or overlapping manuscripts elsewhere, and that the items indicated as personal communications in the text are supported by the referenced person. Also, the protocol letter with the number should be included in the submission article, as well as the name of sponsors (if applicable).

Manuscripts may be submitted within designated categories of communication, including:

- Original basic or clinical investigation (original articles on topics of broad interest in the field of bioengineering and biotechnology applied to health). We particularly welcome papers that discuss epidemiological aspects of international health, clinical reports, clinical trials and reports of laboratory investigations.
- Case presentation and discussion (case reports must be carefully documented and must be of importance because they illustrate or describe unusual features or have important practice implications).
- Brief reports of new methods or observations (short communications brief reports of unusual or preliminary findings).
- State-of-the-art presentations (reviews on protocols of importance to readers in diverse geographic areas. These should be comprehensive and fully referenced).
- Review articles (reviews on topics of importance with a new approach in the discussion). However, review articles only will be accepted after an invitation of the Editors.
- Letters to the editor or editorials concerning previous publications (correspondence relating to papers recently published in the Journal, or containing brief reports of unusual or preliminary findings).
- Editor's corner, containing ideas, hypotheses and comments (papers that advance a hypothesis or represent an opinion relating to a topic of current interest).
- Innovative medical products (description of new biotechnology and innovative products applied to health).
- Health innovation initiatives articles (innovative articles of technological production in Brazil and worldwide, national policies and directives related to technology applied to health in our country and abroad).

The authors should checklist comparing the text with the template of the Journal.

Supplements to the JBTH include articles under a unifying theme, such as those summarizing presentations of symposia or focusing on a specific subject. These will be added to the regular publication of the Journal as appropriate, and will be peer reviewed in the same manner as submitted manuscripts.

Statement of Editorial Policy

The editors of the Journal reserve the right to edit manuscripts for clarity, grammar and style. Authors will have an opportunity to review these changes prior to creation of galley proofs. Changes in content after galley proofs will be sent for reviewing and could be required charges to the author. The JBTH does not accept articles which duplicate or overlap publications elsewhere.

Peer-Review Process

All manuscripts are assigned to an Associate Editor by the Editor-in-Chief and Deputy Editor, and sent to outside experts for peer review. The Associate Editor, aided by the reviewers' comments, makes a recommendation to the Editor-in-Chief regarding the merits of the manuscript. The Editor-in-Chief makes a final decision to accept, reject, or request revision of the manuscript. A request for revision does not guarantee ultimate acceptance of the revised manuscript.

Manuscripts may also be sent out for statistical review ou *ad hoc* reviewers. The average time from submission to first decision is three weeks.

Revisions

Manuscripts that are sent back to authors for revision must be returned to the editorial office by 15 days after the date of the revision request. Unless the decision letter specifically indicates otherwise, it is important not to increase the text length of the manuscript in responding to the comments. The cover letter must include a point-by-point response to the reviewers and Editors comments, and should indicate any additional changes made. Any alteration in authorship, including a change in order of authors, must be agreed upon by all authors, and a statement signed by all authors must be submitted to the editorial office.

Style

Manuscripts may be submitted only in electronic form by www.jbth.com.br. Each manuscript will be assigned a registration number, and the author notified that the manuscript is complete and appropriate to begin the review process. The submission file is in OpenOffice, Microsoft Word, or RTF document file format for texts and JPG (300dpi) for figures.

Authors must indicate in a cover letter the address, telephone number, fax number, and e-mail of the corresponding author. The corresponding author will be asked to make a statement confirming that the content of the manuscript represents the views of the co-authors, that neither the corresponding author nor the co-authors have submitted duplicate or overlapping manuscripts elsewhere, and that the items indicated as personal communications in the text are supported by the referenced person.

Manuscripts are to be typed as indicated in Guide for Authors, as well as text, tables, references, legends. All pages are to be numbered with the order of presentation as follows: title page, abstract, text, acknowledgements, references, tables, figure legends and figures. A running title of not more than 40 characters should be at the top of each page. References should be listed consecutively in the text and recorded as follows in the reference list, and must follow the format of the National Library of Medicine as in Index Medicus and "Uniform Requirements for Manuscripts Submitted to Biomedical Journals" or in "Vancouver Citation Style". Titles of journals not listed in Index Medicus should be spelled out in full.

Manuscript style will follow accepted standards. Please refer to the JBTH for guidance. The final style will be determined by the Editor-in-Chief as reviewed and accepted by the manuscript's corresponding author.

Approval of the Ethics Committee

The JBTH will only accept articles that are approved by the ethics committees of the respective institutions (protocol number and/or approval certification should be sent after the references). The protocol number should be included in the end of the Introduction section of the article.

Publication Ethics

Authors should observe high standards with respect to publication ethics as set out by the International Committee of Medical Journal Editors (ICMJE). Falsification or fabrication of data, plagiarism, including duplicate publication of the authors' own work without proper citation, and misappropriation of the work are all unacceptable practices. Any cases of ethical misconduct are treated very seriously and will be dealt with in accordance with the JBTH guidelines.

Conflicts of Interest

At the point of submission, each author should reveal any financial interests or connections, direct or indirect, or other situations that might raise the question of bias in the work reported or the conclusions, implications, or opinions stated - including pertinent commercial or other sources of funding for the individual author(s) or for the associated department(s) or organizations(s), and personal relationships. There is a potential conflict of interest when anyone involved in the publication process has a financial or other beneficial interest in

the products or concepts mentioned in a submitted manuscript or in competing products that might bias his or her judgment.

Material Disclaimer

The opinions expressed in JBTH are those of the authors and contributors, and do not necessarily reflect those of the SENAI CIMATEC, the editors, the editorial board, or the organization with which the authors are affiliated.

Privacy Statement

The names and email addresses entered in this Journal site will be used exclusively for the stated purposes of this journal and will not be made available for any other purpose or to any other party.

Brief Policies of Style

Manuscript	Original	Review	Birief Comunication	Case Report	Editorial ; Letter to the Editor; Editor' s Corner	Innovative Medical Products	State-of-the-Art	Health Innovation Initiatives
Font Type	Times or Arial	Times or Arial	Times or Arial	Times or Arial	Times or Arial	Times or Arial	Times or Arial	Times or Arial
Number of Words – Title	120	90	95	85	70	60	120	90
Font Size/Space-Title	12; double space	12; double space	12; double space	12; double space	12; double space	12; double space	12; double space	12; double space
Font Size/Space-Abstracts/Key Words and Abbreviations	10; single space	10; single space	10; single space	10; single space	-	-	10; single space	10; single space
Number of Words – Abstracts/Key Words	300/5	300/5	200/5	250/5	-	-	300/5	300/5
Font Size/Space-Text	12; Double space	12; Double space	12; Double space	12; Double space	12; Double space	12; Double space	12; Double space	12; Double space
Number of Words – Text	5,000 including spaces	5,500 including spaces	2,500 including spaces	1,000 including spaces	1,000 including spaces	550 including spaces	5,000 including spaces	5,500 including spaces
Number of Figures	8 (title font size 12, double space)	3 (title font size 12, double space)	2 (title font size 12, double space)	2 (title font size 12, double space)	-	2 (title font size 12, double space)	8 (title font size 12, double space)	8 (title font size 12, double space)
Number of Tables/Graphic	7 title font size 12, double space	2 title font size 12, double space	2(title font size 12, double space)	1(title font size 12, double space)	-	-	7 title font size 12, double space	4 title font size 12, double space
Number of Authors and Co-authors*	15	10	5	10	3	3	15	10
References	20 (font size 10,single space	30(font size 10,single space	15 (font size 10,single space)	10 (font size 10,single space)	10 (font size 10,single space	5(font size 10,single space	20 (font size 10,single space	20

*First and last name with a sequencing overwritten number. Corresponding author(s) should be identified with an asterisk; Type 10, Times or Arial, single space. Running title of not more than 40 characters should be at the top of each page. References should be listed consecutively in the text. References must be cited on (not above) the line of text and in brackets instead of parentheses, e.g., [7,8]. References must be numbered in the order in which they appear in the text. References not cited in the text cannot appear in the reference section. References only or first cited in a table or figures are numbered according to where the table or figure is cited in the text. For instance, if a table is placed after reference 8, a new reference cited in table 1 would be reference 9.1 would be reference 9.

Checklist for Submitted Manuscripts

❑1. Please provide a cover letter with your submission specifying the corresponding author as well as an address, telephone number and e-mail.

❑2. Submit your paper using our website www.jbth.com.br. Use Word Perfect/Word for Windows, each with a complete set of original illustrations.

❑3. The entire manuscript (including tables and references) must be typed according to the guidelines instructions.

❑4. The order of appearance of material in all manuscripts should be as follows: title page, abstract, text, acknowledgements, references, tables, figures/graphics/diagrams with the respective legends.

❑5. The title page must include a title of not more than three printed lines (please check the guidelines of each specific manuscript), authors (no titles or degrees), institutional affiliations, a running headline of not more than 40 letters with spaces.

❑6. Acknowledgements of persons who assisted the authors should be included on the page preceding the references.

❑7. References must begin on a separate page.

❑8. References must be cited on (not above) the line of text and in brackets instead of parentheses, e.g., [7,8].

❑9. References must be numbered in the order in which they appear in the text. References not cited in the text cannot appear in the reference section. References only or first cited in a table or figures are numbered according to where the table or figure is cited in the text. For instance, if a table is placed after reference 8, a new reference cited in table 1 would be reference 9.

❑10. Reference citations must follow the format established by the "Uniform Requirements for Manuscripts Submitted to Biomedical Journals" or in "Vancouver Citation Style".

❑11. If you reference your own unpublished work (i.e., an "in press" article) in the manuscript that you are submitting, you must attach a file of the "in press" article and an acceptance letter from the journal.

❑12. If you cite unpublished data that are not your own, you must provide a letter of permission from the author of that publication.

❑13. Please provide each figure in high quality (minimum 300 dpi: JPG or TIF). Figure must be on a separate file.

❑14. If the study received a financial support, the name of the sponsors must be included in the cover letter and in the text, after the author's affiliations.

❑15. Provide the number of the Ethics Committees (please check the guidelines for authors).